

**Particle Formation in Supercritical
Carbon Dioxide by the RESS Process**

By

Ming Jia

**Department of Chemical and Biochemical Engineering
Faculty of Engineering**

**Submitted in partial fulfilment
of the requirements for the degree of
Master of Engineering Science**

**Faculty of Graduate Studies
The University of Western Ontario
London, Ontario
August, 2003**

© Ming Jia, 2003

ABSTRACT

Jia, Ming. Particle Formation in Supercritical Carbon Dioxide by the RESS Process
(Under the direction of Dr. Paul A. Charpentier)

The objective of this study was to develop and evaluate the rapid expansion of supercritical solution (RESS) process as an environmentally friendly alternative for particle formation. Organic material was dissolved in supercritical carbon dioxide and was used to rapidly expand the supercritical solution through an expansion nozzle. Due to an abrupt decrease of pressure to atmospheric, very high supersaturation values were achieved which led to small particle sizes. Furthermore, as the pressure change traveled at the speed of sound, a rapid propagating mechanical perturbation was obtained and led to an uniform condition within the nucleating medium, and hence in principle to narrow particle size distributions. Previous RESS reports indicate that the RESS process is an extremely attractive technology to form small particles with a narrow particle size distribution.

The goal of this work was to understand the relation between particle size and the RESS process conditions. Understanding this relation can help one to control the particle size and morphology by changing process conditions. Two organic materials, phenanthrene and beclomethasone dipropionate (BECD), were studied in this report. The experimental results show that the RESS apparatus allows forming small particles with narrow particle size distribution for both phenanthrene and BECD. The particle size and morphology

was analyzed by optical microscopy and scanning electron microscopy. The particle size distribution was analyzed using the scion image program.

The solubility of BECD in supercritical CO₂ was studied as a function of temperature and pressure by observing the cloud point. Methyl alcohol was found to be a good co-solvent to enhance the solubility of BECD in supercritical CO₂. It was found that the solubility study aided in the interpretation of the effect of the concentration, and the effect of pressure and temperature on the RESS process.

ACKNOWLEDGEMENTS

I would first like to thank my supervisor, Dr. Paul A. Charpentier, for advising and aiding my graduate studies. I would also like to thank Dr. Xinsheng Li for guiding my project. I thank Dr. Wankei Wan for giving me the advice about particle analysis. I thank Ross Davidson and Brad Kobe for helping me use the scanning electron microscope. I thank Dr. Amin S Rizkalla and Dr. Sohrab Rohani for giving me a lab space. I thank all of my group collages, Rouhong Sui, Yousef Bakhbakhi, Jeff Wood for their friendship and assistance.

At the end, I thank my parents for their support and encouragement. They are in China. They cannot give me so much help on my research, but they always encourage me.

TABLE OF CONTENTS

LIST OF TABLES.....	vii
LIST OF FIGURES.....	viii
NOMENCLATURES.....	xiii
1. INTRODUCTION.....	1
1.1 Supercritical Fluids.....	1
1.2 Properties of Carbon Dioxide.....	5
1.2.1 The Density of Carbon Dioxide.....	5
1.2.2 Physical Properties of Carbon Dioxide.....	8
1.3 Processes and Applications.....	11
2. LITERATURE SURVEY.....	15
2.1 Rapid Expansion of Supercritical Solution Process.....	15
2.2 Literature Review.....	17
3. EXPERIMENTAL APPARATUS AND PROCEDURES.....	31
3.1 Materials.....	31
3.2 Beclomethasone Dipropionate Solubility in Methyl Alcohol and Acetone	33
3.3 Solubility Measurements in Supercritical Solutions.....	36
3.4 RESS Process Experimental Setup.....	38
3.5 RESS System Nozzle Configuration.....	40
3.6 Characterization of Particle Morphology.....	42
3.6.1 Optical Microscopy.....	42

3.6.2	Scanning Electron Microscopy Operational Procedure.....	46
3.6.3	Particle Size Distribution Analysis.....	53
4.	RESULTS AND DISCUSSION.....	55
4.1	Density Calculation of Carbon Dioxide.....	55
4.2	Phenanthrene Solubility in Supercritical CO ₂	60
4.3	The Solubility of Beclomethasone Dipropionate	64
4.4	Phenanthrene Particle Formation in RESS Process.....	74
4.5	Beclomethasone Dipropionate (BECD) Particle Formation in Supercritical CO ₂	83
4.5.1	Different Nozzle Diameter Measurements	85
4.5.2	Different Concentration Measurements.....	90
4.5.3	Different Pressure Measurements.....	98
4.5.4	Different Temperature Measurements.....	107
4.5.5	Different Nozzle Length Measurements.....	111
4.5.6	Different Spray Distance Measurements.....	114
5.	CONCLUSIONS.....	119
6.	REFERENCES.....	122
7.	APPENDIX.....	130
	APPENDIX A. BECD Solubility Measurements.....	130
	APPENDIX B. RESS Operational Procedure.....	135
	APPENDIX C. CO ₂ Density Calculation.....	141

LIST OF TABLES

Table 1.1.1	The Critical Pressure and Temperature of some Organic and Inorganic fluids.....	2
Table 1.2.2.1	Comparison of properties of gases, SCFs, and liquids.....	8
Table 2.2.1	RESS process operation parameters.....	30
Table 4.1.1	Coefficients n_1 through n_{20} for the Bender equation of state.....	56
Table 4.1.2	The density of carbon dioxide from the Bender equation and NIST EOS at 40°C.....	59
Table 4.2.1	Solubility data for naphthalene and benzoic acid in supercritical CO ₂ at 45°C.....	61
Table 4.2.2	Solubility data for phanthrene in supercritical CO ₂ at 45°C.....	62
Table 4.4.1	RESS experiments of phenanthrene using supercritical CO ₂	75
Table 4.5.1.1	RESS experimental conditions for evaluating nozzle diameter.....	86
Table 4.5.2.1	RESS experimental conditions for different concentrations.....	92
Table 4.5.3.1	RESS experimental conditions for different expansion pressures.....	100
Table 4.5.4.1	RESS experimental conditions for different chamber temperatures.....	108
Table 4.5.5.1	L/D ratio of two capillary nozzles.....	111
Table 4.5.5.2	RESS experimental conditions for different nozzle lengths.....	112
Table 4.5.6.1	RESS experimental conditions at the variant spray distance.....	116

LIST OF FIGURES

Figure 1.1.1	Phase diagram of a SCF.....	1
Figure 1.2.1.1	Reduced pressure (P_r) -reduced density (ρ_r) diagrams at various reduced temperatures (T_r).....	5
Figure 1.2.1.2	Solubility parameter of CO ₂	7
Figure 1.2.2.2	Diffusivity of CO ₂ versus temperature at various pressures.....	10
Figure 2.1.1	Schematic diagram of RESS equipment system.....	16
Figure 2.2.1	Processes for the preparation of polymer latexes in water.....	27
Figure 3.1.1	Chemical structure of phenanthrene.....	32
Figure 3.1.2	Chemical structure of Beclomethasone Dipropionate.....	32
Figure 3.3.1.1	SFT phase monitor apparatus.....	36
Figure 3.4.2.1	Rapid expansions of supercritical solutions apparatus.....	38
Figure 3.5.1	Nozzle configuration.....	40
Figure 3.6.1.1	The three-lens optical microscope configuration.....	43
Figure 3.6.1.2	Optical microscope.....	43
Figure 3.6.2.1	A Schematic of SEM.....	47
Figure 3.6.2.2	Sputter coater machine.....	49
Figure 3.6.2.3	The picture of SEM machine.....	49
Figure 4.1.1	The densities of CO ₂ calculated by using the Bender equation.....	58
Figure 4.2.1	Solubility of naphthalene and benzoic acid in supercritical CO ₂ at 45°C.....	61
Figure 4.2.2	Solubility of phenanthrene in supercritical CO ₂ at 45°C.....	62

Figure 4.3.1	The solubility of BECD in pure solvents of methyl alcohol and acetone.....	66
Figure 4.3.2	Solubility of BECD in pure CO ₂ and in CO ₂ with 4 mol% methyl alcohol at T = 35°C.....	67
Figure 4.3.3	The solubility of BECD in pure CO ₂ and CO ₂ with 4 mol% methyl alcohol at T=55°C.....	67
Figure 4.3.4	Solubility of methyl alcohol in CO ₂ as a function of pressure and temperature.....	68
Figure 4.3.5	The effect of temperature and pressure on BECD in CO ₂ at the concentration of 5.91×10^{-5} , 8.44×10^{-5} , 10.97×10^{-5} , 13.51×10^{-5}	68
Figure 4.3.6	The pressure of BECD solutions as a function of weight fraction at various temperatures: 35 °C, 45 °C, 55 °C, and 65°C.....	70
Figure 4.3.7	The solubility of BECD in CO ₂ is a function of density at various temperatures: 35 °C, 45 °C, 55 °C, and 65°C.....	70
Figure 4.3.8	Isothermal properties for carbon dioxide.....	71
Figure 4.3.9	Isobaric properties for carbon dioxide at various pressures: 900psi, 1500psi, 3000psi, and 4000psi.....	71
Figure 4.4.1	Optical microscope photograph of phenanthrene deposited on the carbon tape before vacuuming.....	76
Figure 4.4.2	Optical microscope photograph of phenanthrene deposited on the carbon tape after vacuuming.....	76

Figure 4.4.3	Optical microscope photograph of phenanthrene before RESS process.....	77
Figure 4.4.4	Optical microscope photograph of phenanthrene after RESS process.....	77
Figure 4.4.5	Optical microscope photographs of phenanthrene produced by RESS process at 0.00042 and 0.00064.....	78
Figure 4.4.6	Optical microscope photographs of phenanthrene produced by RESS process at 2000psi and 3000psi.....	79
Figure 4.4.7	Optical microscope photographs of phenanthrene produced by RESS process at spray distance of 1cm and 5cm.....	82
Figure 4.5.1	SEM photographs of BECD before and after the RESS process.....	84
Figure 4.5.1.1	BECD particle size distributions evaluated at different nozzle diameters: 0.010inch, 0.030inch, and 0.040inch.....	86
Figure 4.5.1.2	SEM photographs of BECD produced by RESS using nozzle diameter of 254 micron.....	87
Figure 4.5.1.3	SEM photographs of BECD produced by RESS using nozzle diameter of 762 micron.....	88
Figure 4.5.1.4	SEM photographs of BECD produced by RESS using nozzle diameter of 1016 micron.....	89
Figure 4.5.2.1	BECD size distribution evaluated at different concentration: 3.95×10^{-5} , 6.26×10^{-5} , 7.81×10^{-5} , and 1.63×10^{-4}	92
Figure 4.5.2.2	SEM photographs of BECD produced by RESS at 3.95×10^{-5}	93

Figure 4.5.2.3 SEM photographs of BECD produced by RESS at 6.26×10^{-5}	94
Figure 4.5.2.4 SEM photographs of BECD produced by RESS at 9.81×10^{-5}	95
Figure 4.5.2.5 SEM photographs of BECD produced by RESS at 1.63×10^{-4}	96
Figure 4.5.2.6 Three different RESS process paths from the entrance of nozzle to the exit.....	97
Figure 4.5.3.1 BECD size distribution evaluated at different pressure: 2000psi, 2500psi, and 3000psi.....	100
Figure 4.5.3.2 SEM photographs of BECD produced by RESS at 1900 psi.....	101
Figure 4.5.3.3 SEM photographs of BECD produced by RESS at 2500 psi.....	102
Figure 4.5.3.4 SEM photographs of BECD produced by RESS at 3000 psi.....	103
Figure 4.5.3.5 SEM photographs of BECD produced by RESS at 4100 psi.....	104
Figure 4.5.3.6 The change of particle size and morphology at different pressures.....	105
Figure 4.5.3.7 The jet temperatures of CO ₂ at different pressures.....	106
Figure 4.5.4.1 BECD size distribution evaluated at different temperature: 35 °C, 40 °C, and 50°C.....	108
Figure 4.5.4.2 SEM photographs of BECD produced by RESS at 35°C.....	109
Figure 4.5.4.3 SEM photographs of BECD produced by RESS at 50°C.....	110
Figure 4.5.5.1 BECD size distribution evaluated at different nozzle length: 3cm and 4cm.....	112
Figure 4.5.5.2 SEM photographs of BECD produced by RESS at nozzle length of 4 cm.....	113
Figure 4.5.6.1 BECD size distribution evaluated at different spray distance: 1cm, 3cm, and 5cm.....	116

Figure 4.5.6.2 SEM photographs of BECD produced by RESS at spray distance of 3cm and 5cm.....	117
Figure 4.5.6.3 SEM photographs of BECD particle surface at spray distance of 3cm and 5cm.....	118
Figure A.1. SFT phase monitor apparatus.....	131
Figure B.1 Rapid expansions of supercritical solutions apparatus.....	136

NOMENCLATURE

ρ	Density (g/ml)
ρ_c	Critical density (g/ml)
ρ_{CO_2}	The density of carbon dioxide (g/ml)
$\rho_{methanol}$	The density of methyl alcohol (g/ml)
ρ_r	Reduced density ($\rho_r = \rho / \rho_c$)
a	The fitting parameter of equation 4.2.1
b	The fitting parameter of equation 4.2.1
c	Concentration
$M_{Acetone}$	The molecular weight of acetone (58.08 g/mol)
m_{BECD}	The mass of BECD particles (g)
M_{BECD}	The molecular weight of BECD (521.25 g/mol)
m_{CO_2}	The mass of carbon dioxide (g)
M_{CO_2}	The molecular weight of carbon dioxide (44.01 g/mol)
$m_{Solvent}$	The mass of solvent (g)
$m_{methanol}$	The mass of methyl alcohol (g)
$M_{Methanol}$	The molecular weight of methyl alcohol (32.04 g/mol)
$M_{Phenanthrene}$	The molecular weight of methyl alcohol (178.23 g/mol)
n1-n20	Coefficients of the Bender equation
P	Pressure (psi)
P _c	Critical temperature (psi)

P_{mix}	The pressure of mixture chamber (psi)
P_r	Reduced pressure ($P_r=P/P_c$)
R	Universal gas constant, ($8.314J/(mol.K)$)
T	Temperature ($^{\circ}C$)
T_c	Critical temperature ($^{\circ}C$)
T_{mix}	The temperature of mixture chamber ($^{\circ}C$)
T_r	Reduced temperature ($T_r=T/T_c$)
v_{CO_2}	The volume of carbon dioxide (ml)
v_{methanol}	The volume of methyl alcohol (ml)
$wt\%$	The weight percent of solute in solution (%)
y_{BECD}	The mole fraction of BECD in supercritical carbon dioxide
$y_{\text{benzoicacid}}$	The mole fraction of benzoic acid in supercritical carbon dioxide
y_{methanol}	The mole fraction of methyl alcohol
$y_{\text{naphthalene}}$	The mole fraction of naphthalene in supercritical carbon dioxide
$y_{\text{phenanthrene}}$	The mole fraction of phenanthrene in supercritical carbon dioxide
L/D	Nozzle length to diameter ratio

1. INTRODUCTION

1.1 Supercritical Fluids

A Supercritical fluid (SCF) can be defined either as a compressed gas or as an extended liquid. In other words, a SCF is a substance that displays both gas and liquid-like properties. Unlike a gas, SCFs have considerable solvent strength, and they exhibit considerably better transport properties than liquid solvents. Historically, SCFs have been the subject of research since the early 1800s when Hannay et al. discovered the critical point of a compound (Mchugh et al., 1994). They also observed the effects of pressure on the solubility of the potassium iodide / ethanol system. The progress of SCF technology was slow until the late 1970s and early 1980s when a number of processes were commercialized and research intensified.

Thermodynamically, the definition of a SCF is a fluid, which is at a temperature greater than its critical temperature, and at a pressure greater than its critical pressure (Arai et al., 2002). Figure 1.1.1 shows a typical phase diagram indicating the region where a SCF exists.

Table 1.1.1 shows the critical pressure and temperature of several organic and inorganic fluids. Each substance has its own critical temperature and critical pressure. In terms of practical use, only a few fluids can be used under supercritical conditions because some fluids are corrosive or toxic. Ethane and ethene are flammable, so they need special safety precautions to be used. Methanol has a high solvent strength, but methanol is not generally used alone as a SCF due to its high critical temperature. However, methanol is

commonly employed with other fluids, like carbon dioxide, as a modifier. Although ammonia has the potential for dissolving polar compounds, it can also dissolve pump seals, thereby making it difficult to pump. In addition to its high polarity, it is also dangerous due to its high reactivity. From Table 1.1.1, nitrous oxide (N_2O) is expected to be very similar to CO_2 according to its critical properties. N_2O has a small dipole moment whereas CO_2 does not have permanent dipole moment. Therefore, N_2O can be expected to dissolve more polar analytes. For example, N_2O is better than CO_2 at displacing solutes from adsorption sites on a matrix (Dean, 1993). However, only a few

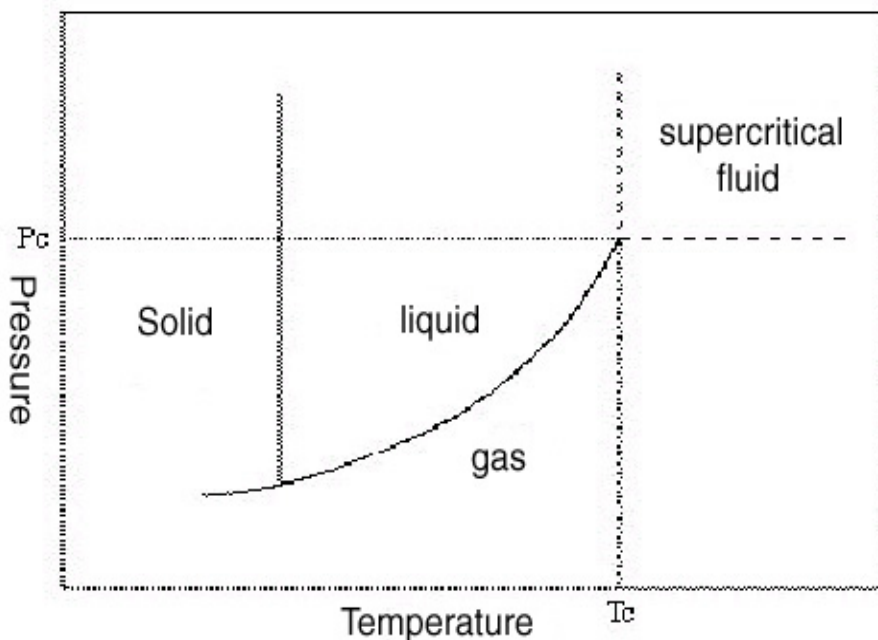


Figure 1.1.1 A typical phase diagram indicating the region where a SCF exists

publications and patents involving N_2O have been reported. Indeed, it is an important factor that N_2O supports combustion and tends to decompose spontaneously under certain

conditions (Taylor, 1996). Promising results have also been obtained using chlorodifluoromethane, which has a higher dipole moment than CO₂ and thus can be expected to solubilize more polar compounds in its supercritical state (Liu et al., 1990).

Table 1.1.1 The Critical Pressure and Temperature of Some Organic and Inorganic Fluids
(McHugh et al., 1986)

Fluid	Critical temperature (T _c) °C	Critical pressure (P _c)	
		Bar	Psi
Carbon dioxide	31.1	73.8	1070.4
Ethane	32.4	48.8	707.8
Methanol	240.1	80.9	1173.4
Ammonia	132.4	113.5	1646.2
Nitrous oxide	36.6	72.4	1050.1
Xenon	16.7	58.4	847.0
Water	374.4	221.2	3208.2
Chlorodifluoromethane	96.3	49.7	720.8
Benzene	289.0	48.9	709.2

However, CO₂ is the most widely used solvent in supercritical technology. The benefits of supercritical CO₂ are summarized as follows:

- 1) Low toxicity and reactivity

- 2) Relatively low critical temperature and pressure
- 3) Does not support combustion
- 4) High purity at low cost
- 5) Environmentally compatible (not a volatile organic compound)

The main problem with supercritical carbon dioxide is its relatively low solvent strength at typical pressures. Pure CO₂ limits solvating of non-polar analytes such as hydrocarbons, halogenated hydrocarbons, steroids, fats, organochlorine pesticides etc. Often, addition of modifiers is required (Mchugh et al., 1986).

1.2 Properties of Supercritical Carbon Dioxide

1.2.1 The Density of Carbon Dioxide

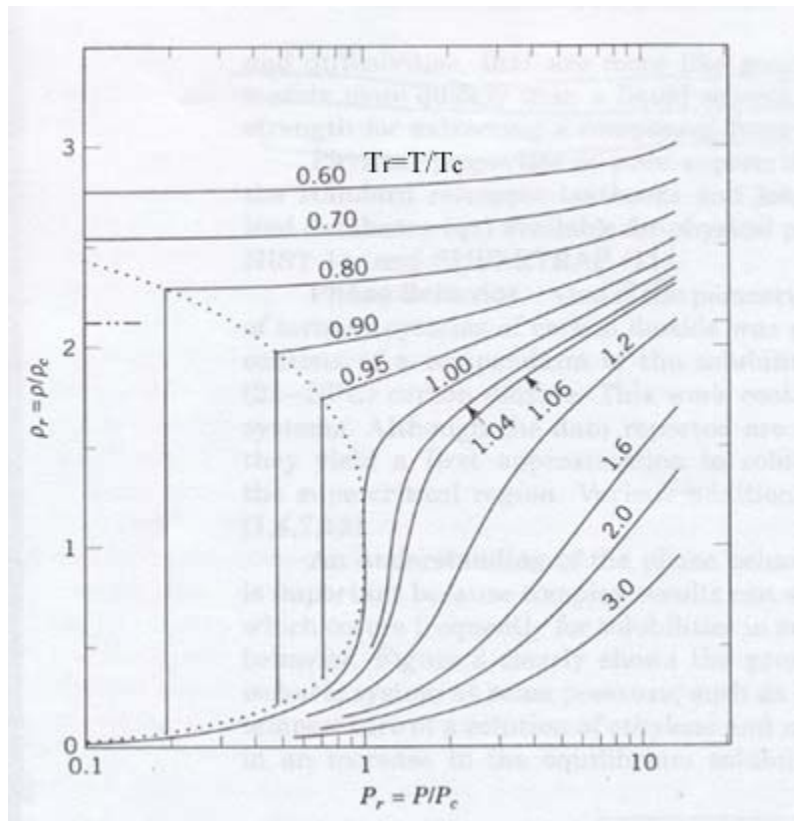


Figure 1.2.1.1 Reduced pressure (P_r) -reduced density (ρ_r) diagrams at various reduced temperatures (T_r) (Dixon et al., 1997)

The density of pure carbon dioxide is sensitive to pressure and temperature, especially near the critical point. It is important to know how the density changes with pressure and temperature for the various engineering applications of interest. Figure 1.2.1.1 shows a graph of pure carbon dioxide in terms of reduced pressure (P_r) -reduced density (ρ_r) at various reduced temperatures (T_r). We define the PT region in terms of reduced pressure

($P/P_c=P_r$), reduced temperature ($T/T_c=T_r$) and reduced density ($\rho/\rho_c=\rho_r$). The critical point is the reduced pressure P_r that equals the reduced temperature, $T_r=1$. At high values of T_r , the fluid density may be reduced to the point where solvent properties are no longer favorable. From Figure 1.2.1.1, it can be observed that a small increase in pressure at $T_r=1.0-1.2$ results in a dramatic increase in density. However, when T_r increases to 1.5, the same change in pressure hardly changes the fluid density. Such knowledge is important for controlling solubility.

It is recognized that the solvating strength of a given SCF is related directly to the fluid density (Dean, 1993). Generally, increasing the density of supercritical CO₂ results in higher solubilities of various compounds in carbon dioxide. In SCF fractionation, small incremental changes in the density of carbon dioxide are invoked with successive solvation (Dixon et al., 1997). In addition, the carbon dioxide density practically never exceeds the density of the comparable liquid, regardless of the pressure (Taylor, 1996).

Although the relationship between solubility and density is simple, the relationship between solubility and temperature and pressure is more complicated. When carbon dioxide is near the critical temperature, small changes in the pressure can create large changes in density. The variation of solvency of CO₂ with pressure is shown in Figure 1.2.1.2 (Johnston et al., 1988). The solubility parameter δ is the square root of the cohesive energy density. The δ for gaseous CO₂ is essentially zero. However, the value for liquid CO₂ is comparable with that of a hydrocarbon (Johnston et al., 1988). At –30°C, there is a large increase in δ upon condensation from gas to liquid. Above the

critical temperature, Figure 1.2.1.2 indicates that the solubility parameter can be tuned continuously over a wide range with a small pressure change.

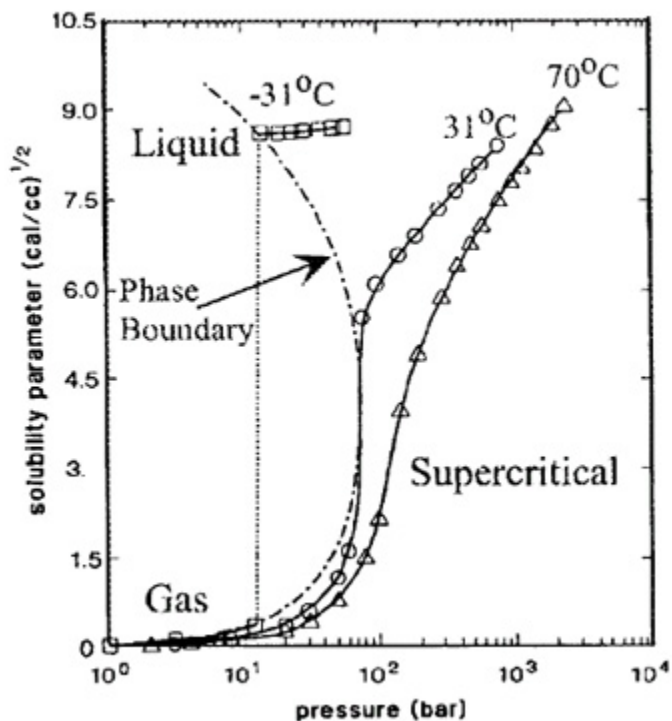


Figure 1.2.1.2 Solubility parameter of CO₂ (Johnston et al., 1988)

Near the critical pressure, carbon dioxide exhibits a decrease in solubility with an increase in temperature, because the density is reduced with increased temperature. However, at higher pressures, the solubility may increase with increasing temperature because the solute vapor pressure becomes significant. At constant SCF density, a temperature increase increases the solute solubility (Tom et al., 1991a).

Although the carbon dioxide density is an indicator of solvent strength, the polarizability along the bond joining the molecules of carbon and oxygen may be a separate function of carbon dioxide solvent strength. The use of polarizability or density alone is insufficient, but this concept has not been well recognized in the literature (Johnston et al., 1996). For a single solvent, however, density is still a good indicator of solvent strength as a function of temperature and pressure.

1.2.2 Physical Properties of Carbon Dioxide

Table 1.2.2.1 Comparison of Properties of Gases, SCFs, and Liquids
(Dixon et al., 1997)

	Gases	SCFs	Liquids
Density, g/cm ³	0.001	0.2-1.0	0.6-1.6
Diffusivity, cm ² /s	0.1	0.001	0.00001
Viscosity, g/(cm.s)	0.0001	0.001	0.01

Another particularly attractive and useful feature of SCFs is the physico-chemical properties of a SCF, which are intermediate between those of a liquid and a gas. Table 1.2.2.1 compares the properties of gases, SCFs and liquids. A SCF has a greater liquid-like density and subsequent greater solvating strength than a gas. Mass transfer, relative to a liquid, is rapid in a SCF. For pressures between 50 and 500 atm, the diffusivity of supercritical CO₂ varies between 10⁻⁴ and 10⁻³ cm²/sec. The values of binary diffusion

coefficients under the same conditions are similar. These values are as much as 100 times higher than those values typically observed in conventional liquids (Dixon et al., 1997).

From Figure 1.2.2.2, it can be observed that the values for diffusivity are dependent on temperature and pressure. When the pressure is increased, the diffusivity of the supercritical CO₂ approaches that of a liquid. With an increase in temperature, the diffusivity will increase.

The change of viscosity with pressure and temperature is opposite compared with diffusivity. A review of these important points is as follows (Taylor, 1996):

Fixed density: temperature ↑ diffusivity ↑ viscosity ↓
Fixed temperature: density ↑ diffusivity ↓ viscosity ↑

The gas-like diffusivity and viscosity, the liquid-like density, and the pressure-dependent solvating power of a SFC are attractive features for the potential applications of various SCF technologies.

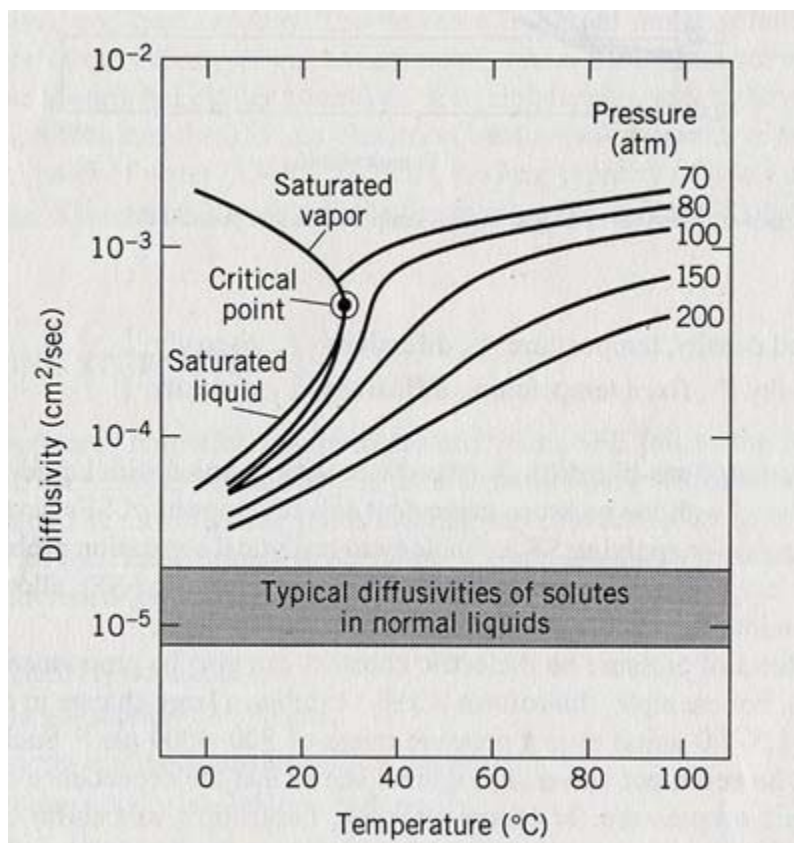


Figure 1.2.2.2 Diffusivity of CO₂ versus temperature at various pressures. (Taylor, 1996)

In summary, regardless of the polarizability, the solvating strength in the supercritical region is a direct function of density, which depends on temperature and pressure. There is no break in the continuity of solvent strength as the material goes from the near critical to the sub-critical region. Thus, it is possible to change the solvating strength of the SCF by varying the temperature and pressure. This is not possible in the liquid state because the liquid is incompressible compared with SCF. Hence, solvation is “tunable”. For some specific applications, adding small quantities of co-solvent to the supercritical CO₂ will increase its polarity.

1.3 Processes and Applications

A variety of SCF processes have been commercialized, or are in the process of being commercialized. In the SCF extraction process, SCFs are used as extraction solvents in commercial food, pharmaceutical, environmental and petroleum applications. Supercritical CO₂ is the most commonly used solvent in extraction processes, although supercritical propane is also used. In fractionation processes, Kerr-Mcgee developed the ROSE (residuum oil supercritical extraction) process for separating the heavy components of crude oil. About 14 companies have licensed this process worldwide (Sun, 2002). For chemical reactions, SCFs are attractive as alternative solvents. Solvent properties such as solvent strength, viscosity, diffusivity and the dielectric constant can be adjusted by varying pressure and temperature. Subsequently, these changes can be used to affect reaction conditions.

In particle formation, SCFs offer many opportunities to form particles with improved properties. From a processing aspect, producing particles by SCFs can be classified into three processes. The first method is based on precipitation from supercritical solutions and is termed the rapid expansion of supercritical solutions (RESS) process. The second process is gas (or SCF) anti-solvent (GAS/SAS) process. This process uses SCFs as an anti-solvent or non-solvent to precipitate particles. The last method is particle formation from gas-saturate solutions (PGSS) process. This process is based on solubilization of SCFs in the substrate, or dispersion of SCFs in the substrate (Tan et al., 2001).

Particle formation in SCFs is presently a major development for SCF applications, mainly in the pharmaceutical, nutrient, cosmetic and specialty chemical industries. For drug delivery, the drug must get to the right place at the right time. The particle size of pharmaceutical products is important because it can limit the bioavailability of poorly soluble active components. Atkinson studied the concentration of griseofulvin in blood as a function of particle size over given intervals of time after dosing (Atkinson et al., 1962). The quantity of griseofulvin absorbed for a particle size of 2.7 microns is 2 times that obtained with a particle size of 10 microns. For inhaling applications targeted to reach deep lung regions, the particle size and distribution of the drug should be from 1 to 5 microns (York et al., 1996). However, such small particle sizes cannot be obtained directly, and in the list of the United States pharmacopoeia, one third of drugs are water insoluble or poorly water-soluble (Pace et al., 2001).

The traditional methods for small particle formation can be classified into two categories: attrition and controlled precipitation (Sun, 2002; Tom et al., 1991). The physical properties of drugs, the crushing mechanism, and the relationship of grinding mechanism to the failure contact mechanism can influence the attrition process. Even though attrition is a simple method, some of the disadvantages it has are the inefficiency of energy expended, particle agglomeration, heat generation, the formation of irregularly shaped particles, and wide particle size distributions. Another traditional micronization technology is controlled precipitation. The particle size and distribution can be controlled, but organic solvents must be removed in a careful procedure. The removal process is not only tedious and time consuming, but also very difficult. Failing to control

particle size and distribution will delay or block the development of many new drugs and other biologically useful compounds. It may also prevent the much-needed reformulation of several currently marketed drugs.

Recent developments in SCF technology, especially the use of supercritical carbon dioxide, seem to offer an alternative technology that attempts to overcome several of the limitations of the traditional methods for small particle formulation. Potential applications of SCFs in the pharmaceutical industry include (Tan et al., 2001):

1. Generation of small size drug particles to enhance dissolution and therefore bioavailability of poorly water soluble or insoluble drugs.
2. Encapsulation of proteins, peptides and vaccines.
3. Targeted delivery of biologicals.
4. Parenteral formulation (e.g. injectable) applications.
5. Metered dose and dry powder for inhaler applications.

Compared with the conventional methods, using low critical temperature solvents can make the process work at mild temperatures, and lead to the formation of very fine and mono-disperse powders. Hence, supercritical technology can provide the possibility to obtain solvent-free products after a single processing step, as the supercritical solvents are dilute gases, which are vented to leave the desired product.

Numerous drugs have been micronized by the rapid expansion of supercritical solutions (RESS) processes, or gas anti-solvent (GAS) processes. It has been found that pharmaceuticals prepared by SCF processing are smaller, and the size distribution is narrower than those prepared by other means. The particle size and distribution are more appropriate for drug delivery requirements. Therefore, the RESS process provides significant justification to be developed as a particle formation technique for processing pharmaceuticals.

2. LITERATURE SURVEY

2.1 Rapid Expansion of Supercritical Solution Process

The rapid expansion of supercritical solution (RESS) process is used for drugs that are soluble in supercritical solutions. The solution of drugs is depressurized through a nozzle to a low-pressure chamber. Since the density of the solution is changed greatly on going through the nozzle into the lower pressure condition, the solvating capacity is also reduced rapidly. Supercritical solutions can lead to very high supersaturation ratios. This high enhancement factor can lead to massive nucleation, which produces very small particles. Decompression of the solution yields mechanical perturbations that can lead to uniform conditions within the solution, and subsequent particles with narrow size distribution (Tom et al., 1991b). After the rapid expansion, the fluid becomes a gas and is vented or recycled; whereas the particles are deposited in the expansion vessel.

Figure 2.1.1 depicts a simplified system of the RESS process using CO₂ as the SCF. The drug material is placed into the extraction vessel. The SCF is delivered from a cylinder and is pumped to the desired pressure and preheated to the extraction temperature through a heat exchanger. The SCF then flows through the high-pressure extraction vessel. The extraction unit could be a single autoclave or several autoclaves in series. In the precipitation unit, the supercritical solution is sprayed through a capillary or laser-drilled nozzle. During the spraying, the particles are precipitated due to the high degree of solute supersaturation.

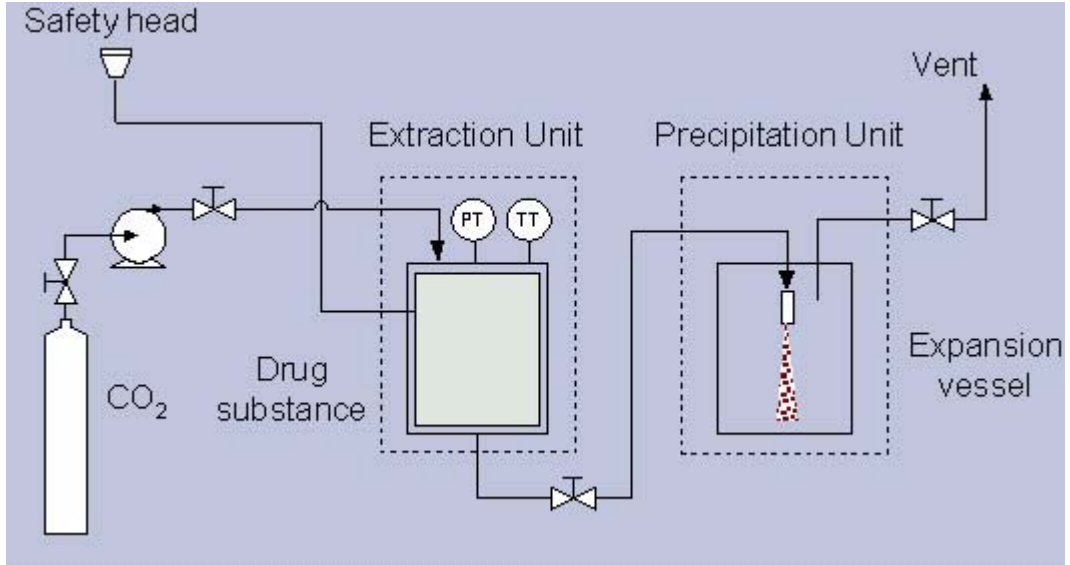


Figure 2.1.1 Schematic diagram of RESS equipment system

2.2 Literature Review

The first study of changes in particle size and morphology upon expansion of supercritical solutions was made by Hannay and Hogorth 120 years ago (Jung et al., 2001). The solid was crystalline when it precipitated by a sudden reduction in pressure. They describe this phenomenon as a solid that was brought down as a “snow” in the gas, or on a glass as a “frost”. For more than one century, this concept lay dormant until 1984 when Krukoniis said, “Maybe we can use this phenomenon as a way of tailoring the size and size distribution of difficult-to-comminute organic materials.”(Krukoniis, 1984)

Larson and King were one of the first groups to report the use of the RESS process in pharmaceutical applications (Larson et al., 1986). They studied the nucleation of several drugs. The RESS process, as used for pharmaceutical applications, requires the solubility of pharmaceutical compounds in the SCF. In 1993, Phillips and Stella reported the solubility of several pharmaceutical compounds in several SCFs (Phillips et al., 1993).

Only a few patents have been filed on the RESS apparatus or RESS-based applications. After the pioneering work of Krukoniis, the Battelle Institute Researching Work made the RESS concept easier to understand and develop by issuing two patents in 1986 and 1988. Smith et al. patented a process and apparatus for deposition of solid films or formation of fine powders on a surface according to the RESS process. They used two different types of nozzles. Several examples were chosen for demonstrating the two systems: deposition

of polystyrene films on platinum and fused silica, and deposition of silica on platinum and glass.

The Smith patents from the Battelle Institute only disclosed the physical processes such as solvent evaporation to form films. In 1990, Sievers and co-workers (US Patent No 4, 970, 093) described a chemical process for depositing a film of a desired material on a substrate. At least one reagent was dissolved in a SCF comprising at least one solvent. The supercritical solution was expanded through a nozzle to produce a vapor or aerosol, which was directed onto a heated surface. A chemical reaction was induced on that surface such that a film of the desired material was deposited. This method was called SCF transport chemical deposition (SFT-CD). Several mixed metal oxide films of Y, Ba, Cu, Pd, AC, Cr, Zn and Ag were produced by the system using various supercritical solvents, such as diethylether, pentane, acetone, N₂O and CO₂.

The Smith US Patent No 4, 582,731 and the Siever and co-workers US Patent No 4,970,093 disclosed the use of SCFs for powder and film formation, but did not include the use of powders for pharmaceutical applications. Sievers and co-workers in US Patent No 5,301,664 published in 1994, responded to the parent application. This patent describes using SCFs for delivery of pharmaceutical agents directly to the lung. The medicaments were dissolved by a SCF and were rapidly expanded into a physiologically active substance that was delivered to a patient. The SCF process provided particles of the desired size range (1 to 5 microns) for administration to the patients' lungs.

In 2000, there was another patent published by Sievers and co-workers. They used a mixture consisting of a SCF with an immiscible liquid, such as supercritical carbon dioxide mixed with a water solution, to process the desired substance to form aerosols or vapors. After the rapid expansion, the gas-borne dispersions of solids or liquids were formed with an average diameter between about 0.1 and about 6.5 microns. This process is different from the traditional RESS process, because the SCF is immiscible with the other liquid.

In 1999, Godinas et al. succeeded in using the RESS process to prepare a suspension of sub-micron particles of water-insoluble compounds, particularly drugs. In this process, two kinds of modifiers were used. The first modifier was used to dissolve the water-insoluble drug into a compressed gas. The second modifier was used to form an aqueous suspension in an aqueous solution that the compressed gas solution was expanded into. This process can stabilize the aqueous suspension of water-insoluble drugs and the produced particle sizes ranged from 50 to 200 nm. A fine suspension of fenofibrate was obtained with a mean particle size of about 200 nm by expanding a liquefied carbon dioxide solution containing fenofibrate (2g), liquid E-80 (0.2g), and Tween-80 (0.2g). Another example is that liquefied carbon dioxide solution containing 1g of cyclosporine and 0.2 g of Tween-80 is expanded into an aqueous dispersion of egg phospholipid and mannitol. As a result, a translucent aqueous suspension of about 23 nm particle size was obtained (Godinas et al., 1999).

In 2001, Baush et al. in US Patent 6,299,906 asserted that the process described in the Godinas patent might be difficult to realize on an industrial scale due to variations in temperature, and aggregation or flocculation of particles dissolved in the supercritical solution causing clogging of the tubes or spray-nozzles. The suspension on an industrial scale could be destabilized. In their patent, a biologically active compound was dissolved under elevated pressure in a compressed gas, liquid or SCF, containing a surface modifier. The dissolved compound could be precipitated by expanding the compressed solution into a chamber. They described a separate process where a biologically active compound was dissolved in compressed dimethylether, which might or might not require a surface modifier. The compressed solution was sprayed into an antisolvent phase, which might optionally contain a surface modifier, under vacuum, atmospheric pressure or elevated pressure. Expansion of orlistat (Tetrahydrolipstatin THL) and Saquinavir were studied in this patent. The THL was dissolved in supercritical CO₂ with a surface modifier and was expanded into water. The THL particles were formed with an average particle size of 1.5 microns. The Saquinavir was dissolved in supercritical dimethylether with a surface modifier and was expanded into water. The Saquinavir particles' diameters were found to be from 1 to 3 microns, depending on the condition.

The patents discussed above show several RESS techniques that people have found and created in the past 20 years. During this time, the RESS process has been applied to a wide range of materials, including inorganic, organic and polymeric materials, as well as pharmaceutical compounds. In some publications, micron and nano-particles have been directly prepared by the RESS process. For elaboration of inorganic materials, the spray

technique is widely used. However, there are relatively few examples of the production of inorganic powders by using the rapid expansion of supercritical CO₂ process due to the low solubility of inorganic compounds in supercritical CO₂. Therefore, supercritical water is frequently used for inorganics. In 1987, Matson et al. used a range of supercritical solvents to study the formation of powders, thin films and fibers by the RESS process. Manipulating process conditions such as temperature was found to change the morphology of silicon dioxide particles from a solid film to individual particles. GeO₂ is another inorganic material studied in this report. The main reason that supercritical water cannot be widely used is due to its high critical temperature and pressure. Supercritical water has a critical pressure of 221.2 bars, and critical temperature of 374.1°C (compared with CO₂ of 73.8bars and 31.1°C). Supercritical water is aggressive to many solutes, especially organic pharmaceutical compounds, which limits the use of this solvent.

The RESS process can also be used as a crystallization and size reduction technique for organic materials that are not pharmaceuticals. There have been several reports on the crystallization of benzoic acid, naphthalene and phenanthrene from supercritical CO₂ as these organic solids exhibit reasonably good solubility in supercritical CO₂.

Mohammed et al. (1989) studied the effect of pre and post expansion conditions on the morphology of naphthalene powders by the RESS process. One year later, P. G. Debenedetti explored the evolution of the nucleation rate along different expansion paths (Debenedetti et al., 1990). His study was based on phenanthrene in CO₂. Researching

the nucleation rate can help one to understand the optimal nozzle and expansion conditions for the RESS process. The solvent recompression cost could be reduced if the CO₂ is recycled in the system and the product size distribution could be greatly controlled. C. Y. Tai and C. Cheng published a report that focused on exploring the growth phenomena, mechanisms, and kinetics of naphthalene seed crystals in a supercritical CO₂ solution (Tai et al., 1995). The growth phenomenon of naphthalene was observed and the growth rate measured. The growth mechanism was inferred from the observed phenomena, and the corresponding growth rate equations were derived to interpret the measured growth rates.

Liu and Nahahama (1996, 1997) investigated the solubility of an anthracene and phenanthrene mixture in supercritical CO₂ and the precipitation behavior of pure anthracene, pure phenanthrene, and the mixture of anthracene and phenanthrene by the RESS process. This was the first study on the separation of a solute mixture by the RESS technique. According to the results, the composition and morphology of mixtures precipitated from supercritical CO₂ was highly influenced by conditions during the expansion process. The naphthalene composition of the precipitate was increased compared to the composition of the pre-expansion mixture solution with the increase of pre and post expansion temperature. The morphology of precipitation changed from flat sheets to needlelike crystals when the composition of phenanthrene was increased in the pre-expansion mixture solution.

Domingo and co-workers (1996) studied the formation of benzoic acid powders by the RESS process. However, compared to the report published earlier, a porous sintered metal plate was developed as an expansion nozzle instead of an orifice or a capillary tube. The particles were flat and mostly isometric in shape. The average size of the particles was smaller than 1 micron. However, a number of particles with 2 to 10 micron and larger were also observed. With a capillary nozzle, benzoic acid particles had an average size of 2 - 5 microns. Although this report showed findings that the benzoic acid crystal obtained using a porous plate nozzle was smaller in size than those obtained from a capillary nozzle, the particle size still depended on the process conditions. Domingo (1997) also used a frit nozzle instead of the traditional capillary nozzle and the porous plate nozzle that were used previously. Benzoic acid, salicylic acid, aspirin and phenanthrene were studied in this report. The experimental results showed that the particles obtained with the frit nozzle were smaller than those obtained using the capillary nozzle, except for phenanthrene.

Helfgen (2000) also studied benzoic acid particle formation by the RESS process using CO₂ as the solvent. They investigated the influence of various parameters like pre-expansion temperature and pressure and nozzle temperature on the RESS process. The benzoic acid particle size was found to lie within the range of 0.2 to 1.4 microns after rapid expansion. Compared to the results that Domingo (1996,1997) obtained, the particles formed using the capillary nozzle were not larger than those precipitated with the frit nozzle or the porous plate nozzle. Therefore, the construction of the nozzle is an important parameter that must be considered when studying particle formation. The

particle size, size distribution and morphology can also be influenced by other operating parameters.

One potential application of precipitation from supercritical solutions to polymer processing is the production of polymer microsphere matrices that can be used for controlled drug delivery. For example, a given drug is uniformly dispersed into the polymer carrier, and either diffuses through pores in a non-erodible matrix, or is released as the polymer disintegrates due to the action of body fluids. In 1991, Debenedetti et al. investigated the biocompatible and bioerodible polymers, polyhydroxy acid [poly (L-lactic acid)(L-PLA), poly- (D, L-Lactic acid) (DL-PLA), and poly- (glycolic acid) (PGA)], for controlled delivery of pharmaceuticals. These polymers were approved by the Food and Drug Administration (FDA) for vivo sutures and bone repair implants. After the RESS process, they found that the molecular weight of the precipitated polymers was lower than that of the pre-expansion polymer. Debenedetti surmised that RESS might be limited to low molecular weight polymers. In addition, the polyhydroxy acid produced irregularly shaped particles that were fairly uniform in size ranging from 10 to 12 microns.

From studies on polymeric materials, researchers found that polymers are particularly interesting solutes for use in the RESS process because they can form fibers or thin films. The relationship between operating conditions and precipitate morphology needs to be understood. In 1992, Lele and Shine studied the morphology of polymers from the RESS process. From this study, it was found that polycaprolactone, poly (methyl methacrylate)

and a styrene/methyl methacrylate block copolymer precipitated from supercritical chlorodifluoromethane. Increasing temperature, increasing polymer concentration, decreasing pressure, or decreasing L/D ratio of the capillary caused a change in morphology from fine diameter powders to high aspect ratio fibers. However, there were two limitations in this study. One limitation was that the phase behavior of the binary solution was not studied. The other limitation was that the concentration of polymers was always unknown. In 1994, Lele and Shine reported a new experimental procedure for RESS. They offered a theoretical and conceptual framework for predicting whether fibers or particles were produced by RESS. If precipitation of a polymer rich phase occurs later in the nozzle, the structure of formation time is greatly diminished, only 10^{-6} s, and particles are formed. On the other hand, if a polymer rich phase precipitates upstream of the nozzle, the time structure formation time is long, 10^1 s, and fibers are formed instead. This time scale conception explains the reason for forming different shapes by the RESS process, and accounts for the effect on polymer morphology by varying the pressure, temperature, and concentration.

The polymers that Lele and Shine used were insoluble in supercritical CO₂; hence they used supercritical chlorodifluoromethane as the solvent. In 1995, Mawson et al. studied the formation of poly (1,1,2,2, -tetrahydroperfluorodecyl acrylate) by the RESS process. Because of the high solubility of this polymer in CO₂, the highest solution concentration was well above that used in most of the previous RESS studies. The results from this polymer system support the mechanism of Lele and Shine.

Another potential application of the RESS process relating to polymers is coating. In the coating industry, the problem of the release of harmful volatile organic compounds (VOCs), such as hydrocarbon and oxygenated organic solvents, delay or block the development of new paints (Matsuyama et al., 2001). Carbon dioxide might be utilized as an environmentally benign solvent substitute to reduce these emissions and maintain the coating quality. A report published by K. Matsuyama et al. (2001), described how the RESS process can be used to produce nano-agglomerated micron sized powders for powder coatings and other applications. Because the solubility of most high molecular weight polymers in CO₂ is very low, a cosolvent, ethanol, was added to the RESS process. Several polymers were studied and the resulting coatings gave a smooth and coherent film.

At the same time, Shim and co-workers investigated rapid expansion of poly (2-ethylexyl acrylate) (2-EHA) suspensions in supercritical CO₂, containing a hydrophilic and a CO₂-philic surfactant to produce stable aqueous latexes (Shim et al., 2001). They used three possible methods to make polymer-latexes. In the first method, polymer suspensions obtained by polymerization of 2-EHA with a CO₂-philic surfactant and a hydrophilic surfactant were expanded rapidly through a capillary tube into water to make a stable emulsion. In the second method, the polymer, which can be made by conventional polymerization or by SCF polymerization, is directly transferred into water and the mixture was agitated. In the third method, the depressurized polymer suspension was re-pressurized and re-suspended in order to obtain a polymer suspension. The aqueous latexes can be formed by the RESS process after depressurization and re-suspension of

the polymer dispersion in CO₂. The polymer latex made by the direct transfer method is not stable. This study provides the possibility of using water instead of organic solvent as a solvent, and offers the possibility of new environmentally benign coatings and adhesives.

In review of the production of polymeric micro-spheres for controlled drug delivery, there are still a lot of publications describing the production of ultra fine and ultra pure drug particles in the pharmaceutical industry by the RESS process. Some organic materials, like phenanthrene, naphthalene, and benzoic acid, have good solubility in supercritical CO₂; but not all the organic materials have such good solubility. In order to make use of the RESS process to reduce the particle size and narrow the particle size distribution, the addition of some type of co-solvent during the RESS process may be necessary.

Larson and co-workers (1986) studied pharmaceutical formation with a co-solvent by the RESS process. The solubility of lovastatin in supercritical carbon dioxide was enhanced from 0.04 wt% to 0.45 wt% at 379 bars and 40 °C, when CO₂ was saturated with methanol. The precipitated particles contained both needles and irregularly shaped particles with a range of diameters from 10 to 50 microns. However, increasing the solubility by increasing the co-solvent concentration may result in larger particles having a larger particle size distribution. This is due to particle re-crystallization from the liquid co-solvent phase, which condenses following expansion. The use of other SCFs, instead of CO₂, is another method to enhance the solubility of compounds in SCFs. In 1995,

Reverchen et al. investigated the solubility and micronization of griseofulvin in supercritical CHF₃. Two different morphologies of griseofulvin were observed: quasispherical particles and needles. The pre-expansion chamber temperature was the key parameter to control griseofulvin morphology. Increasing temperature gave a change in morphology from quasi-spherical particles to needles.

Reverchen et al. (1993) studied salicylic acid solubility in supercritical CO₂, and its micronization by RESS. They found that pre-expansion temperature and expansion chamber temperature had a significant influence on the morphology of salicylic acid crystals. The pre-expansion temperature influenced particle dimensions, while the expansion chamber temperature mainly influenced the particle size distribution.

Besides temperature, the RESS experiments by Charcenchaitrakod et al. (2000) also involved the study of the effect of spray distance, the pre-expansion pressure and nozzle length on particle size. Ibuprofen was studied in this report. In the range of operating conditions studied, the pre-expansion pressure and nozzle length had no effect on the particle size or morphology, and increasing spraying distance slightly decreased the particle size and degree of aggregation.

Most materials particle size, as reported in the literature produced from the RESS process, range between 5 and 10 microns. However, from theoretical calculations, it should be possible to form particles down to 20-25 nanometers (Young et al., 2000). Due to particle growth during collisions in the free jet, it makes it difficult to approach the

theoretical limit. In 2000, Young produced stable suspensions of sub-micron particles of cyclosporine, a water insoluble drug, formed by rapid expansion from SCF to aqueous solution. According to the results, the particles were an order of magnitude smaller than those produced by RESS into air, without the surfactant solution. The cyclosporine concentration was as high as 38 mg/ml for the 100-400 nanometer particles produced.

There are still a multitude of pharmaceuticals that are being investigated by the RESS process. Loth and Hemisberg (1986) studied precipitation of phenacetin from supercritical CO₂, and Hemisberg et al. investigated the particle formation of cholesterol, dipalmitoylphosphatidylcholine (DPPC), and lazaroide in supercritical CO₂ with the RESS process. Two steroid drugs, progesterone and medroxyprogesterone, were studied by the RESS process (Alessi et al., 1996). Domingo et al. (1997) studied the precipitation of aspirin using the RESS process. Turk et al. (2002) studied micronization of griseofluvin and β -sitosterol by the RESS process.

In summary, most current research is aimed towards an improved understanding of the relationship between process parameters and particle characteristics, as well as exploring RESS for the application to nanoscale materials. Table 2.2.1 shows several operating parameters studied by various reports (Tom et al., 1991a; Tan et al., 2001; Phillips et al., 1993).

Table 2.2.1 RESS Process Operation Parameters (Tom et al., 1991a; Tan et al., 2001; Phillips et al., 1993)

RESS process operation variable	
SCF	Choice, flow rate, pressure, and temperature.
Sample	Sample condition, size, matrix, analyte type, e.g. polarity, molecular weight.
Extraction cell	Geometry, agitation, cell size, extraction temperature.
Nozzle	Geometry, diameter, length/diameter, temperature,
Precipitation unit	Geometry, unit size, pressure, temperature.

3. EXPERIMENTAL APPARATUS AND PROCEDURES

Section 3.1 discusses the properties of materials used by the rapid expansion in supercritical solutions (RESS) process. The solubility measurement technique is discussed in sections 3.2 and 3.3. A discussion of the RESS process and nozzle configuration is given in sections 3.4 and 3.5. Section 3.6 describes the apparatus and experimental procedure to characterize the particle size and particle size distribution.

3.1 Materials

There were two types of materials studied in this report: phenanthrene and beclomethasone dipropionate (BECD).

Phenanthrene is one of a group of chemicals called polycyclic aromatic hydrocarbons (PAHs). Naphthalene and anthracene also belong to this group. Figure 3.1.1 shows the chemical structure of phenanthrene. Phenanthrene is a colorless crystal-like solid, with molecular weight of 178.23 g/mol. Phenanthrene was purchased from Aldrich, and used as received. Like most PAHs, phenanthrene can be used to make dyes, plastics and pesticides, explosives and drugs. It has also been used to make bile acid, cholesterol and steroids.

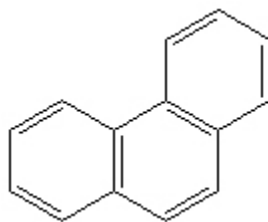


Figure 3.1.1 Chemical structure of Phenanthrene

Beclomethasone dipropionate (BECD) is a synthetic steroid of the glucocorticoid family. Figure 3.1.2 shows the structure of BECD. BECD is a white to creamy white, odorless powder with a molecular weight of 521.25 g/mol. It is slightly soluble in water, very soluble in acetone and in methyl alcohol. When it is used in an inhaler, the medication goes directly into the lungs, and very little finds its way into the rest of the body. Beclomethasone is used for the control of bronchial asthma in persons requiring continuous treatment. The BECD used in this work was donated by Glaxo Smithkline, and used as received.

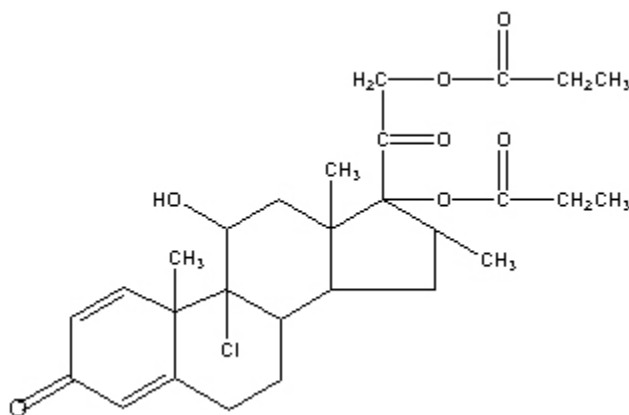


Figure 3.1.2 Chemical structure of Beclomethasone Dipropionate

3.2 Beclomethasone Dipropionate Solubility in Methyl Alcohol and Acetone

As a co-solvent was used to enhance the BECD solubility in supercritical CO₂ for this research, the solubility of the BECD material was first studied in the co-solvent. In this report, the BECD solubility in pure methyl alcohol and acetone was measured. The objectives of these measurements were to find a good solvent for BECD. The procedure is as follows.

First, a desired amount of BECD material was weighed using a Mettler-Toledo balance. A small sample container was placed onto the balance and the balance reading was set to zero. The desired amount of BECD was placed into the container, then removed from the balance. An empty sample bottle with a cap was placed onto the balance and the balance reading was zeroed. A desired amount of acetone was placed into the bottle and the acetone weight was read from the balance. BECD material was loaded into the sample bottle slowly until the solution was supersaturated with excess BECD being undissolved. The BECD container was then re-weighed. The weight difference before and after loading BECD into the acetone was the mass of BECD material inside the sample bottle. The sample bottle was placed into a slowly heated water bath (Cimarec 2) to dissolve the remainder of the BECD material. The mole fraction of BECD in the acetone was calculated using equation 3.2.1:

$$y_{BECD} = \frac{\frac{m_{BECD}}{M_{BECD}}}{\frac{m_{Acetone}}{M_{Acetone}} + \frac{m_{BECD}}{M_{BECD}}} \quad 3.2.1$$

The water bath was allowed to cool slowly using ambient cooling with the solubility temperature being recorded as the temperature at which the BECD material started to crystallize from solution. The water heating and cooling procedure were repeated with the average value reported. Based on the mole fraction of the previous measurement, a greater or lesser amount of BECD was placed into the sample bottle for the solubility measurement at the next temperature of interest.

BECD solubility in methanol was measured using the same procedure described above.

The mole fraction of BECD in solution was calculated using equation 3.2.2:

$$y_{BECD} = \frac{\frac{m_{BECD}}{M_{BECD}}}{\frac{m_{Methanol}}{M_{Methanol}} + \frac{m_{BECD}}{M_{BECD}}} \quad 3.2.2$$

It was determined experimentally that the BECD solubility in methanol was much lower compared to the solubility in acetone. Hence, the loading procedure must be slow in order to avoid loading too much BECD into the sample bottle. Otherwise, the BECD material would not be dissolved completely by methyl alcohol, even at relatively high temperatures.

Both acetone and methyl alcohol are relatively volatile solvents. The boiling points of acetone and methyl alcohol are 56.3°C and 64.8°C, respectively. Therefore, all the

measurements were run at low temperatures as after loading the BECD material, the sample bottle cap was closed in order to prevent the solvent from vaporizing.

3.3 Solubility Measurements in SCF

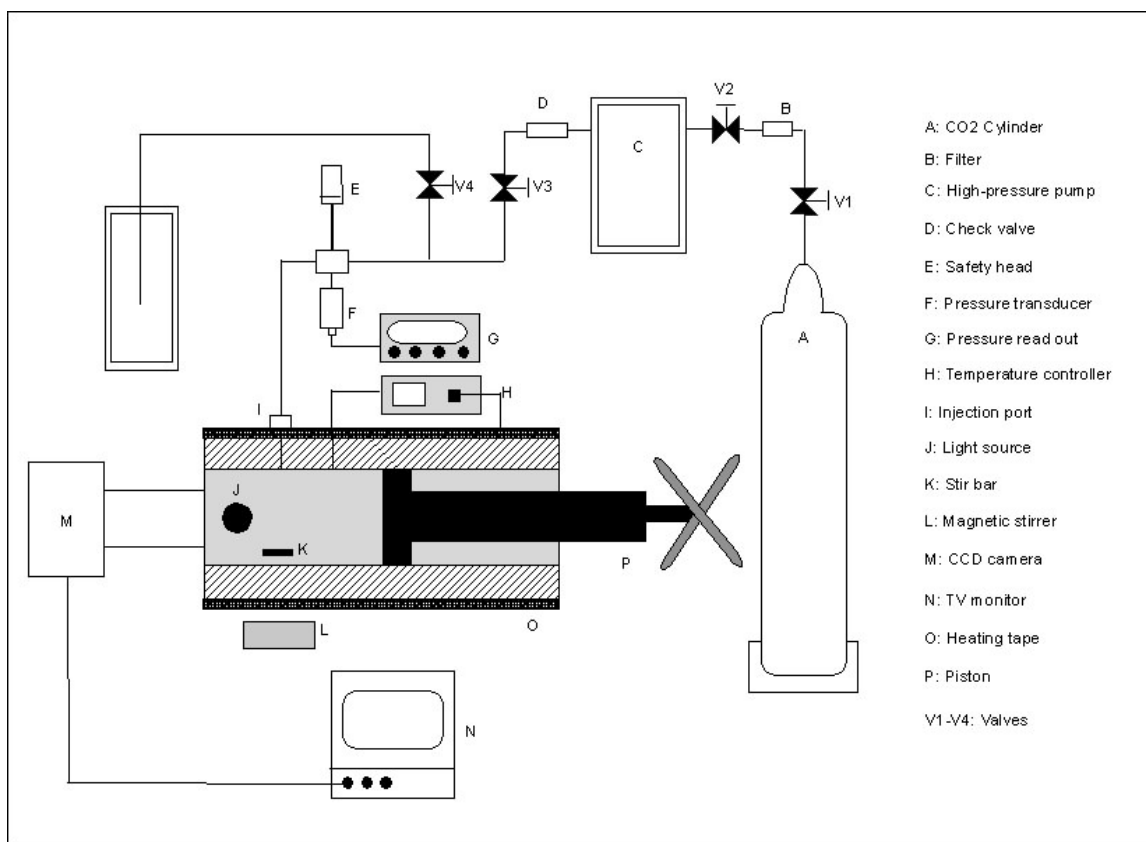


Figure 3.3.1 SFT phase monitor apparatus: A), CO₂ tank; B), filter; C), high-pressure pump; D), check valve; E), safety head; F), pressure transducer; G), pressure read out; H), temperature controller; I), injection port; J), light source; K), stir bar; L), magnetic stirrer; M), CCD camera; N), TV monitor; O), heating tape; P), piston; V1-V4), valves

In this report, a phase monitor (Supercritical Fluid Technologies, US) was used to determine the solubility of various materials in supercritical fluids. The phase monitor provides direct visual observation of materials under supercritical conditions, which can be controlled by the user. Figure 3.3.1 provides a schematic of the SFT phase monitor.

The system consists of a 30ml capacity variable volume syringe; a high-pressure vessel with quartz windows, a mixer, a variable light source, and a variable focus video camera. The pressure sensor is accurate to ± 2 psi and the pressure transducer was calibrated from 700-10,000psi. The temperature control system can heat up to 300°C, and the temperature sensor has an accuracy of $\pm 0.5^\circ\text{C}$.

A desired amount of BECD material and co-solvent was loaded into the SFT phase monitor vessel. The vessel was heated to the desired temperature by the SFT heating jacket, and pressurized to the desired pressure by a high-pressure syringe pump (Isco, 260D). The BECD/CO₂/cosolvent solution was formed as a homogeneous phase under these conditions. Then, the pressure was dropped gradually (25 psi/minute) by backing the piston off until the phase separation process began. The solute precipitated from solution, giving a cloudy appearance. The cloud-point pressure was typically measured three times at constant temperature and composition. The three measurements were reproducible within $\pm 5\%$ (i.e. ± 150 psi at 3000psi) at each temperature and composition. Experimental data were taken first at a lower temperature. The detailed operational procedure is provided in Appendix A.

3.4 RESS Process Experimental Setup

The rapid expansion of supercritical solution (RESS) experimental setup used for particle formation is shown schematically in Figure 3.4.2.1.

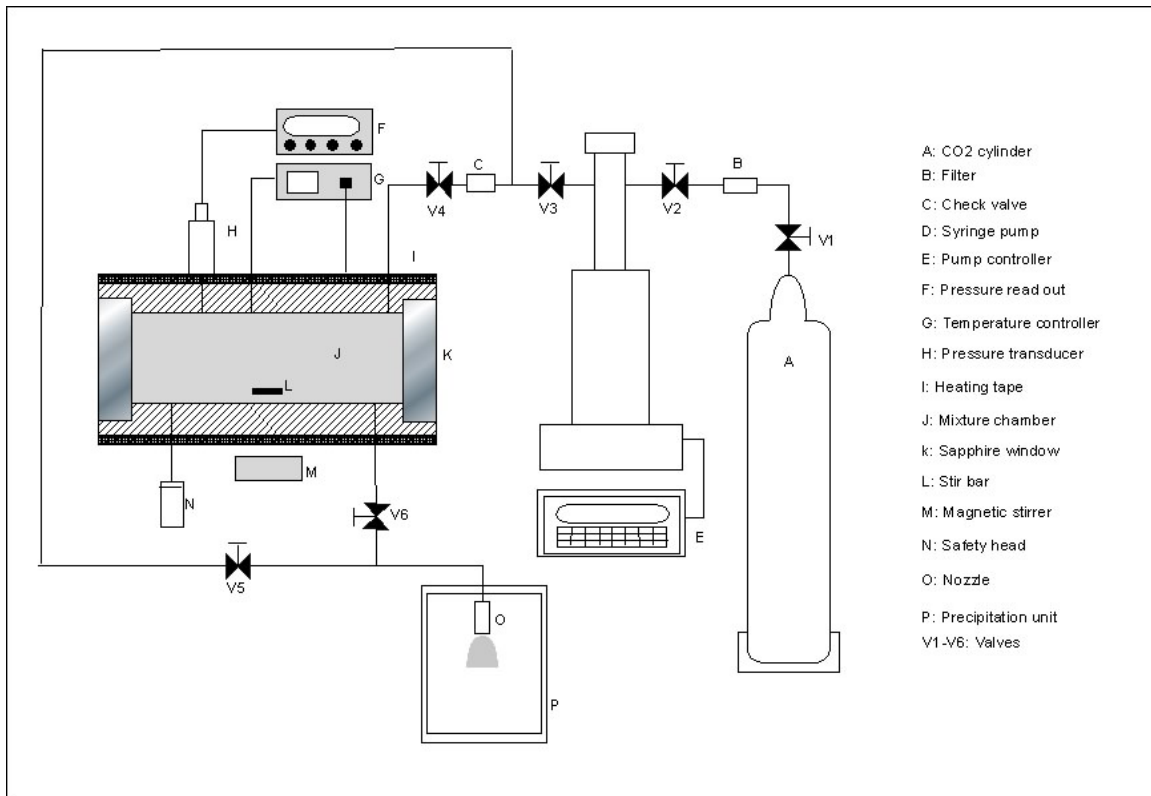


Figure 3.4.2.1 Rapid expansion of supercritical solutions apparatus: A), CO₂ tank; B), filter; C), check valve; D), syringe pump; E), pump controller; F), pressure readout; G), temperature controller; H), pressure transducer; I), heating tape; J), mixture chamber; K), sapphire window; L), stir bar; M), magnetic stirrer; N), safety head; O), nozzle; P), precipitation unit; V1-V6), valves

Liquid CO₂ (BOC Gases) was filled into the syringe pump and pumped to the desired pressure. The mixture chamber is a high-pressure 316 stainless steel view cell with sapphire windows (Insaco). The material and CO₂ were mixed in the mixture chamber at the desired temperature and pressure. The solution normally took 10-20 minutes to become transparent. The pressure was controlled by a syringe pump (ISCO 260 D) whereas the temperature was controlled by a temperature controller (FUJI, PXW-4). Temperature and pressure were maintained constant during the expansion. The syringe pump can pressurize CO₂ up to 7500psi and the flow range is from a few microliters/min to 100ml/min. The temperature was maintained within $\pm 0.5^{\circ}\text{C}$ by the temperature controller and the pressure controlled $\pm 30\text{psi}$ during the spray experiments. The particles were collected in a precipitation unit. In this thesis, a silicon wafer was placed in the precipitation vessel. The material was sprayed onto the silicon plate directly. After spraying, the silicon wafer was placed in a sample bottle to avoid contamination. The detailed procedures can be found in Appendix B.

3.5 RESS System Nozzle Configuration

Figure 3.5.1 presents the nozzle configuration used in this report. Two kinds of nozzles were tested. The majority of the results were obtained from a geometry that terminated with a 3cm long capillary tube. Other results were obtained using a nozzle terminating with a 4cm long capillary tube. Both of their outer diameters are 1587.5 microns (1/16") and inner diameter is 127micron (0.005"). The capillary tube was held in place by a pressure gland and sleeve. The components of the nozzle were purchased from High Pressure Equipment (HIP). Capillary tubes were purchased from Sigma-Aldrich, Supelco.

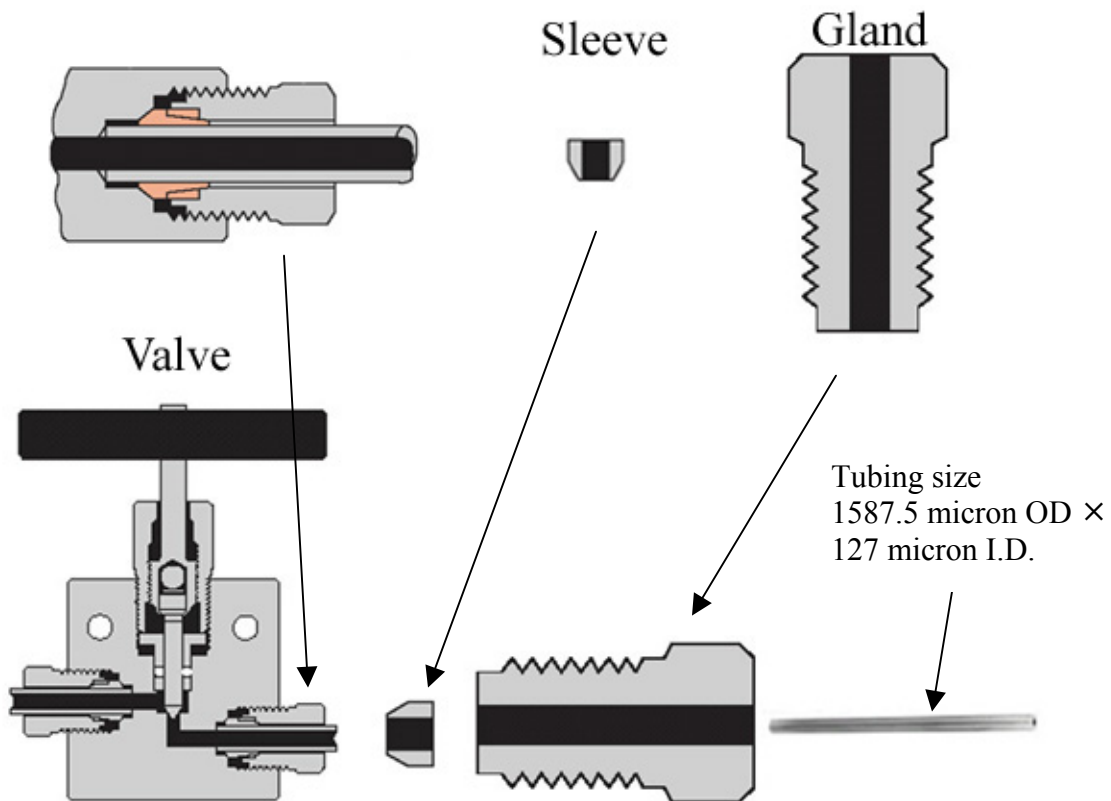


Figure 3.5.1 Nozzle Configuration

It was found that this nozzle type was easy to replace when it became plugged. When the nozzle became plugged, the nozzle was removed from the RESS system and put into an acetone bath as BECD has good solubility in acetone. After rinsing with solvent, high pressure CO₂ was used to flow through the capillary nozzle for further cleaning. The volume flow was measured and compared with the volume flow before the RESS process, in order to ensure complete plug removal. In this work, 3000-4000psi CO₂ was used to clean the nozzle. For the nozzle length of 3cm, the volume flow of CO₂ at 3000psi is 52±3ml/min and the volume flow of CO₂ at 4000psi is 63±3ml/min.

3.6 Characterization of Particle Morphology

Scanning Electron Microscopy (SEM) and optical microscopy were used to analyze the morphology of particles. The particle size distribution was subsequently determined by counting at least 100 particles from the SEM photographs and optical microscope photographs. The software used to measure particle sizes was Scion Image™.

3.6.1 Optical Microscopy

Optical microscopy enables the human eye to see smaller objects than are discernible with the naked human eye. The optical microscope uses glass lenses to focus light to produce a magnified image of an object. Figure 3.6.1.1 shows the three-lens optical microscope configuration. As optical microscope improved, smaller and smaller objects could be seen and more and more discoveries were made. Presently, a good optical microscope can distinguish objects as small as 200nm. In this thesis, a Mitutoyo FS70 microscope was used to observe the particle morphology (Figure 3.6.1.2).

In order to control contrast and visibility under the microscope, the interactions between light and matter should be understood. The principal interactions of light with matter are reflection, refraction, absorption, polarization, fluorescence and diffraction (Bradbury, 1984). In this thesis, the particles were sprayed onto a silicon wafer. Therefore, the main interactions of light with matter are reflection and diffraction.

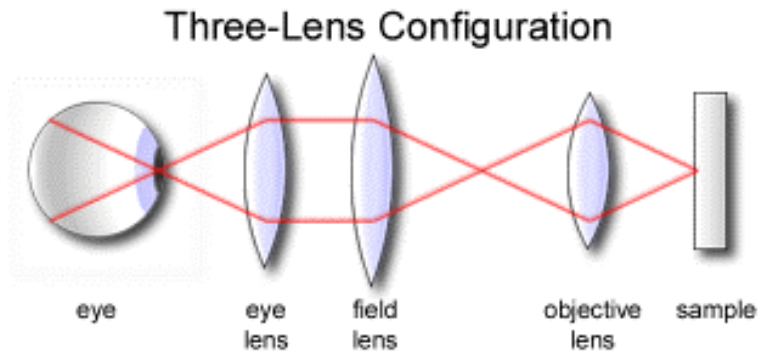


Figure 3.6.1.1 The three-lens optical microscope configuration



Figure 3.6.1.2 Optical microscope

For observing samples with the optical microscope, the silicon wafer was first placed on the stage and held using the clips. The internal lamp was turned on and a movable internal mirror inside the stand was used to direct the light to an incident illuminator mounted above the objective. In some cases, the internal lamp could not supply enough light. In those cases an external lamp was used to supply extra light. Before getting an image on the computer, the silicon plate was focused starting with minimum magnification, then gradually increasing. The distance between the silicon wafer and the objective mounted on the revolver was set to approximately 95mm. As the magnification of the objective was increased gradually, the fine adjustment knob was turned to focus the silicon wafer.

After getting a sharply focused image, a image of the work piece could be obtained on the computer by using a camera (Leica DC). The phototube on the optical microscope has a lens system to compensate for extra tube length and to ensure that the image will be focused on the photographic lens. By using “Vision Gauge” software (“live video” function), the image can be focused on a screen. After setting the image properties, the image was acquired by pushing the acquire button on the software. When the process was finished, the image acquisition window would close. At the end, the picture was saved in the vision gauge window.

3.6.2 Scanning Electron Microscopy:

Traditional light microscopes are limited by the physics of light to 500x or 1000x magnification, and a resolution of 200 nanometers. It is impossible to use light microscopes to observe samples requiring 10000x plus magnification like the structure of organic cells (Goldstein et al., 1992). Electron microscopes use a beam of highly energetic electrons to examine objects. Topography of an object, morphology of particles, composition of elements and compounds, and crystallographic information in the objects can be observed by electron microscopes. Scanning electron microscopy (SEM) is one of the types of electron microscopes. In this thesis, a Hitachi S-4500 Field Emission SEM was used to observe BECD particle size and morphology.

Figure 3.6.2.1 shows a schematic of the SEM. The electron gun generates a stream of monochromatic electrons. The condenser lens 1 and 2 condense the stream of electrons. The condenser aperture eliminates the high-angle electrons from the beam. A set of scan coils moves the focused beam back and forth across the specimen, row by row. The final lens, the objective lens, is used for focusing the scanning beam onto the desired section of the sample. When the beam strikes the sample, secondary electrons are generated because of interactions between the beam and the sample. A detector counts these electrons and sends the signals to an amplifier. The final image is built up from the number of electrons emitted from each spot on the sample. The process is repeated until the grid scan is finished and repeated (Goldstein et al., 1992).

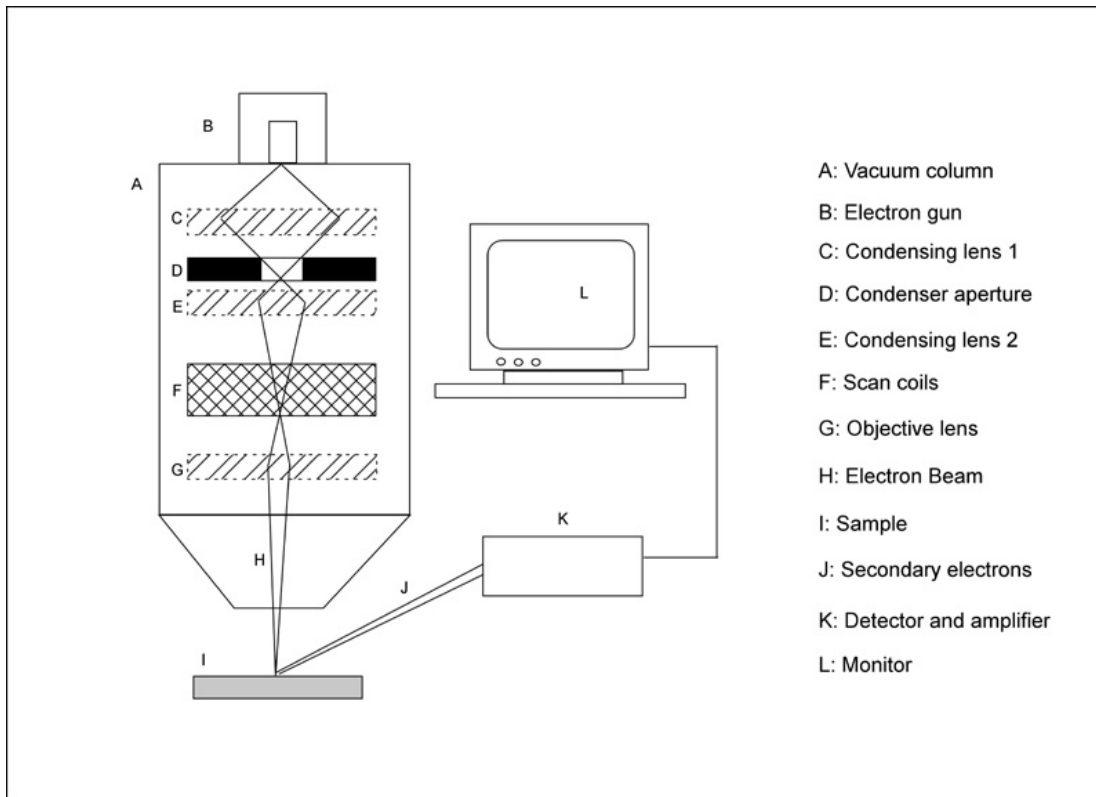


Figure 3.6.2.1 A Schematic of a SEM: A, vacuum column; B, electron gun; C, condensing lens1; D, condenser aperture; E, condensing lens2; F, scan coils; G, objective lens; H, electron beam; I, sample; J, secondary electrons; K, detector and amplifier; L, monitor (Goldstein et al., 1992)

Since SEM uses electrons to produce an image, most conventional SEMs require that the samples are electrically conductive. For example, metallic samples are conductive whereas organic materials are largely non-conductive. Although specially designed environmental SEMs are available to observe non-conductive samples or even wet samples directly, the SEM used in this thesis can only observe conductive samples.

As the analyzed materials used in this research were not conductive, a sputter coater was used to coat the sample with gold atoms in order to make samples electrically conductive. Figure 3.6.2.2 shows the picture of the sputter coater used in this work. First, a sample was placed in the specimen chamber. When the machine was turned on, the chamber vacuum would start automatically. At the same time, the leak valve was closed down finger tight. The coating time was set to 1-2 minutes when the pump evacuated the chamber down to below 100 milli-torr, as indicated by the vacuum gauge. The leak valve was opened slowly to get a reading of 10 milliamperes. Argon gas was introduced into the chamber and an electric field was used to ionize the argon atoms to make them positive. The argon ions were then attracted to a negatively charged piece of gold foil. Gold atoms from the surface of the foil settled onto the surface of the sample, producing a gold coating. For this sputter coater, a 14-nanometer layer gold coating was placed on the sample surface every minute. Coating time depends on the property of samples. If samples are sensitive to the electron beam, a longer coating time is needed. When the coating timer was finished, the pump was turned off and leak valve was opened. The sample was then removed from the specimen chamber.

After the coating process, the sample was loaded into the SEM. Figure 3.6.2.3 shows the picture of SEM machine used in this work. The detailed operational procedure used for running the SEM instrument is given in Appendix C.



Figure 3.6.2.2 sputter coater machine



Figure 3.6.2.3 Picture of Hitachi S-4500 Field Emission SEM

3.6.3 Particle Size Distribution Analysis

Scion Image™ software, which is an image processing and analysis program that can be used to measure area, mean, centroid, perimeter, etc. for user defined regions of interest, was used for this research. This program reads and writes TIFF and BMP image files and can acquire, display, edit, enhance, analyze and animate images.

Scion Image™ can analyze particles automatically by counting and measuring objects in binary images. The program scans across the image until it finds the boundary of an object, outlines the object using an algorithm, measures the object using the equivalent of the measure command, and then redraws the object in a different gray level so that it becomes invisible to the scanning process. However, as the SEM photographs taken were not binary images, they had to be converted into binary images. It was found that the particle analysis tools of the software could not recognize the outlines of all the particles, such that most of the particles were miscounted. Hence, the automatic particle analysis function was not found useful for this work.

For the SEM photographs analyzed in this report, particle size was measured manually.

The operational procedure was:

1. Use the line selection tool to make a straight line that corresponds to the magnification bar of SEM photographs on the photographs.
2. Bring up the set scale dialog box.

3. Select micron unit as the unit of measurement.
4. Enter the known distance from photographs.
5. Measure at least 100 particles with the Scion Image™ program.

As not all particles have high sphericity, the maximum length of the particles were used as the primary particle size of interest in this thesis. Likewise, the minimum diameter, Feret's diameter, or other quantity, can also be used. Aspect ratios, or length/diameter ratio of the particles, were also measured.

4. RESULTS AND DISCUSSION

4.1 The Density Calculation of Carbon Dioxide

As the density of carbon dioxide was used to calculate the mass of carbon dioxide in the vessel, and was also used to predict the supercritical solvating strength, it was crucial to know its value. The relationship between density and pressure and temperature is complex. There are several equations of state (EOS) available to evaluate carbon dioxide thermodynamic and volumetric properties. The Bender EOS (Bender, 1970), as provided in equation 4.1.1, was cited by several references (Reverchon et al., 1995; Gamse et al., 2000) and is particularly suitable to predict carbon dioxide properties. Hence, in this report, the density of carbon dioxide, depending on pressure and temperature, was calculated with the equation of Bender,

$$P = \frac{RT\rho}{M_{CO_2}} + B\rho^2 + C\rho^3 + D\rho^4 + E\rho^5 + F\rho^6 + (G + H\rho^2)\rho^3 \exp(-n_{20}\rho^2) \quad 4.1.1$$

with

$$B = n_1T + n_2 + \frac{n_3}{T} + \frac{n_4}{T^2} + \frac{n_5}{T^3} \quad 4.1.2$$

$$C = n_6T + n_7 + \frac{n_8}{T} \quad 4.1.3$$

$$D = n_9T + n_{10} \quad 4.1.4$$

$$E = n_{11}T + n_{12} \quad 4.1.5$$

$$F = n_{13} \quad 4.1.6$$

$$G = \frac{n_{14}}{T^2} + \frac{n_{15}}{T^3} + \frac{n_{16}}{T^4} \quad 4.1.7$$

$$H = \frac{n_{17}}{T^2} + \frac{n_{18}}{T^3} + \frac{n_{19}}{T^4} \quad 4.1.8$$

Table 4.1.1 Coefficients n_1 through n_{20} for the Bender Equation of State (Bender, 1970)

$n_1 = 0.22488558$	$n_{11} = 0.12115268$
$n_2 = -0.13717965 \times 10^3$	$n_{12} = 0.10783386 \times 10^3$
$n_3 = -0.14430214 \times 10^5$	$n_{13} = 0.43962336 \times 10^2$
$n_4 = -0.29630491 \times 10^7$	$n_{14} = -0.36505545 \times 10^8$
$n_5 = -0.20606039 \times 10^9$	$n_{15} = 0.19490511 \times 10^{11}$
$n_6 = 0.45554393 \times 10^{-1}$	$n_{16} = -0.29186718 \times 10^{13}$
$n_7 = 0.77042840 \times 10^2$	$n_{17} = 0.24358627 \times 10^8$
$n_8 = 0.40602371 \times 10^5$	$n_{18} = -0.37546530 \times 10^{11}$
$n_9 = 0.40029509$	$n_{19} = 0.11898141 \times 10^{14}$
$n_{10} = -0.39436077 \times 10^3$	$n_{20} = 0.50000000 \times 10^1$

The coefficients n_1 through n_{20} are given in Table 4.1.1. B, C, D, E, F, G, and H are defined by means of polynomial expressions, which are temperature dependent and are correlated with those 20 coefficients n_1 through n_{20} . R is the universal gas constant. For carbon dioxide, R is divided by the carbon dioxide molecular weight.

$$M_{CO_2} = 44 \text{ g/mol}$$

$$R = 8.314 \text{ J/(mol.K)}$$

The Bender EOS was solved using Matlab™. Carbon dioxide densities were calculated in the temperature range from 293K to 393K, and in the pressure range from 0 bar to 1200 bar. These values are reported in Figure 4.1.1. The Matlab™ program for the Bender EOS is provided in appendix D.

The critical temperature, critical pressure, and critical density of carbon dioxide are 304.13K (30.98°C), 73.773bar (1069.98psi) and 0.4676g/ml. From this isothermal figure, there is a large slope $(\partial P/\partial \rho)_T$ around the critical point region. Therefore, small changes in pressure give significant differences in density. We also can see that increasing temperature at a constant pressure results in a decrease in the carbon dioxide density. Therefore, the solvating strength of supercritical carbon dioxide can be changed or “tuned” by adjusting pressure and temperature.

Another source for the density of carbon dioxide is from National Institute of Standards and Technology (NIST) website. This EOS is based on Span and Wagner’s work in 1996

(Span et al., 1996). Table 4.1.2 compares the density of carbon dioxide calculated from the Bender EOS and that from the NIST EOS, at 40°C. It is clear from this table that the density of carbon dioxide calculated by the Bender EOS is very similar to the Span-Wagner EOS used by NIST.

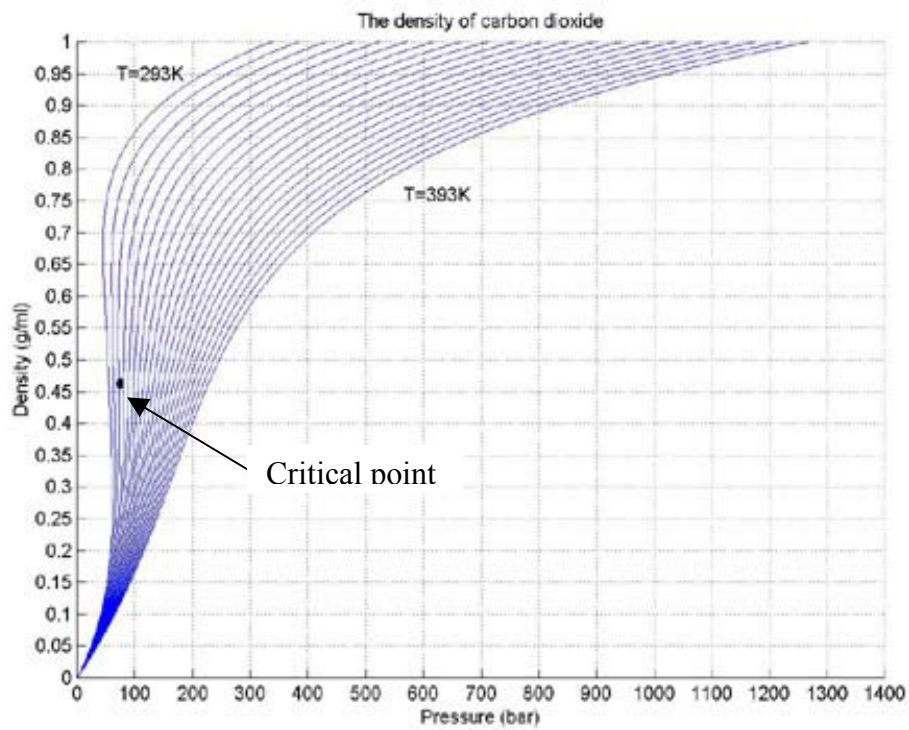


Figure 4.1.1 The densities of CO₂ calculated by using the Bender EOS.

Table 4.1.2 The Density of Carbon Dioxide from the Bender Equation and NIST EOS at
40°C.

Pressure (psi)	The density of carbon dioxide (g/ml)	
	Bender equation	NIST
2000	0.75897	0.75932
2100	0.77155	0.77173
2200	0.78287	0.78285
2300	0.79306	0.79293
2400	0.80238	0.80218
2500	0.81103	0.81073
2600	0.81905	0.81869
2700	0.82654	0.82614
2800	0.83356	0.83314
2900	0.84028	0.83976
3000	0.84661	0.84604

4.2 Phenanthrene Solubility in Supercritical CO₂

As discussed in the introduction, many organic materials have a relatively high solubility in supercritical CO₂, and have been processed by the RESS method. However, on account of the solute solubility requirement, not all materials can be used for the RESS process. Phenanthrene, naphthalene and benzoic acid were studied by the RESS process by several authors, as these materials have good solubility in pure supercritical CO₂ (Sauceau et al., 2000; Lee et al., 2001). Compared with phenanthrene and benzoic acid solubility in supercritical CO₂, the solubility of naphthalene in supercritical CO₂ is higher due to its low molecular mass and low polarity. At 45 °C and 2200 psi, 1-gram of carbon dioxide can dissolve approximately 0.06-gram of naphthalene (Sauceau et al., 2000).

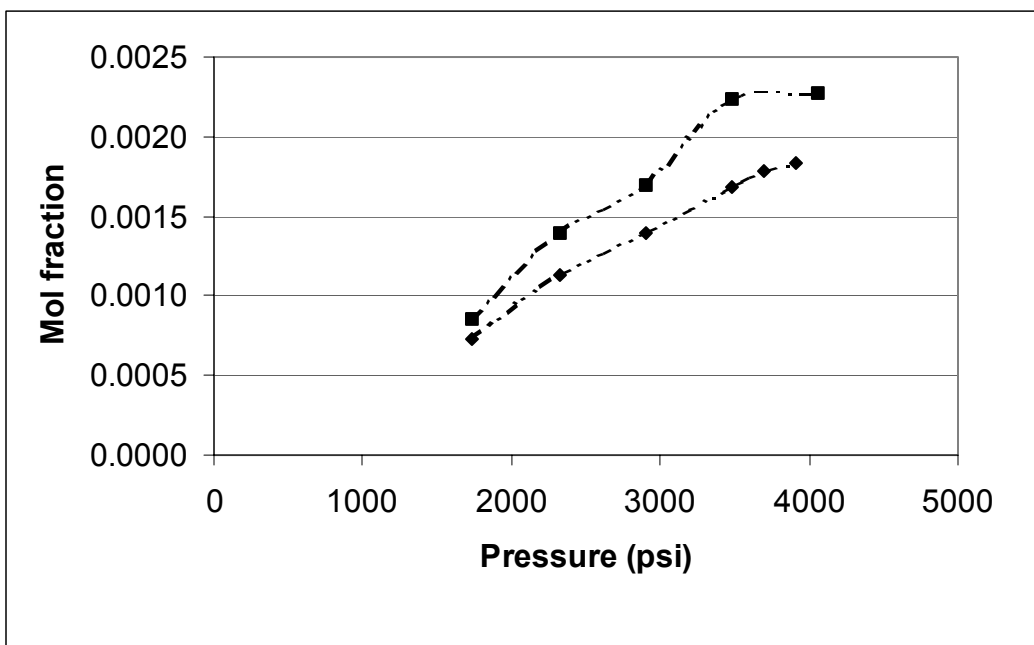


Figure 4.2.1 Solubility of phenanthrene in supercritical CO₂ at 45°C

Kurnlk et al., 1981 (■); Lee et al., 2001 (◆)

As of 2003, there have been literally thousands of reports of material solubility in supercritical CO₂. There are eighty-three reports for phenanthrene solubility in supercritical CO₂. From Kurnlk in 1981 to Goodorznia in 2002, various researchers have used various methods and models to measure and calculate phenanthrene solubility in supercritical CO₂. The results are different for each report due to the use of different measurement methods and apparatus. The results of phenanthrene solubility in supercritical CO₂ at 45°C from two references are plotted in Figure 4.2.1 (Kurnlk et al., 1981; Lee et al., 2001).

Due to the abundance of literature data on solubility of phenanthrene in CO₂, only one phenanthrene solubility experiment was run using the SFT phase monitor. The mole fraction of phenanthrene in this experiment is 1.16×10^{-3} . The cloud point pressure was measured to be 1980 psi at 45°C. According to the result of Kurnlk and co-workers in 1981, the cloud point pressure is around 2000 psi at the temperature of 45°C. According to the results of Lee and co-workers in 2001, the cloud point pressure is around 2350 psi at a temperature of 45°C. This close agreement with literature values provides confidence in our experimental technique for the following BECD results.

4.3 The Solubility of Beclomethasone Dipropionate (BECD)

In order to establish the best technique for the micronization of BECD using supercritical fluids, the solubility of BECD needs to be determined. The effect of different physicochemical parameters can be best understood on the RESS process if solubility in the supercritical fluid is known as a function of temperature and pressure. In addition, the solubility measurement is important to understand the effect of concentration on the RESS process.

According to literature results, the solubility of beclomethasone dipropionate (BECD) in pure carbon dioxide is low (Dean, 1995). Carbon dioxide has limited ability to dissolve polar molecules, even at relatively high densities (Taylor, 1996). In addition to the polarity of BECD, the high molecular mass of BECD is another factor to inhibit solubility in CO₂ (Sahle-Demessie et al., 2003). To study the solubility of BECD in supercritical CO₂, 10 mg BECD was placed in a 24.33 ml view cell. Pure carbon dioxide was filled into the vessel and pressurized to 3000 psi at a constant temperature, 45°C. Under even this very low weight percent, not all of the BECD was soluble in supercritical carbon dioxide. At this temperature and pressure, the density of CO₂ is 0.81997g/ml. According to the following equation, the mole fraction of BECD in CO₂ is 4.23×10^{-5} :

$$y_{BECD} = \frac{\frac{m_{BECD}}{M_{BECD}}}{\frac{\rho_{CO_2} V_{CO_2}}{M_{CO_2}} + \frac{m_{BECD}}{M_{BECD}}} \quad (4.3.1)$$

Hence, it was determined that the solubility of BECD in pure CO₂ is too low to be used in the RESS process system.

As discussed in the introduction, solubility of analytes in supercritical CO₂ can be enhanced by adding a polar, second compound. The second component is referred to as a modifier, co-solvent, or entrainer. These substances are liquids under ambient conditions. It should be noted that not all polar liquids are miscible with supercritical fluids. For example, water is only slightly soluble in CO₂; acetone and methyl alcohol can be miscible with supercritical CO₂ below a specific mole fraction. Figure 4.3.1 shows the solubility of BECD in pure acetone and pure methyl alcohol. Two experiments were performed to compare solubility of BECD in the co-solvent/CO₂ mixture. At the same conditions (40°C, 3500psi), the same number of moles (0.025mol) of acetone and methyl alcohol were separately added into the high-pressure view cell and mixed with supercritical solution containing 0.0204g BECD. It was visually observed that not all the BECD material was soluble in the solutions containing acetone. The solution containing methyl alcohol was clear. Although the solubility of BECD in pure acetone was higher than in pure methyl alcohol, methyl alcohol was found to be a better co-solvent compared with acetone to enhance BECD solubility in supercritical CO₂.

For a constant temperature and pressure, the co-solvent effect depends predominantly on the concentration of co-solvent (Wang et al., 1986; Sahle-Demessie et al., 2003). In each experiment, the mole fraction of acetone and methyl alcohol in the supercritical carbon dioxide was the same. The co-solvent effect also depends on its polarity. According to

the solubility of BECD in pure acetone and methyl alcohol, acetone's dissolving power for BECD was higher than methyl alcohol. In addition to these two factors, the solubility enhancement factor also depends on specific solute and co-solvent interactions such as hydrogen bond formation. Acetone is a H-bond acceptor because it contains a C=O group. However, methyl alcohol is a strong H-bond donor as a result of its -OH group (Foster et al., 1993). From its structure, BECD can be assumed to be a H-bond acceptor in the respect that it contains three C=O groups. So methyl alcohol is a suitable co-solvent for BECD. Figure 4.3.2 shows the solubility of BECD in pure CO₂ and in CO₂ with 5 mol% methyl alcohol at T = 35°C. Figure 4.3.3 shows the solubility of BECD in pure CO₂ and CO₂ with 5 mol% methyl alcohol at T=55°C. From Figure 4.3.2 and Figure 4.3.3, it is obvious that the addition of a small amount of a liquid co-solvent to the compressed CO₂ can enhance the solubility of BECD significantly.

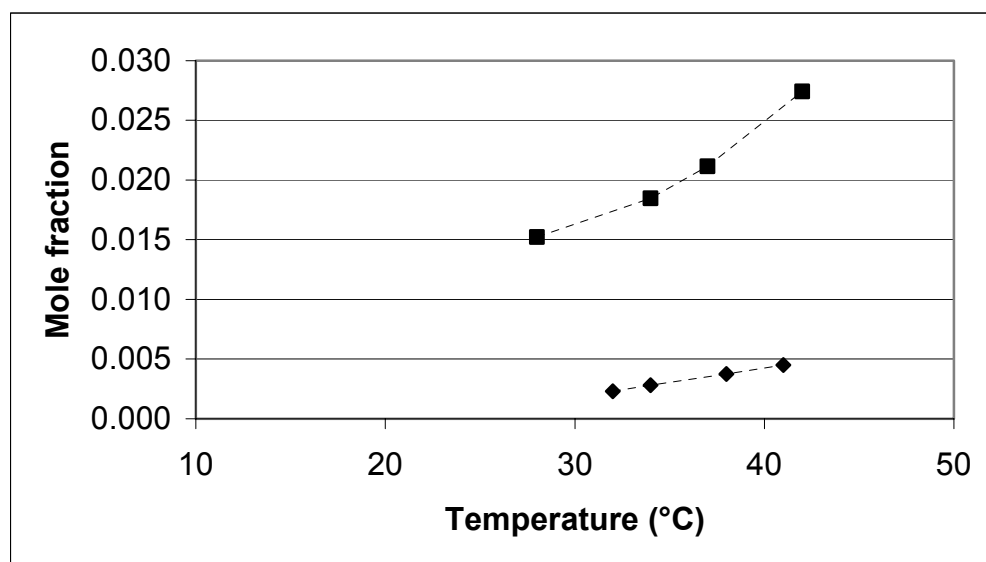


Figure 4.3.1 The solubility of BECD in pure solvents of methyl alcohol (◆) and acetone (■).

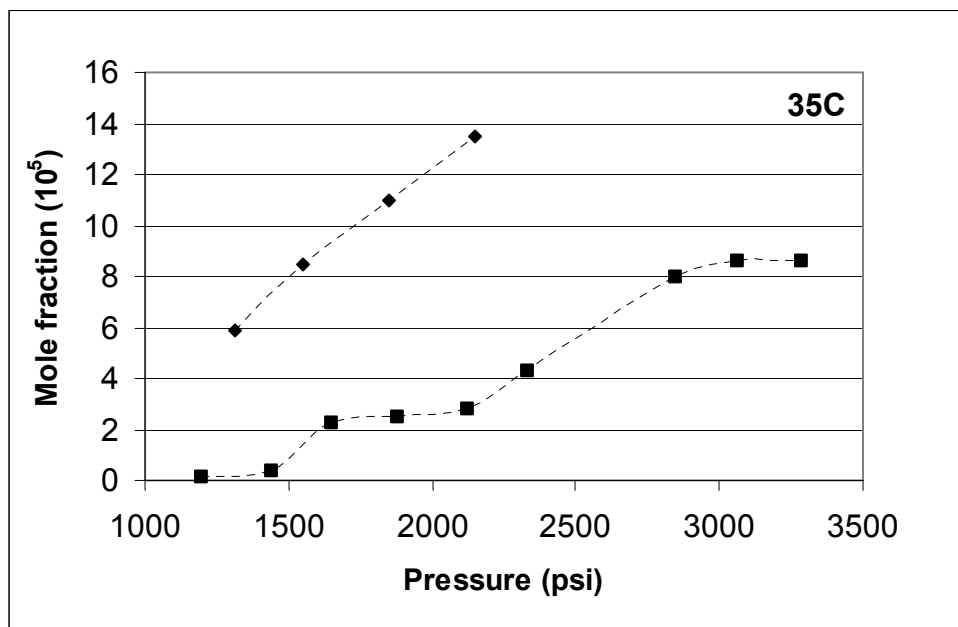


Figure 4.3.2 The solubility of BECD in pure CO₂ (■) (Dean, 1995) and in CO₂ with 5 mol% methyl alcohol (◆) at T = 35°C

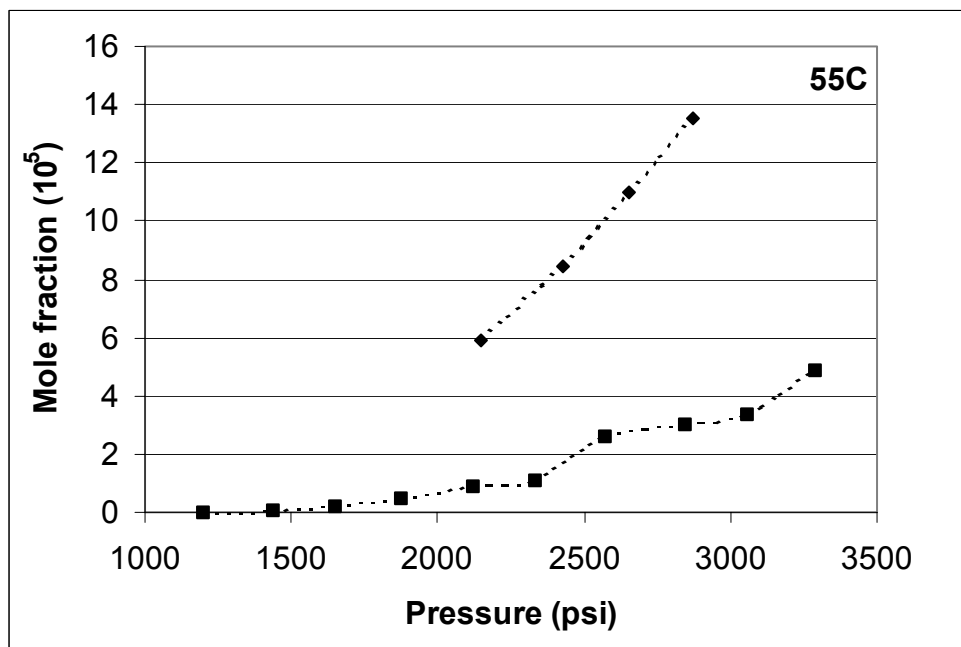


Figure 4.3.3 The solubility of BECD in pure CO₂ (■) (Dean, 1995) and CO₂ with 5 mol% methyl alcohol (◆) at T=55°C

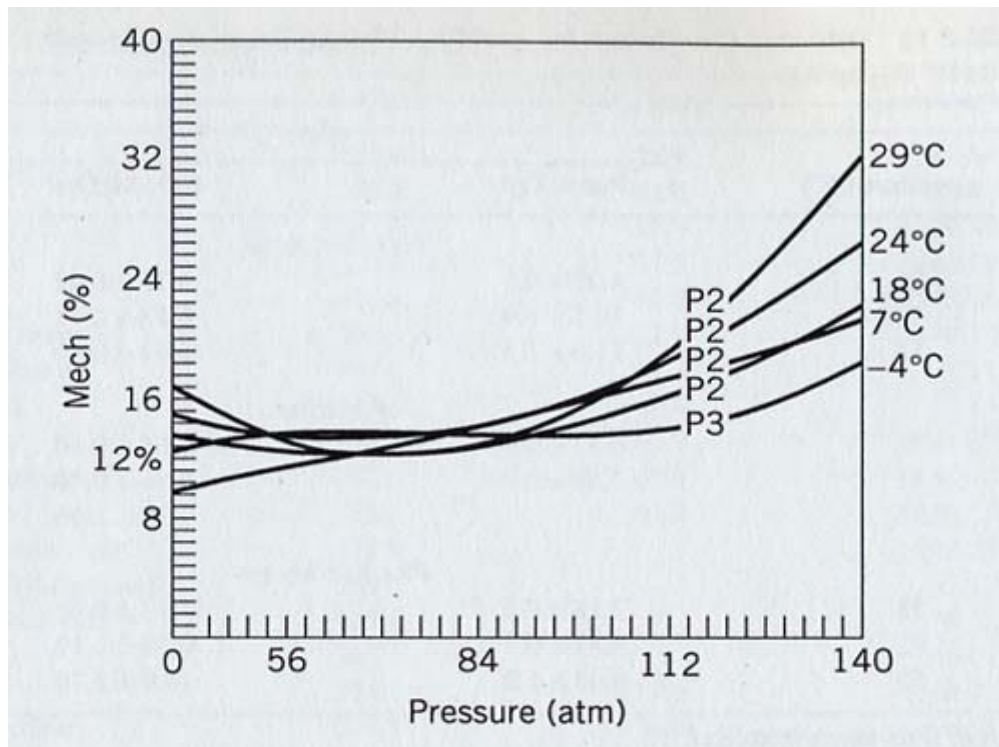


Figure 4.3.4 Solubility of methyl alcohol in CO₂ as a function of pressure and temperature (Maguire et al., 1988)

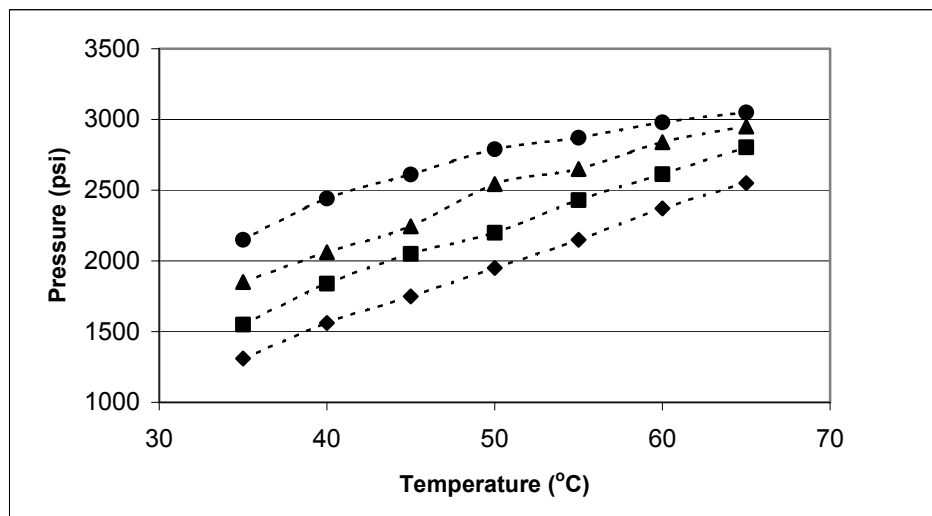


Figure 4.3.5 The effect of temperature and pressure on BECD solubility in CO₂/methanol at the mole fraction of 5.91×10^{-5} (◆), 8.44×10^{-5} (■), 10.97×10^{-5} (▲), and 13.51×10^{-5}

(●)

In order to keep the methyl alcohol and CO₂ mixture homogeneous, the methyl alcohol concentration needs to be considered. Figure 4.3.4 shows the solubility of methyl alcohol in CO₂ at various temperatures and pressures (Maguire et al., 1988). According to this figure, the concentration of methyl alcohol must be kept below 12mol% when the temperature is between -4 and 29°C (sub-critical temperatures). An increase in pressure can increase the solubility of methyl alcohol in CO₂. In this thesis, each experiment was run under the same co-solvent concentration, 5mol%, and at temperatures above 29°C (i.e. under supercritical conditions for temperature and pressure). Hence, the methyl alcohol/ CO₂ mixture was homogeneous.

Figure 4.3.5 shows the effect of temperature and pressure on the solubility of BECD in CO₂/methanol. The cloud point pressures of the solutions were measured at four mole fractions (5.91×10^{-5} , 8.44×10^{-5} , 10.97×10^{-5} and 13.51×10^{-5} of BECD) along seven isotherms (35, 40, 45, 50, 55, 60 and 65°C). Each reported data value was an average of the three or four replicate measurements. The reproducibility of the measurements is generally within 5% (i.e. ± 100 psi at 2000psi). In this work, cloud point pressure is defined as the pressure at which the image started to become light. Mawson et al. defined cloud point as the point when a light, directed into the vessel, no longer reflected off the smooth stainless steel face as the solution turned slightly translucent (Mawson et al., 1995). Meilchen et al. defined the cloud point as the point at which it was no longer possible to observe the stir bar (Meilchen et al., 1991). Blasig et al. defined the cloud point as the point at which the piston inside the vessel first became invisible (Blasig et al., 2002). Hence, the cloud point value depends on the individual operators' procedure.

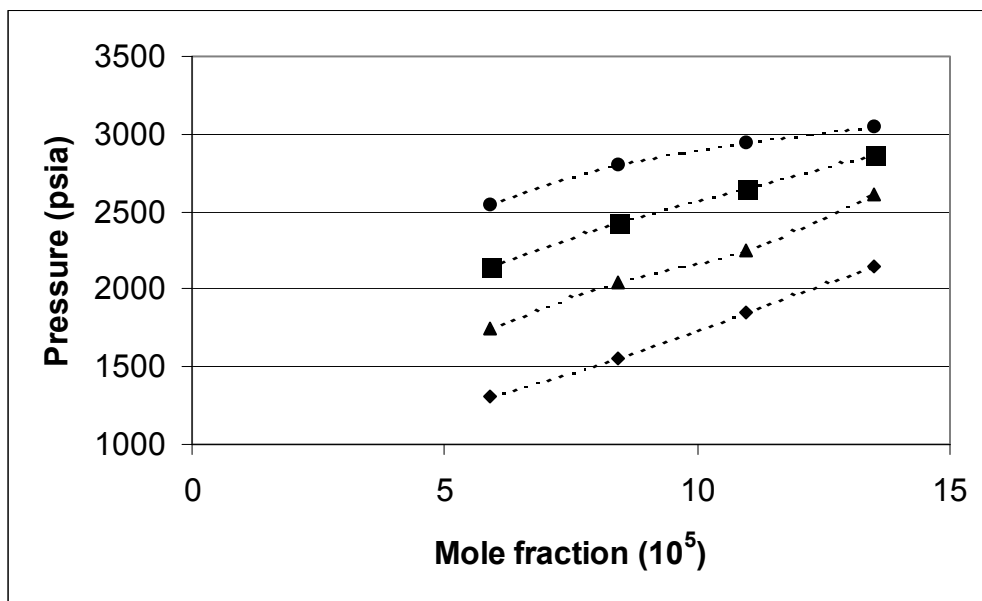


Figure 4.3.6 The pressure of BECD solutions as a function of mole fraction at various temperatures: 35 °C (◆), 45 °C (▲), 55 °C (■), and 65 °C (●)

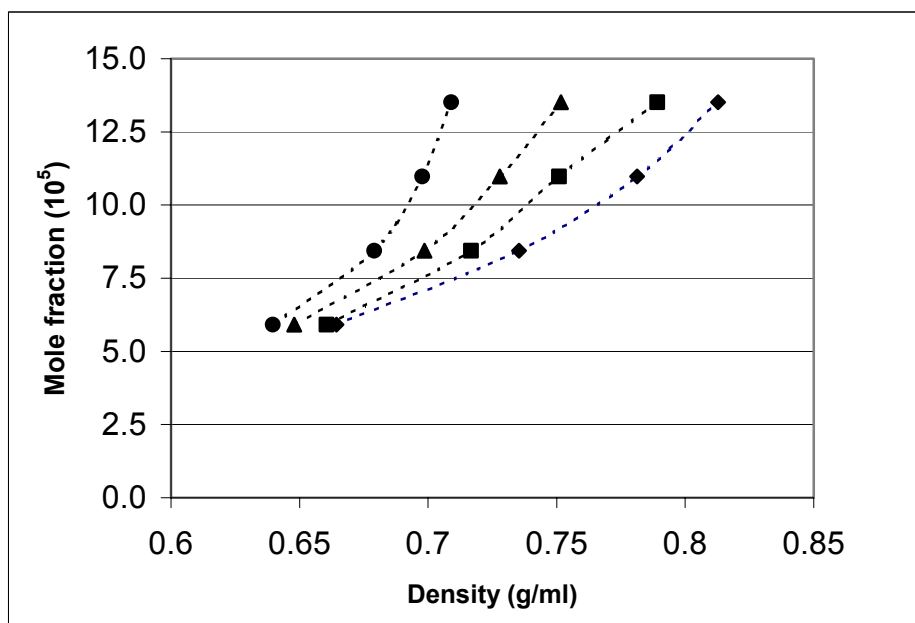


Figure 4.3.7 The solubility of BECD in CO₂ is a function of density at various temperatures: 35 °C (◆), 45 °C (■), 55 °C (▲), and 65 °C (●)

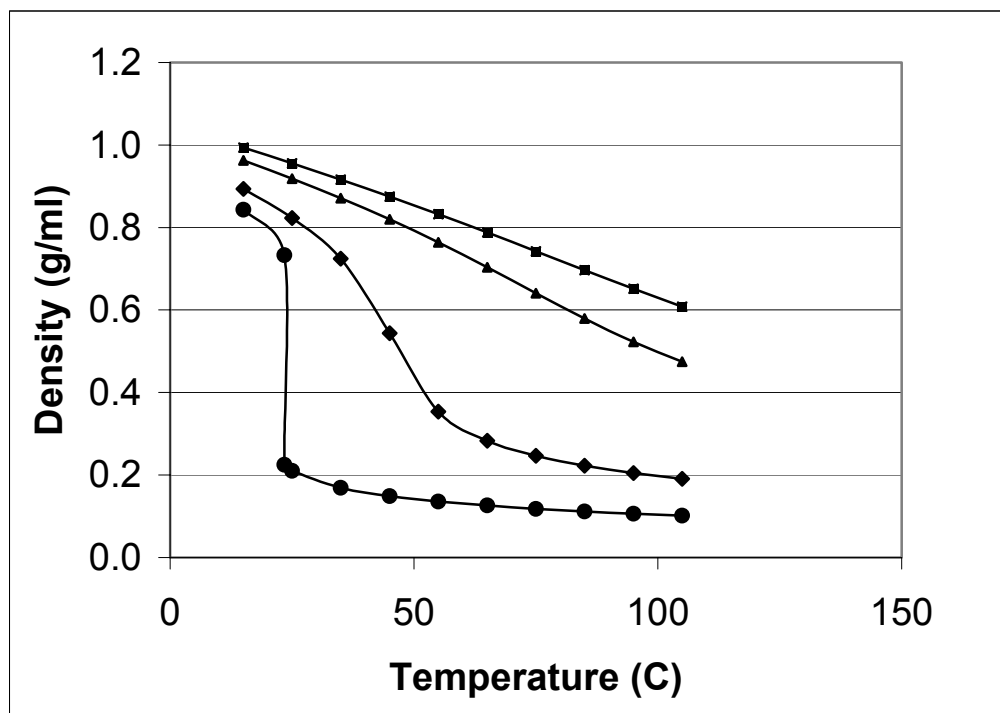


Figure 4.3.8 Isobaric properties for carbon dioxide at various pressures: 900psi (●), 1500psi (◆), 3000psi (▲), and 4000psi (■)

Figure 4.3.6 shows the cloud-point pressure of BECD solutions as a function of weight fraction at various temperatures. Figure 4.3.7 shows the solubility of BECD in CO₂ is a function of density at various temperatures.

The effect of pressure on the solubility is mainly due to the effect of pressure on the solvent density. From Figure 4.1.1, the density increases with an increase in pressure. Near the critical region, the density increases significantly with a small increase in pressure. As a result, the solubility is increased significantly with a small increase in pressure.

The effect of temperature on the solubility is complex due to the effect of temperature on the density and vapor pressure. From Figure 4.3.8, increasing temperature at constant pressure results in a decrease in density. At the lower pressures (near the critical pressure, 1070psi), the density decreases significantly with a small increase in temperature. Regardless of the vapor pressure, the solvent power of CO₂ decreases with increasing temperature. However, from Figure 4.3.7, the solubility of BECD in CO₂ increased with temperature at a given density. This indicates that solute vapor pressure is another factor that influences the solvating power of CO₂. The higher solubility was found by increasing the vapor pressure of BECD (vapor pressures of solutes increase with increasing temperature). Also at a higher pressure, the effect of temperature on density becomes less. Therefore, the effect of temperature on the solubility is complicated and cannot be described by density alone.

4.4 Phenanthrene Particle Formation using the RESS Process

There are eight reports about phenanthrene particle formation using the RESS process. The particle sizes reported range from 1 to 25 microns, which vary due to the use of different RESS systems and various working conditions. In this report, phenanthrene was mixed with supercritical CO₂ in the mixing chamber and sprayed out from the nozzle. The experimental conditions are summarized in Table 4.4.1. Phenanthrene particles could not be observed under the Scanning Electron Microscope (SEM) by reason that phenanthrene was sublimated under the vacuum. Figure 4.4.1 and Figure 4.4.2 show the optical microscope photographs taken before and after exposure to vacuum for two minutes. As clearly indicated, the white mark from phenanthrene disappeared after vacuum exposure.

Table 4.4.1 RESS Experiments on Phenanthrene Using Supercritical CO₂

Run no.	T _{mix} (°C)	P _{mix} (psi)	Capillary diameter (micron)	Length (cm)	Concentration <i>y</i> _{phenanthrene}	Spray distance (cm)
Increasing concentration						
1	34	3000	127	3	2.2×10^{-4}	1
2	34	3000	127	3	4.2×10^{-4}	1
3	34	3000	127	3	6.4×10^{-4}	1
Increasing pressure						
4	34	2000	127	3	2.2×10^{-4}	1
5	34	3000	127	3	2.2×10^{-4}	1
Increasing spray distance						
6	45	4500	127	3	6.9×10^{-4}	1
7	45	4500	127	3	6.9×10^{-4}	5

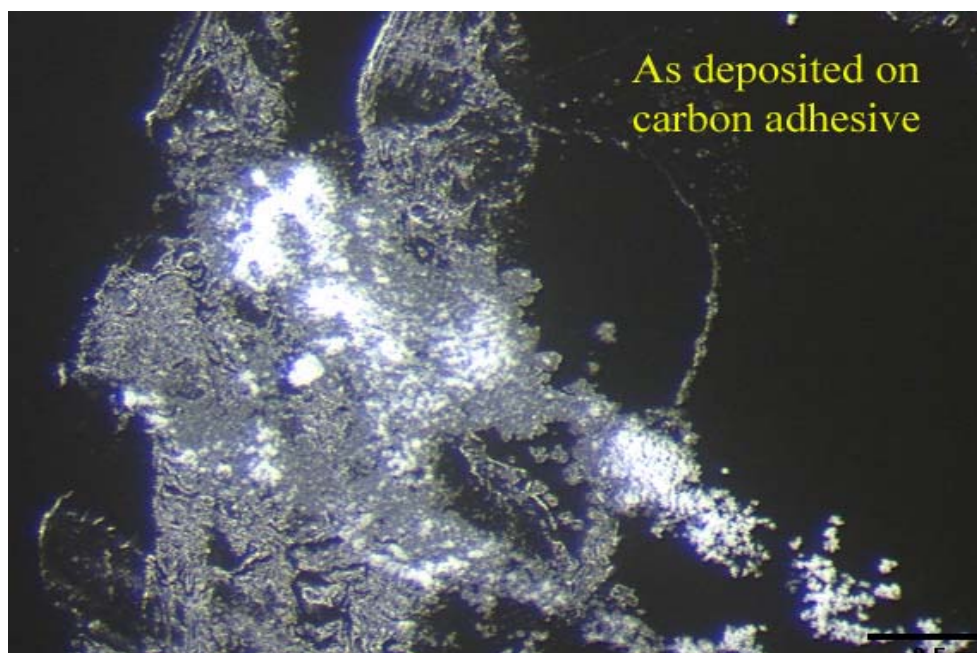


Figure 4.4.1 Optical microscope photograph of phenanthrene deposited on the carbon tape before vacuuming

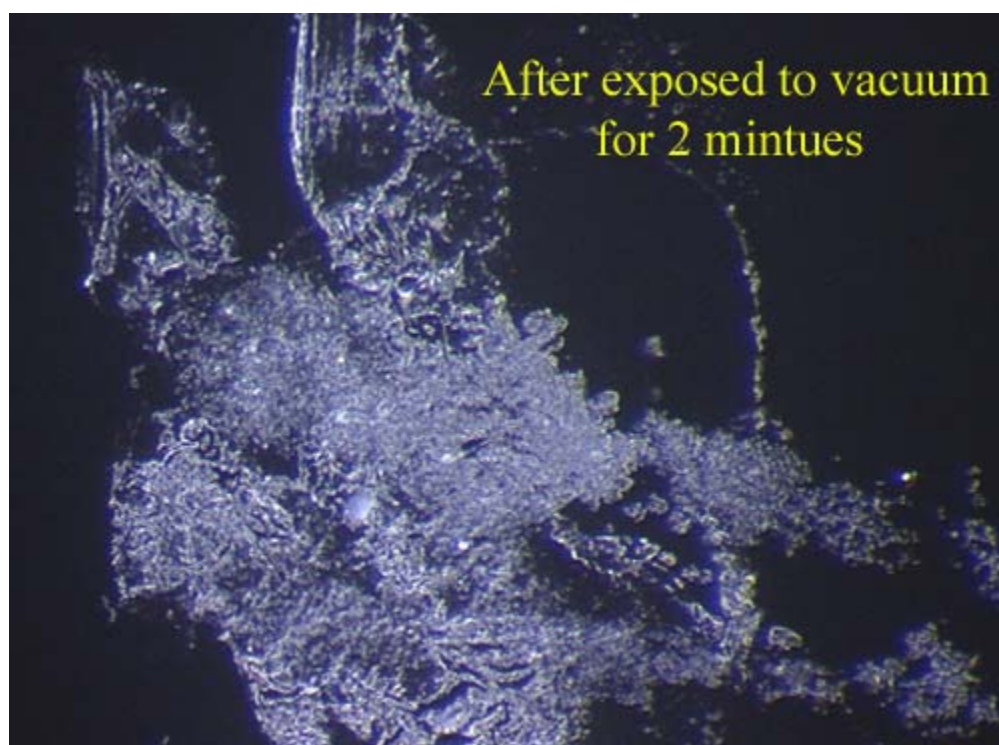


Figure 4.4.2 Optical microscope photograph of phenanthrene after vacuuming

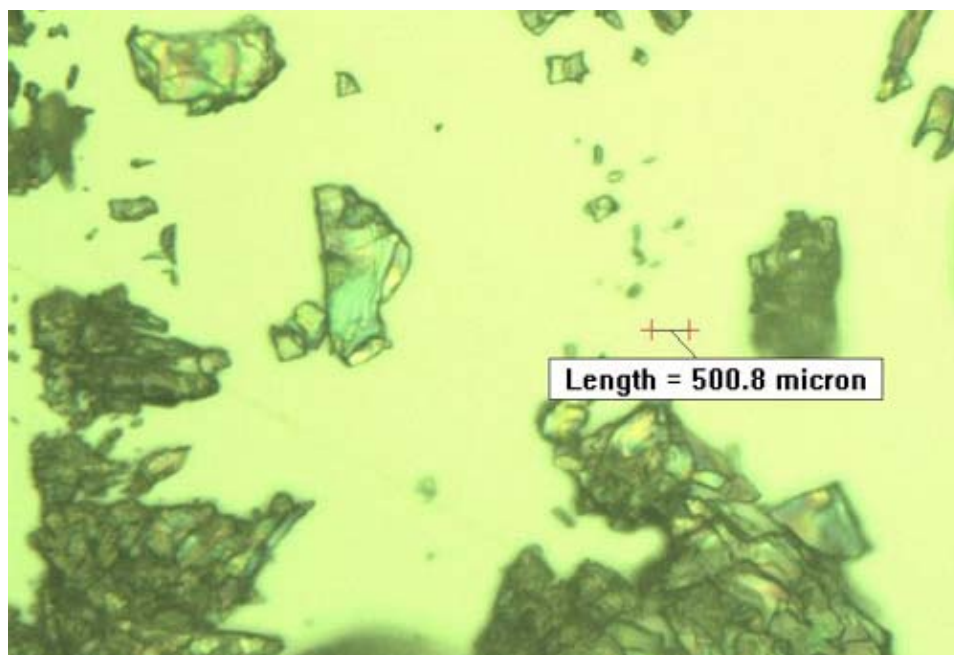


Figure 4.4.3 Optical microscope photograph of phenanthrene before RESS process

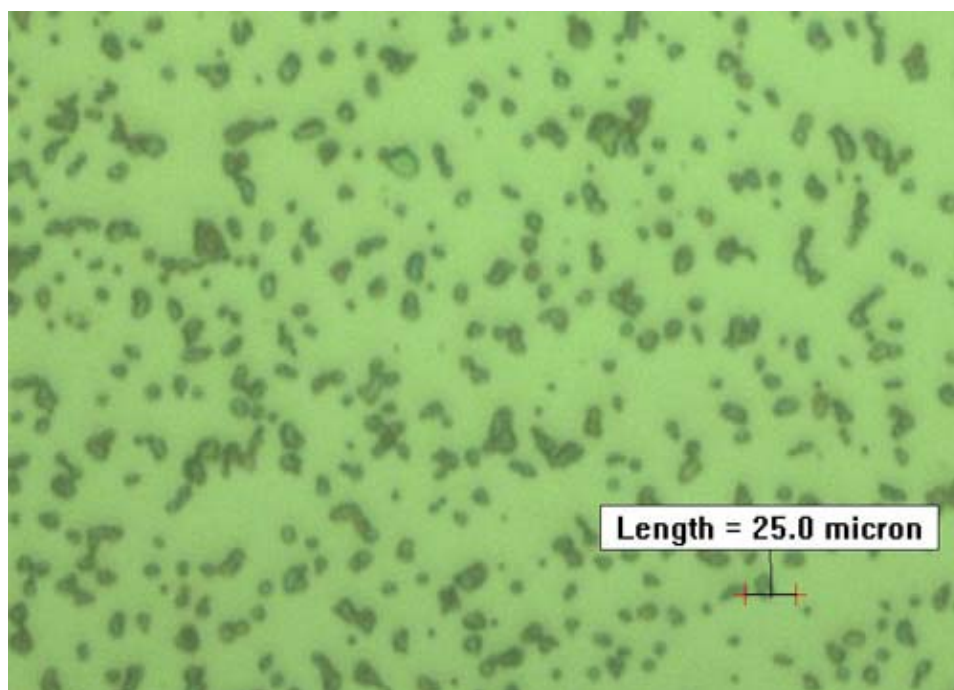
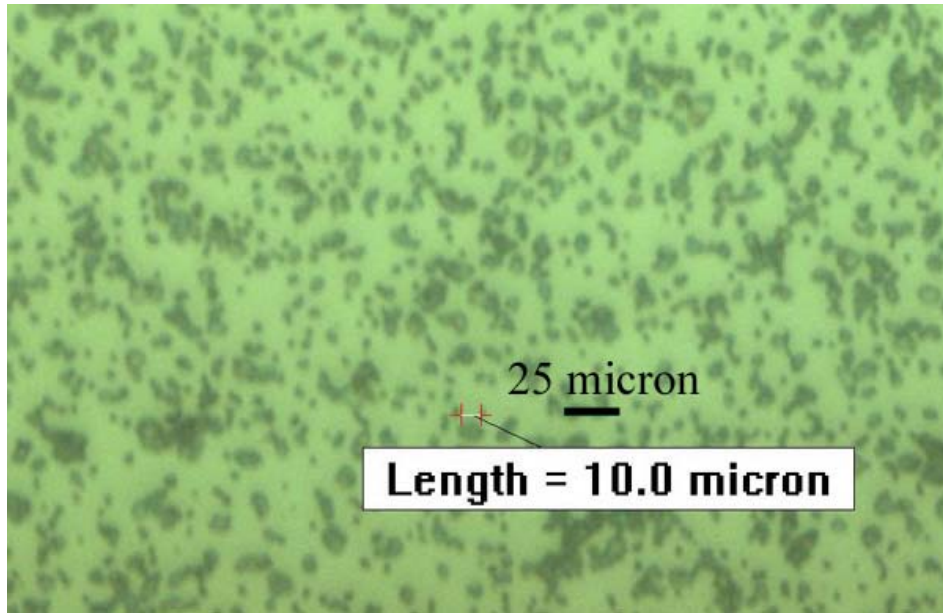
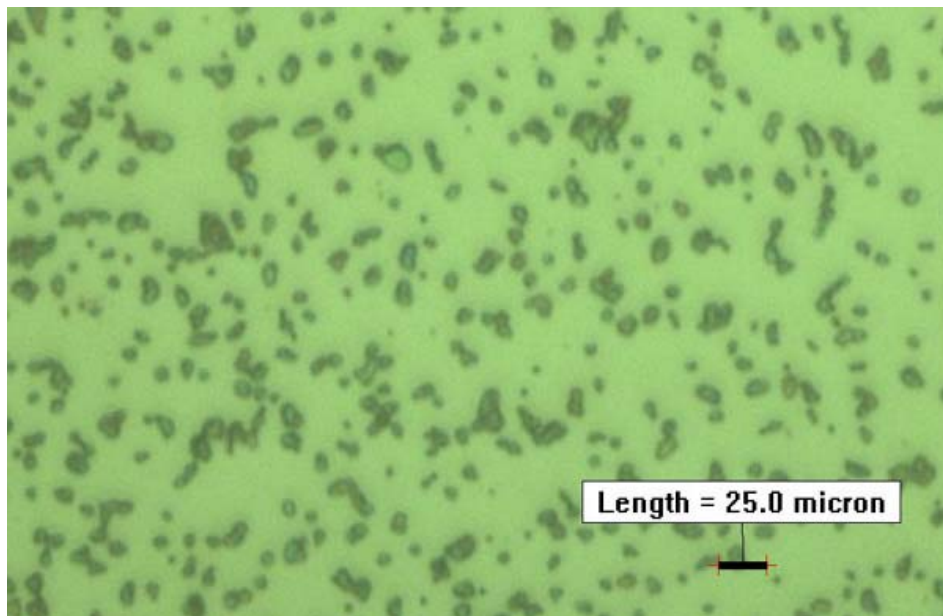


Figure 4.4.4 Optical microscope photograph of phenanthrene after the RESS process.

The experiment conditions were $T_{\text{mix}}=34^{\circ}\text{C}$, $P_{\text{mix}}=3000\text{psi}$, Capillary diameter=127microns, $y_{\text{phenanthrene}}=6.4 \times 10^{-4}$, and Spray distance=1cm

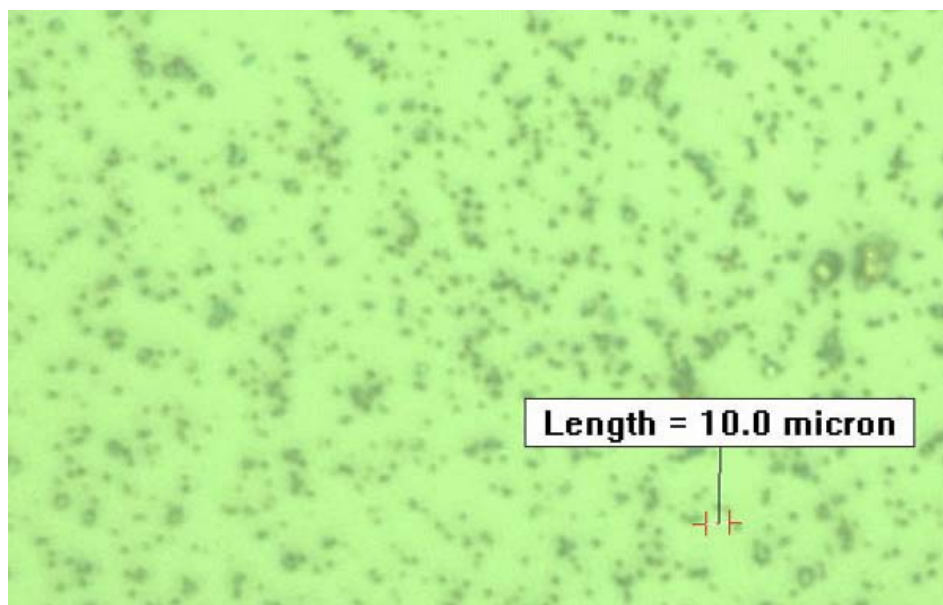


(a)

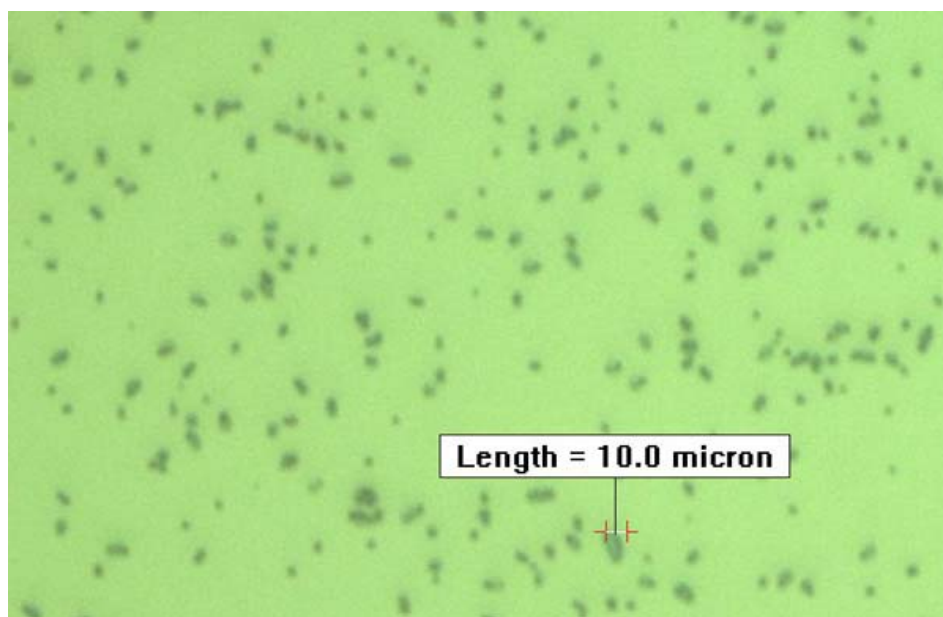


(b)

Figure 4.4.5 Optical microscope photographs of phenanthrene produced by the RESS process at the different mole fraction. The experiment conditions were $T_{\text{mix}}=34^{\circ}\text{C}$, $P_{\text{mix}}=3000\text{psi}$, Capillary diameter= 127microns , $y_{\text{phenanthrene}} = 4.2 \times 10^{-4}$ (a) 6.4×10^{-4} (b), and Spray distance= 1cm



(a)



(b)

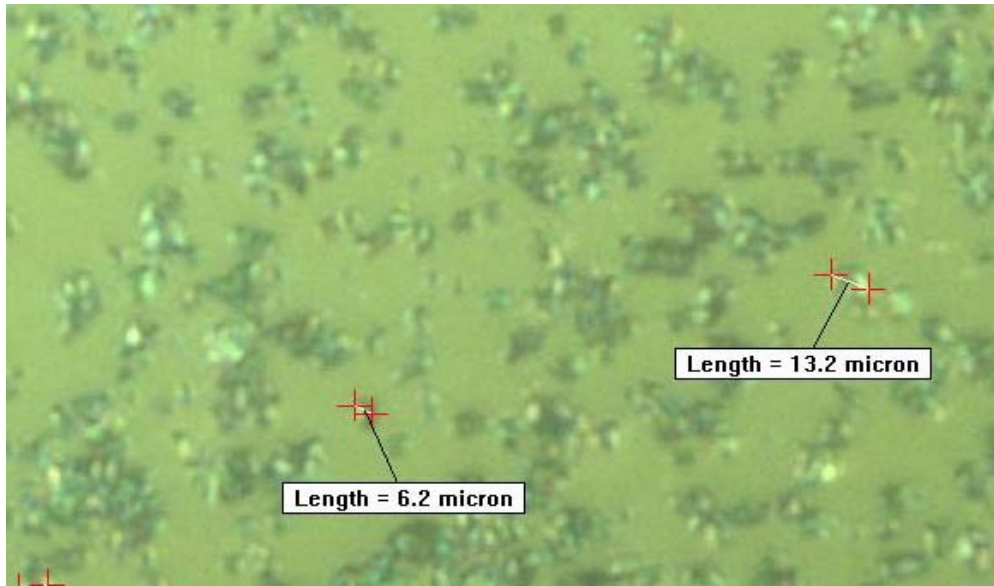
Figure 4.4.6 Optical microscope photographs of phenanthrene produced by the RESS process at different expansion pressure. The experiment conditions were $T_{\text{mix}}=34^{\circ}\text{C}$, $P_{\text{mix}}=2000\text{psi}$ (a); 3000psi (b), Capillary diameter= 127microns , $y_{\text{phenanthrene}} = 2.2 \times 10^{-4}$, and Spray distance= 1cm

Figures 4.4.3 and 4.4.4 show the optical microscope photographs before and after the RESS process. The phenanthrene particle size became smaller after processing by RESS, ranging from 1 to 15 microns. Two points are evident from these two pictures; 1) the RESS process enables one to form smaller phenanthrene particles than are present with those before the RESS process, and 2) the phenanthrene particle size distribution becomes narrower after the RESS process.

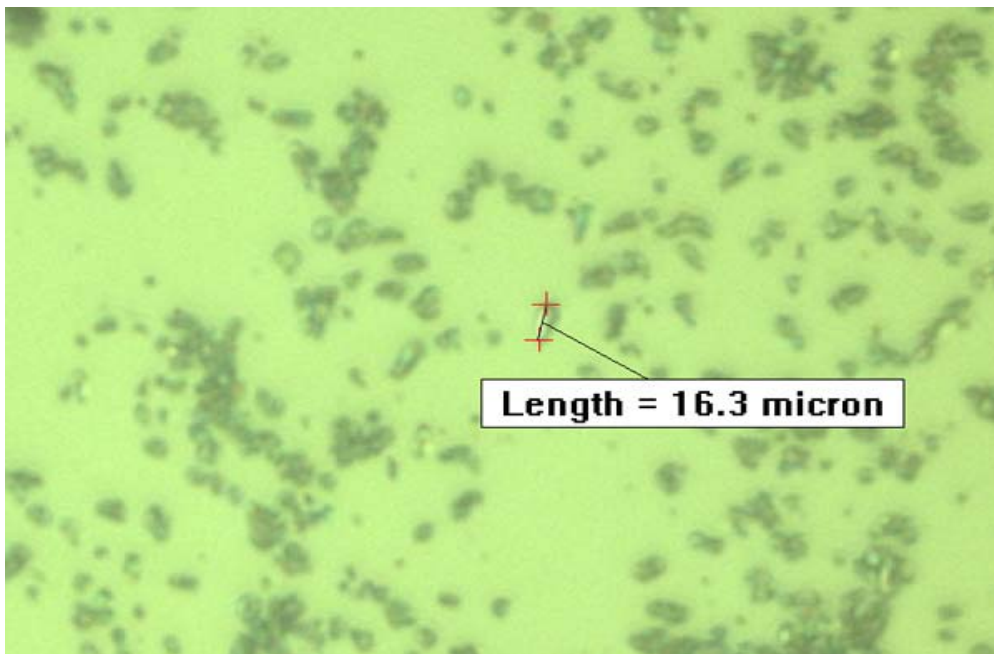
In this report, three process parameters, the concentration, pressure and spray distance, were studied using phenanthrene. Figure 4.4.5 shows the optical microscope graphs of phenanthrene from the RESS process at two different phenanthrene concentrations. The phenanthrene concentration had no significant effect on particle shape, for the conditions studied. However, the particle size increased slightly with an increase in concentration by comparing the optical microscope photographs at the three studied concentrations. Owing to the properties of light, the optical microscope cannot observe particles that are smaller than 0.2 microns. Although the size of the phenanthrene particles was above the smallest size limitation, the edge of the particles was indistinguishable on the graphs. If the particle size were measured by the automatic Scion Image™ software, the error would be at least $\pm 30\%$ (i.e. ± 3 micron at 10micron). However, the optical microscope photographs are still useful to observe the trend of particle size and can be used to compare with BECD SEM graphs.

Figure 4.4.6 shows optical microscope graphs of phenanthrene from the RESS process at two pressures (2000 and 3000 psi). According to previous literature results, increasing the expansion pressure decreased phenanthrene particle size slightly (Liu et al., 1996). However, the particle size was too small to be analyzed accurately from optical microscope photographs. The effect of expansion pressure on the phenanthrene particle shape in the studied region was not significant.

Figure 4.4.7 shows optical microscope graphs of phenanthrene from the RESS process at different spray distances. The particle size and morphology did not change significantly at two-spray distances. However, as we will see in the next section, particle size and morphology of BECD were strongly influenced by the spray distance.



(a)



(b)

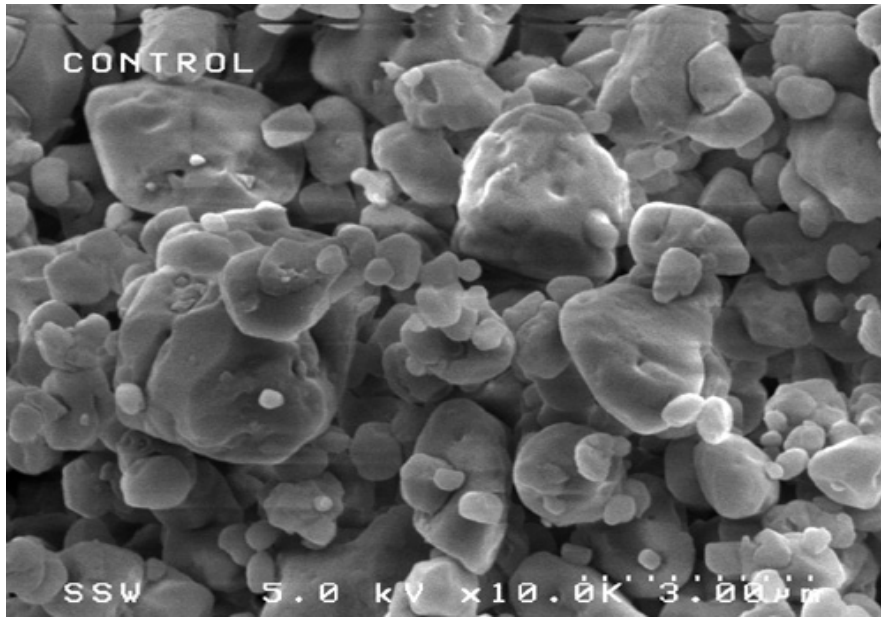
Figure 4.4.7 Optical microscope photographs of phenanthrene produced by the RESS process at different spray distance. The experiment conditions were $T_{\text{mix}}=34^{\circ}\text{C}$, $P_{\text{mix}}=2000\text{psi}$ (a); 3000psi (b), Capillary diameter= 127microns , $y_{\text{phenanthrene}} = 6.9 \times 10^{-4}$, and Spray distance= 1 cm (a); 5 cm (b)

4.5 Beclomethasone Dipropionate (BECD) Particle Formation in Supercritical CO₂

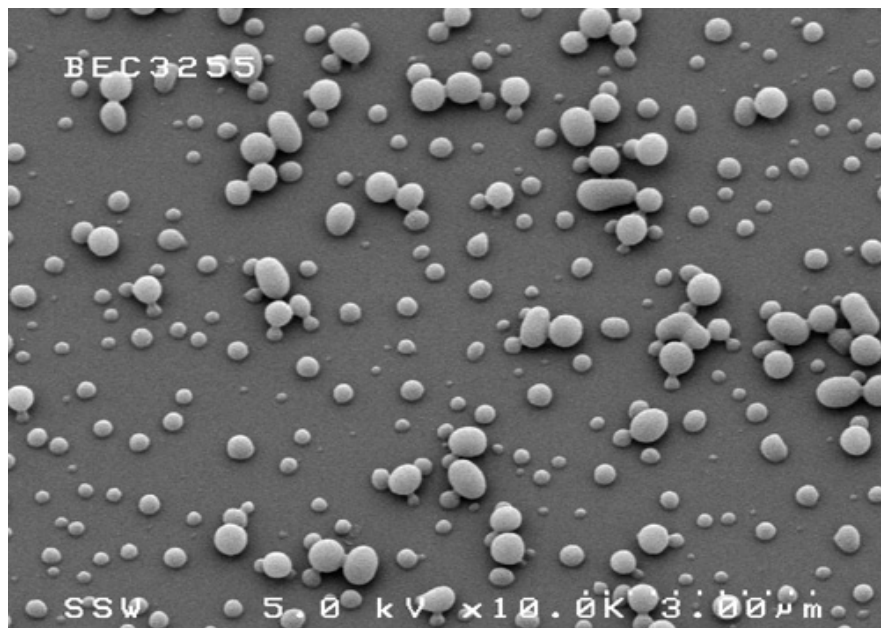
BECD is a synthetic steroid used in an inhaler for the treatment of bronchial asthma. Presently, there is only one report about BECD particle formation in supercritical CO₂. Steckel tried to use an aerosol solvent extraction system to micronize BECD particles (Steckel et al., 1997). BECD particles were dissolved in an organic solvent and sprayed into supercritical carbon dioxide. However, no BECD particles were obtained due to the fact that BECD was extracted by the supercritical carbon dioxide under the applied conditions.

In this report, the rapid expansion of supercritical solution (RESS) process was used to micronize BECD particles. BECD particles were obtained by the RESS process and the particle size was smaller than 1 micron in some cases. Figure 4.5.1 shows BECD particles before and after the RESS process. Before the RESS process, the original BECD particle size was already very small. The particle size ranged from 0.4 - 5 microns and the particle shape was irregular. However, the particle size became much smaller after the RESS process (experimental condition 1 in Table 4.5.2.1). For this set of experimental conditions, the particle size range was from 0.2 - 1.0 microns. The size distribution also became narrower after the RESS process. Particle shape changed from irregular to unitary spheres.

In this section, several parameters will be discussed in order to understand the relationship between particle size and operational conditions.



(a)



(b)

Figure 4.5.1 SEM photographs of BECD; (a) received (b) after the RESS process. The experiment conditions were $T_{\text{mix}}=43^{\circ}\text{C}$, $P_{\text{mix}}=4600\text{psi}$, Capillary diameter=127microns, Nozzle length=3cm, $y_{\text{BEC D}} = 3.95 \times 10^{-5}$, Methanol concentration= 5mol%, and Spray distance=1cm

4.5.1 Effect of Nozzle Diameter

In this work, four nozzles of different diameters were studied using the RESS process. When a 127-micron internal diameter nozzle was used, significant plugging occurred under this working condition. When BECD particles precipitate inside the nozzle, the effective nozzle diameter decreases from plugging. Larger diameter nozzles were found to minimize the effect of plugging.

Table 4.5.1.1 shows the RESS experimental conditions used for studying different nozzles. Figure 4.5.1.1 shows BECD particle size distributions evaluated at different nozzle diameters. Table 4.5.1.2 shows the mean diameter, standard deviation, the size of range and the aspect ratio of BECD particles at the different nozzle diameters. The effect of nozzle diameter on particle size is such that the particle size increases with an increase of nozzle diameter. Figures 4.5.1.2, 4.5.1.3 and 4.5.1.4 show SEM photographs of BECD produced by RESS using different nozzle diameters. At a nozzle diameter of 254 micron, the morphology of BECD is micron sphere. At a nozzle diameter of 762 micron, small fibers were formed. At a nozzle diameter of 1016 micron, larger elongated crystals were present after the RESS process.

Table 4.5.1.1 RESS Experimental Conditions for Evaluating Nozzle Diameter

Run no.	T _{mix} (°C)	P _{mix} (psi)	Capillary diameter (micron)	Capillary length (cm)	BECD mole fraction	Methanol concentration (mol%)	Spray distance (cm)
1	40	3000	254	3	2.50×10^{-3}	5	1
2	40	3000	762	3	2.50×10^{-3}	5	1
3	40	3000	1016	3	2.50×10^{-3}	5	1

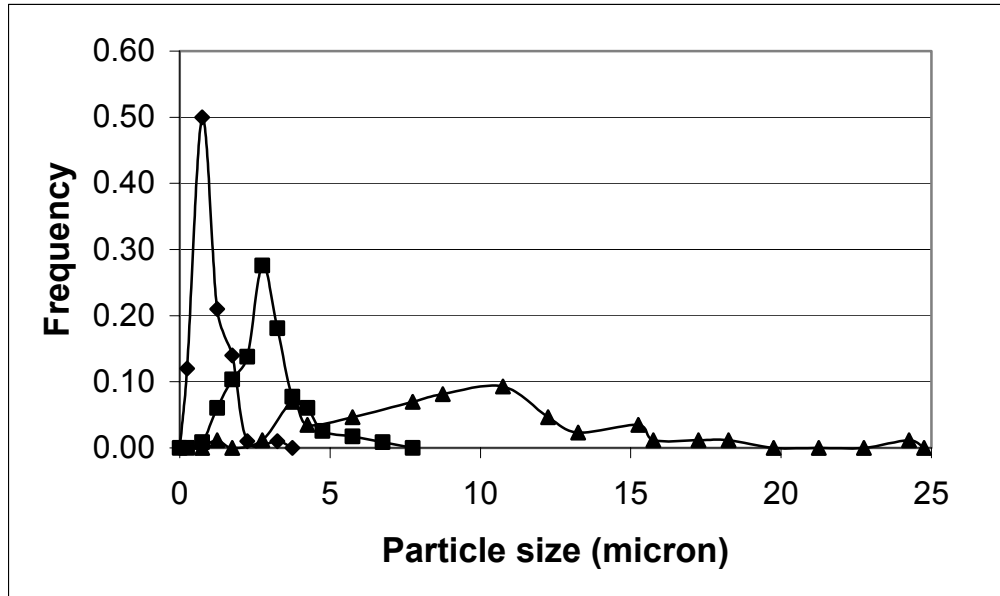
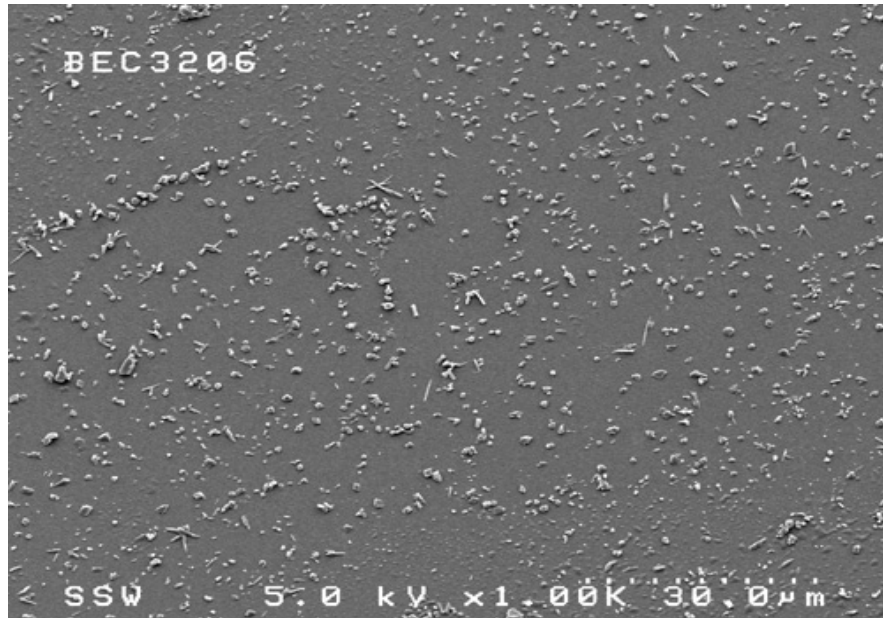


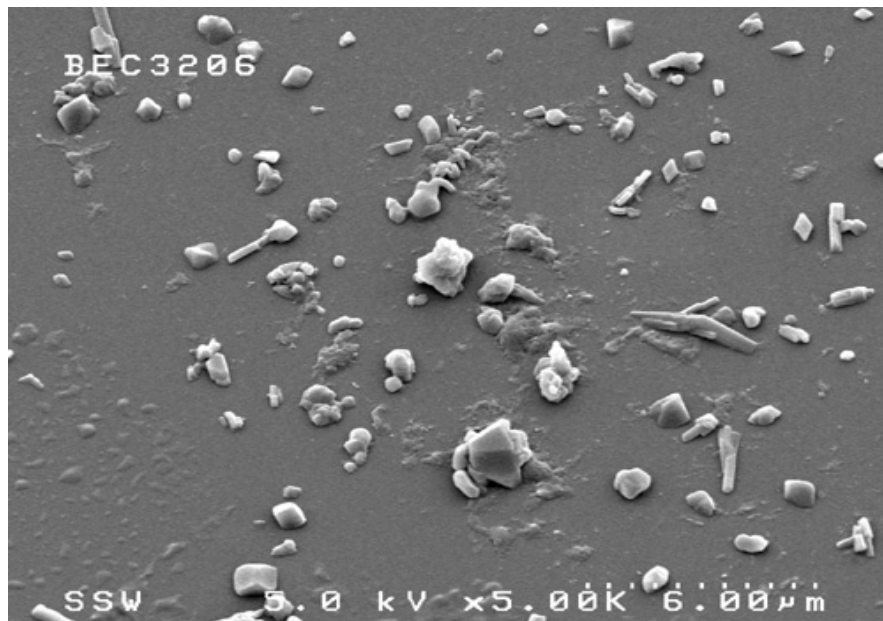
Figure 4.5.1.1 BECD particle size distributions evaluated at different nozzle diameters: 254microns (◆), 762microns (■), and 1016microns (▲). The experiment conditions were $T_{mix}=40^{\circ}C$, $P_{mix}=3000psi$, Nozzle length=3cm, $y_{BECD} = 2.50 \times 10^{-3}$, Methanol concentration= 5mol%, and Spray distance=1cm

Table 4.5.1.2 The Mean Diameter, Standard Deviation, Size of Range and Aspect Ratio of BECD Particles at the Different Nozzle Diameters

Run no.	Nozzle diameter (micron)	Mean diameter (micron)	Standard deviation (micron)	Size of range (micron)	Aspect ratio
1	254	1.01	5.21	0.30 – 3.15	1.86
2	762	2.97	11.96	1.10 – 6.60	4.10
3	1016	9.16	37.06	2.50 - 18.40	5.33



(a)

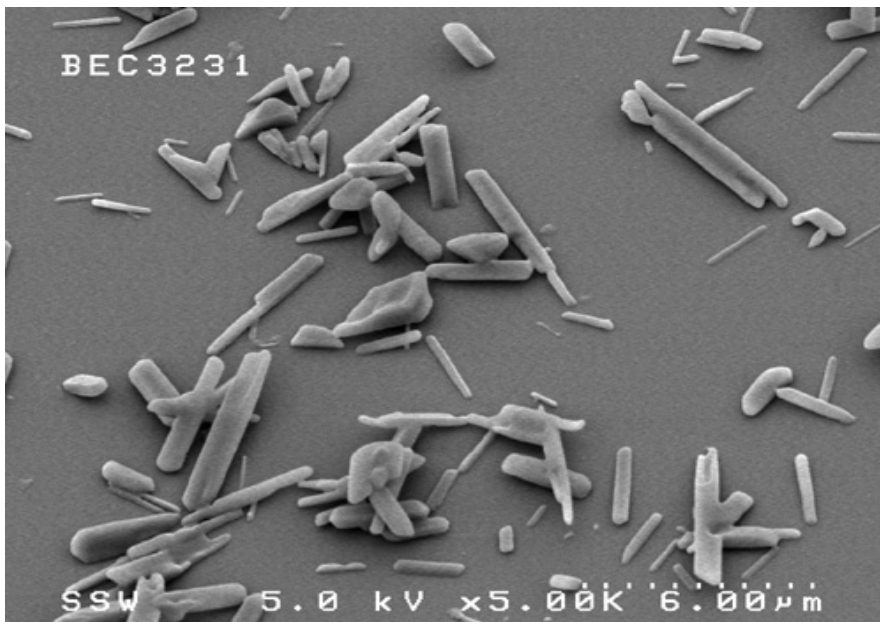


(b)

Figure 4.5.1.2 SEM photographs of BECD produced by RESS using nozzle diameter of 254 micron. The experiment conditions were $T_{\text{mix}}=40^{\circ}\text{C}$, $P_{\text{mix}}=3000\text{psi}$, Nozzle length=3cm, $y_{\text{BECD}} = 2.50 \times 10^{-3}$, Methanol concentration= 5mol%, and Spray distance=1cm

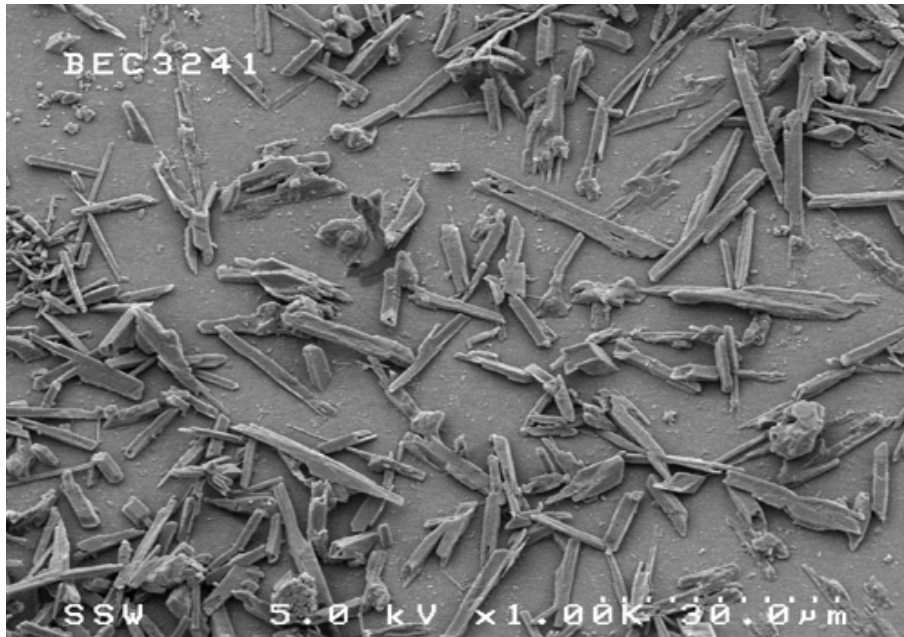


(a)

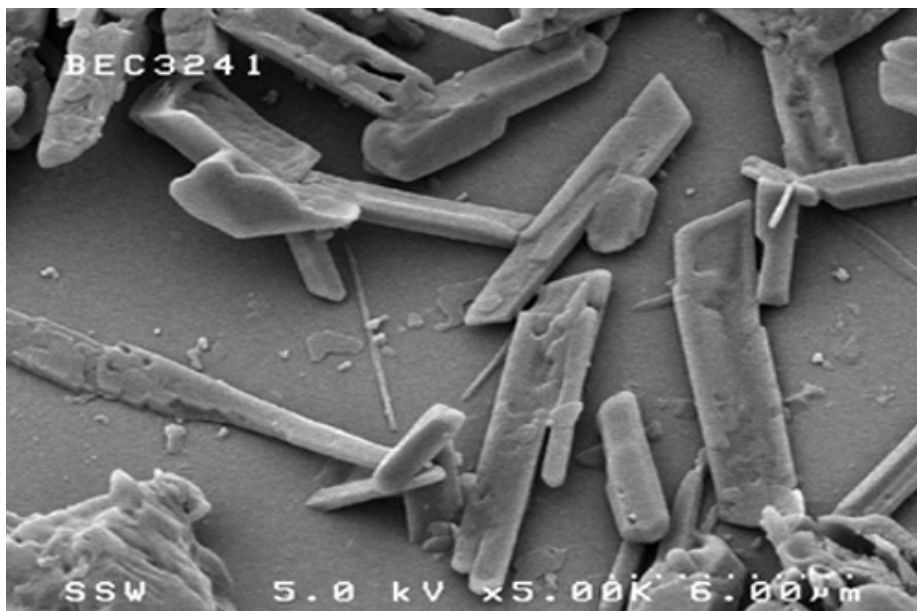


(b)

Figure 4.5.1.3 SEM photographs of BECD produced by RESS using nozzle diameter of 762 micron. The experiment conditions were $T_{\text{mix}}=40^{\circ}\text{C}$, $P_{\text{mix}}=3000\text{psi}$, Nozzle length=3cm, $y_{\text{BECD}} = 2.50 \times 10^{-3}$, Methanol concentration= 5mol%, and Spray distance=1cm



(a)



(b)

Figure 4.5.1.4 SEM photographs of BECD produced by RESS using nozzle diameter of 1016 micron. The experiment conditions were $T_{\text{mix}}=40^{\circ}\text{C}$, $P_{\text{mix}}=3000\text{psi}$, Nozzle length=3cm, $y_{\text{BECD}} = 2.50 \times 10^{-3}$, Methanol concentration= 5mol%, and Spray distance=1cm

4.5.2 Effect of BECD Concentration

Table 4.5.2.1 shows the RESS experimental conditions at different BECD concentrations. Figure 4.5.2.1 shows BECD size distribution evaluated at different mole fractions. Table 4.5.2.2 shows the mean diameter, standard deviation, size of range and aspect ratio of BECD particles at the different BECD concentrations. Particle size is smaller and the particle size range is narrower for lower concentrations of solute. Figures 4.5.2.2, 4.5.2.3, 4.5.2.4, and Figure 4.5.2.5 show SEM photographs of BECD produced by RESS at different concentrations of solute.

As seen in Figure 4.5.2.1 and Table 4.5.2.2, increasing the concentration of BECD in supercritical CO₂ leads to a larger particle size. At low concentrations, most of the BECD particles are spherical. There are only a few long crystals observed from SEM graphs at the mole fraction of 3.95×10^{-5} and 6.26×10^{-5} . When the concentration was increased to the mole fraction of 7.81×10^{-5} , there were more long crystals formed by the RESS process. When BECD concentration reaches the mole fraction of 1.63×10^{-4} , the morphology of BECD gave long and large crystals.

When supercritical CO₂ is depressurized through a nozzle to a low-pressure chamber, the supercritical solution can generate very high supersaturation ratios. An increase in the BECD concentration leads to a higher supersaturation ratio. According to the classical theory of nucleation (Matson et al., 1987), higher supersaturation ratios produce higher nucleation rates. However, the particle volume is inversely proportional to the nucleation

rate. According to this theory, increasing BECD concentration in supercritical CO₂ reduces particle size. In this report, the RESS nozzle is a capillary, not an orifice. In addition to the supersaturation ratio, another factor should be considered. When supercritical solutions expand across a nozzle, the pressure drop inside the nozzle can arouse precipitation of the solute from the solution driven by nucleation, condensation and particle coagulation. Figure 4.5.2.6 represents three different RESS process paths from the entrance of the nozzle to the exit (Lele et al., 1994; Mawson, et al., 1995). The first case represents how sub-micron particles are produced. Particles begin to nucleate from solution when a homogenous solution is expanded across the nozzle. The second case represents micron-size particles formation after spraying. Particles begin to nucleate at the nozzle entrance and grow very quickly to form micron size particles. The third case represents fiber formation from the RESS process. The precipitation starts upstream of the nozzle entrance, since the solution already has crossed the cloud point. When the solution is expanded through the nozzle, particles grow and coalesce. Fibers are drawn from the nozzle exit or the nozzle is plugged completely by reason of agglomeration. In summary, the location of the initial solute condensation along the expansion path decides the particle size and morphology. Hence, the longer the path length after nucleation, the larger the particle size.

In this research, each experiment was run at a different concentration. When a solution is expanded across the nozzle at the same temperature and pressure, the solution with a higher concentration would cross the cloud point first and particle nucleation will begin earlier. The path length along the nozzle after nucleation is longer than other solutions at

lower concentrations. Therefore, increasing the concentration of BECD resulted in a larger particle size. When the concentration of BECD was 1.63×10^{-4} , the expansion process turned into the third case, and long crystals were formed.

Table 4.5.2.1 RESS Experimental Conditions for Different Concentrations

Run no.	T_{mix} (°C)	P_{mix} (psi)	Capillary diamter (micron)	Capillary length (cm)	BECD concentration y_{BECD}	Methanol concentration (mol%)	Spray distance (cm)
1	43	4600	127	3	3.95×10^{-5}	5	1
2	43	4600	127	3	6.26×10^{-5}	5	1
3	43	4600	127	3	7.81×10^{-5}	5	1
4	43	4600	127	3	1.63×10^{-4}	5	1

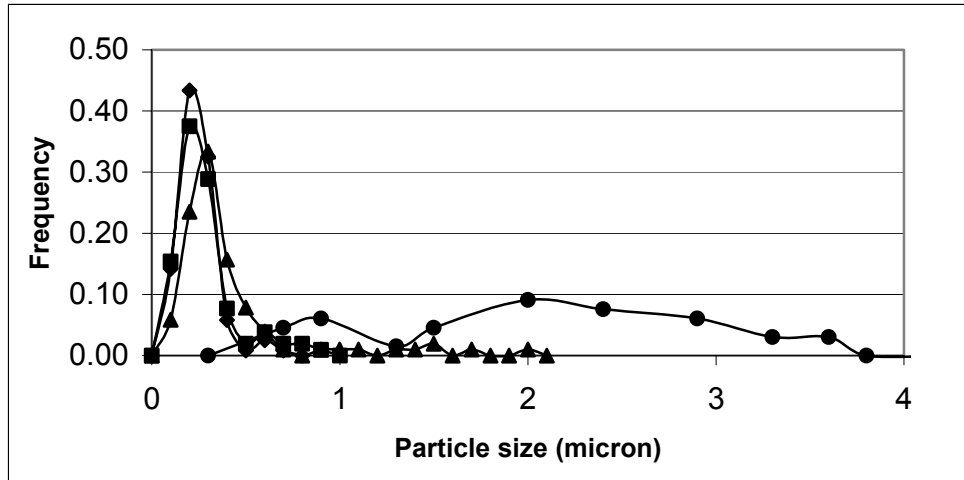


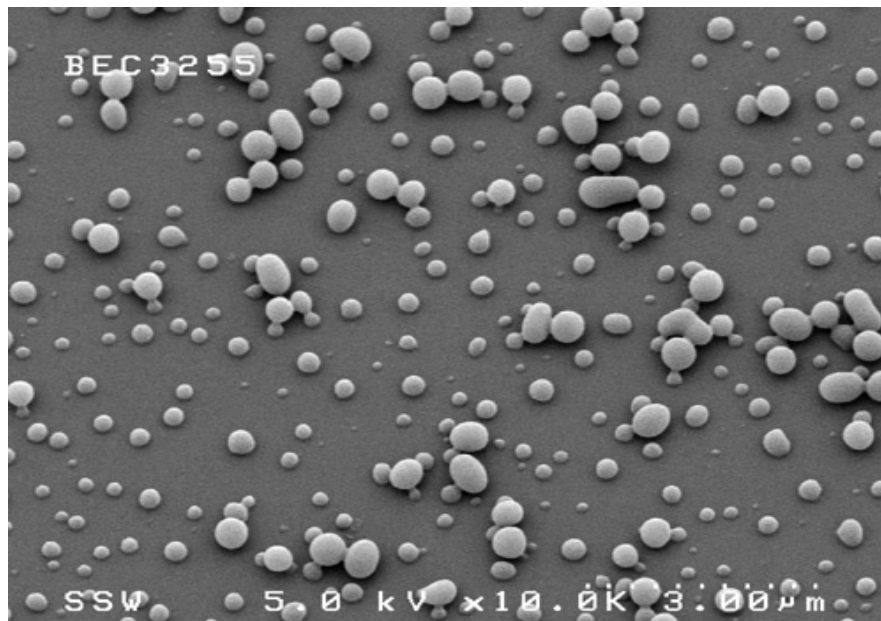
Figure 4.5.2.1 BECD size distribution evaluated at different mole fraction: 3.95×10^{-5} (\blacklozenge), 6.26×10^{-5} (\blacksquare), 7.81×10^{-5} (\blacktriangle), 1.63×10^{-4} (\bullet). The experiment conditions were $T_{\text{mix}}=43^{\circ}\text{C}$, $P_{\text{mix}}=4600\text{psi}$, Capillary diameter=127microns, Nozzle length=3cm, Methanol concentration= 5mol%, and Spray distance=1cm

Table 4.5.2.2 The Mean Diameter, Standard Deviation, Size of Range and Aspect Ratio of BECD Particles at the Different BECD Concentrations

Run no.	BECD concentration (y_{BECD})	Mean diameter (micron)	Standard deviation (micron)	Size of range (micron)	Aspect ratio
1	3.95×10^{-5}	0.24	1.18	0.09 – 1.10	1.22
2	6.26×10^{-5}	0.34	1.86	0.11 – 1.32	1.54
3	7.81×10^{-5}	0.40	3.44	0.10 – 2.20	1.79
4	1.63×10^{-4}	1.94	6.64	0.40 – 3.90	3.59



(a)

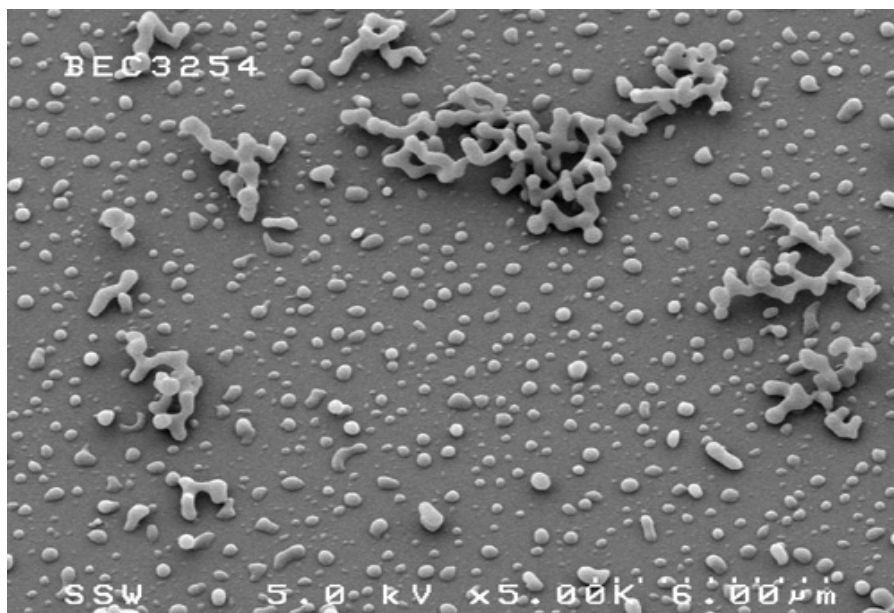


(b)

Figure 4.5.2.2 SEM photographs of BECD produced by RESS at the mole fraction of 3.95×10^{-5} . The experiment conditions were $T_{\text{mix}}=43^{\circ}\text{C}$, $P_{\text{mix}}=4600\text{psi}$, Capillary diameter=127microns, Nozzle length=3cm, Methanol concentration= 5mol%, and Spray distance=1cm



(a)

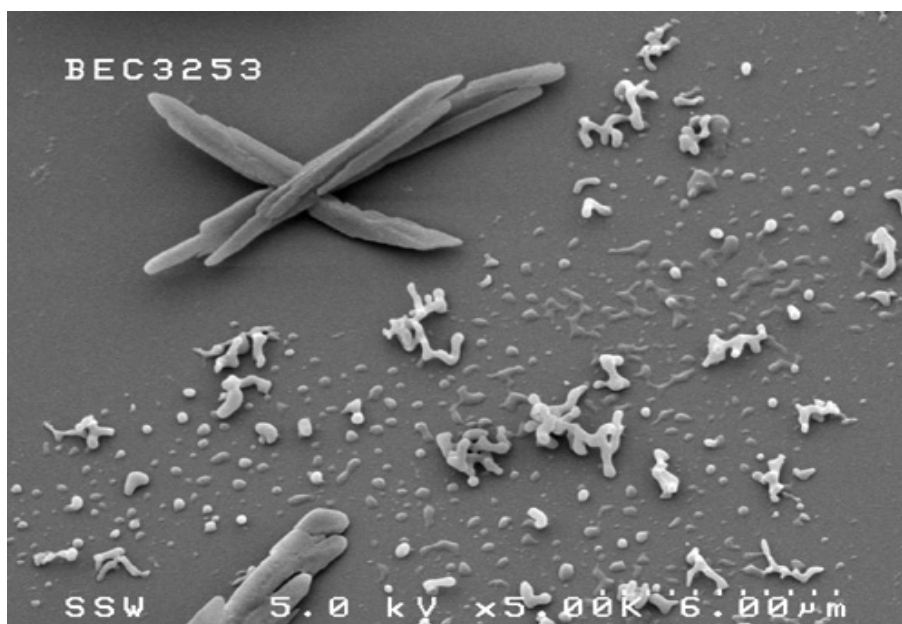


(b)

Figure 4.5.2.3 SEM photographs of BECD produced by RESS at the mole fraction of 6.26×10^{-5} . The experiment conditions were $T_{\text{mix}}=43^{\circ}\text{C}$, $P_{\text{mix}}=4600\text{psi}$, Capillary diameter=127microns, Nozzle length=3cm, Methanol concentration= 5mol%, and Spray distance=1cm

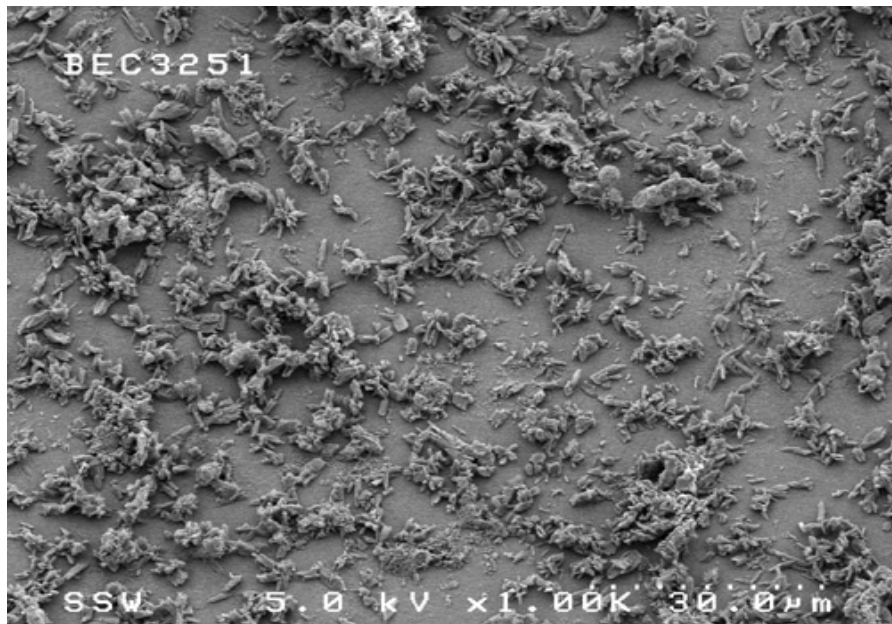


(a)

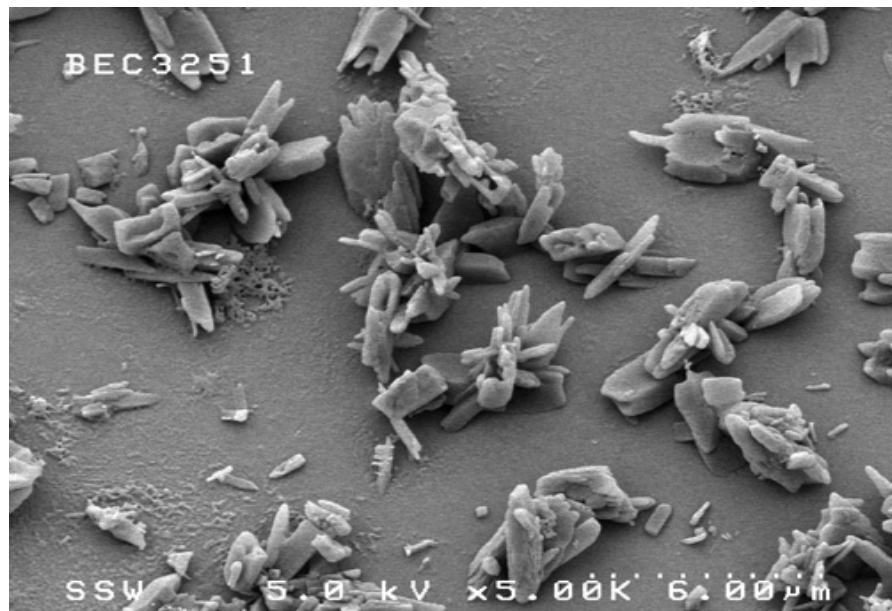


(b)

Figure 4.5.2.4 SEM photographs of BECD produced by RESS at the mole fraction of 7.81×10^{-5} . The experiment conditions were $T_{\text{mix}}=43^{\circ}\text{C}$, $P_{\text{mix}}=4600\text{psi}$, Capillary diameter=127microns, Nozzle length=3cm, Methanol concentration= 5mol%, and Spray distance=1cm



(a)



(b)

Figure 4.5.2.5 SEM photographs of BECD produced by RESS at the mole fraction of 1.63×10^{-4} . The experiment conditions were $T_{\text{mix}}=43^{\circ}\text{C}$, $P_{\text{mix}}=4600\text{psi}$, Capillary diameter=127microns, Nozzle length=3cm, Methanol concentration= 5mol%, and Spray distance=1cm

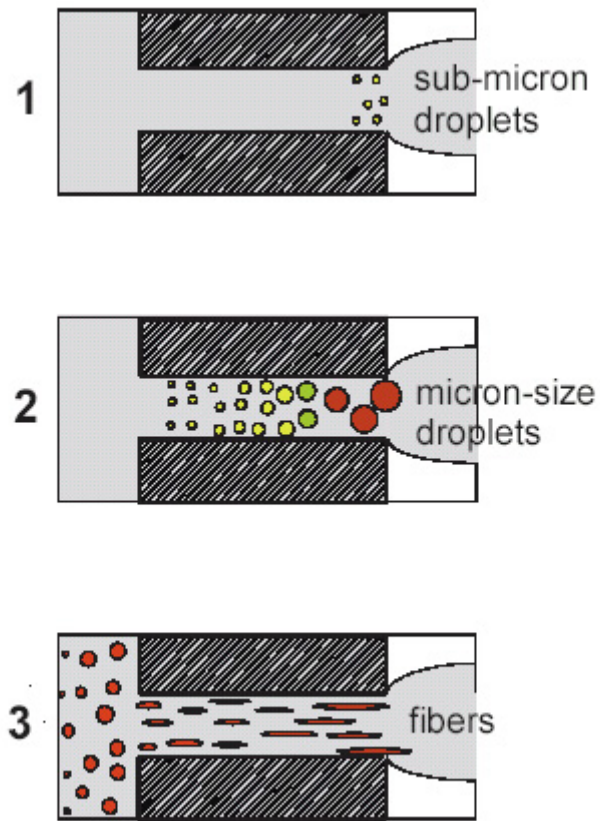


Figure 4.5.2.6 Three different RESS process paths from the entrance of the nozzle to the exit (Lele et al., 1994; Mawson et al., 1995)

4.5.3 Effect of Process Pressure

An increase of expansion pressure in the range of 1900-4100 psi resulted in an increase in particle size. In addition to an increase of particle size, it also produced a larger number of long crystals. Table 4.5.3.1 shows the RESS experimental conditions at the different pressures studied. Figure 4.5.3.1 shows the BECD particle size distribution evaluated at different pressures. Table 4.5.3.2 shows the mean diameter, standard deviation, size of range and aspect ratio of BECD particles at the different expansion pressures.

It is not easy to identify a precise trend for expansion pressure. Expansion pressure was studied by several reports. Turk et al. investigated griseofulvin and β -stirosterol with the solvents CO₂ and trifluoromethane, and found that increasing expansion pressure resulted in a decrease of particle size (Turk et al., 2002). Charoenchaitrakool et al. worked with ibuprofen and CO₂ binary system, and found that increasing expansion pressure had no effect on the particle size and morphology (Charoenchaitrakool et al., 2000). Reverchon et al. studied salicylic acid in supercritical CO₂, and found that increasing pressure led to an increase of particle size (Reverchon et al., 1993). Experimental tests conducted by Domingo and co-workers on several materials proved to be inconclusive (Domingo et al., 1997).

Figures 4.5.3.2, 4.5.3.3, 4.5.3.4 and 4.5.3.5 show SEM photographs of BECD produced by the RESS process at different pressures. From 1900psi to 4100psi, there is an interesting particle size growing progress, which is shown in Figure 4.5.3.6. At 1900psi,

the particle size is small and there is little aggregation. At 2500psi, the particle size becomes larger due to the fact that some particles grow and aggregate together. From the SEM photographs, the aggregate particle size was measured to be between 0.5 and 3 microns. At 3000psi, the particle size increased slightly. However, the aggregate phenomenon becomes obvious and some long crystals are observed from the SEM photographs. At 4100psi, most BECD particles were formed as long crystals, although there were still some small spherical particles.

Rapid expansion of supercritical solutions from the nozzle can cause the nozzle temperature to decrease. There was no heating tape or wire installed on this capillary nozzle. As a result, the nozzle temperature was not maintained constant when the supercritical solution was sprayed at different pressures. A higher expansion pressure results in a lower nozzle temperature (Reverchon et al., 1993). In this thesis, the jet temperatures of CO₂ at the exit of capillary nozzle using a small thermocouple were measured at five different spraying pressures. The temperature difference between two expansion pressures, 4500 and 1900psi would be larger than 40°C. Figure 4.5.3.7 shows the jet temperatures of CO₂ at different pressures. Although it was impossible to measure the surface temperature of particles in the RESS process, the jet temperature indicates that the difference of surface temperature of particles at two expansion pressures was rather large. The BECD particle formation at different pressures might be related to surface roughening. Every surface of a crystal has a characteristic temperature for surface roughening. This is called the transitional temperature of roughening which is much lower than the melting temperature of the substance (Larson et al., 1986). The

particle surface is roughened partly by the cold supercritical CO₂. On the roughened surface, the crystal growth-rate is very high by reason of selective aggregation (Karpenko et al., 1997). Therefore, long crystals grow at relative high pressures in RESS.

Table 4.5.3.1 RESS Experimental Conditions for Different Expansion Pressures

Run no.	T _{mix} (°C)	P _{mix} (psi)	Capillary diamter (micron)	Capillary length (cm)	BECD concentration y_{BECD}	Methanol concentration (mol%)	Spray distance (cm)
1	40	1900	127	3	8.44×10^{-5}	5	1
2	40	2500	127	3	8.43×10^{-5}	5	1
3	40	3000	127	3	8.44×10^{-5}	5	1
4	40	4100	127	3	8.44×10^{-5}	5	1

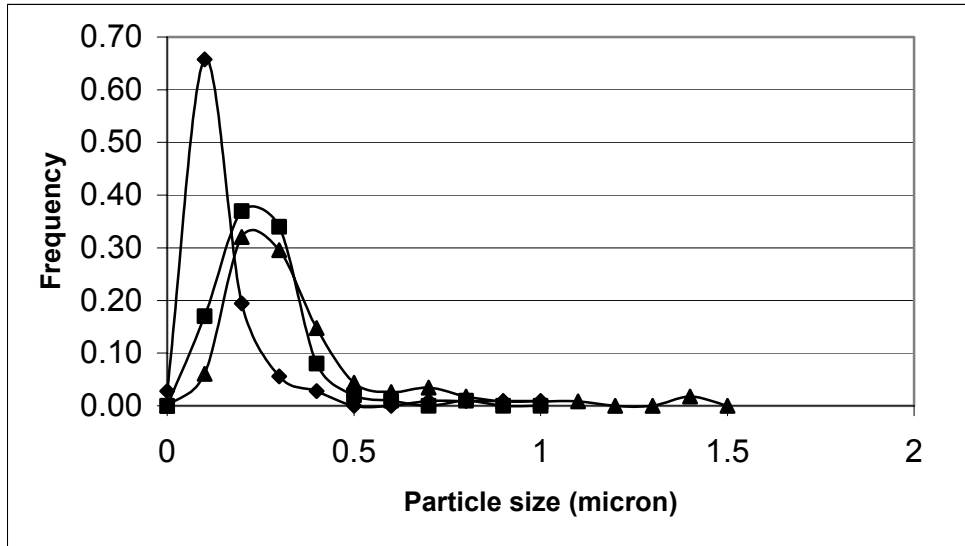
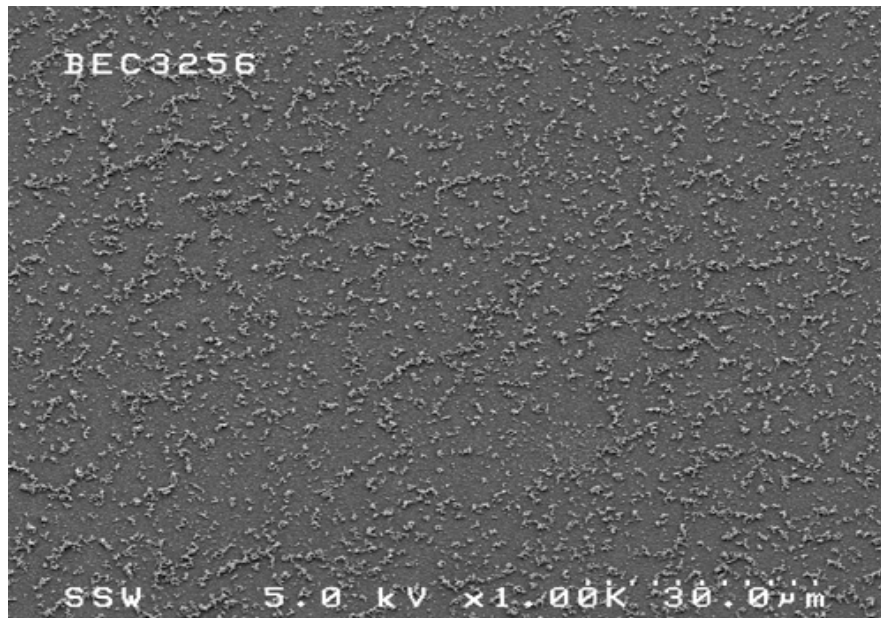


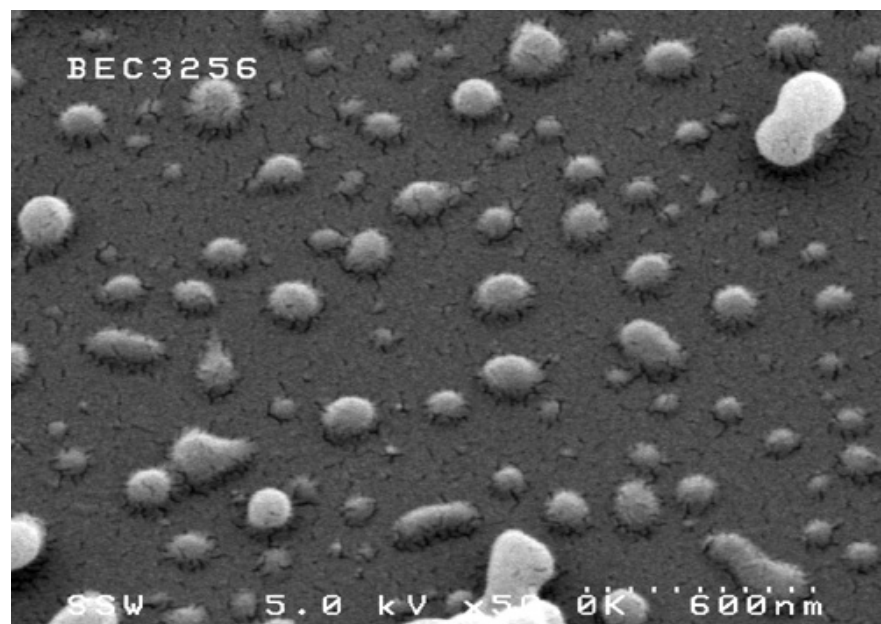
Figure 4.5.3.1 BECD size distribution evaluated at different pressure: 1900psi (◆), 2500psi (■), and 3000psi (▲). The experiment conditions were $T_{\text{mix}}=40^{\circ}\text{C}$, Capillary diameter=127microns, Nozzle length=3cm, $y_{\text{BECD}}=8.44 \times 10^{-5}$, Methanol concentration=5mol%, and Spray distance=1cm

Table 4.5.3.2 The Mean Diameter, Standard Deviation, Size of Range and Aspect Ratio of BECD Particles at the Different Expansion Pressures

Run no.	P_{mix} (psi)	Mean diameter (micron)	Standard deviation (micron)	Size of range (micron)	Aspect ratio
1	1900	0.16	1.60	0.02 – 0.98	1.45
2	2500	0.24	1.11	0.07 – 1.01	1.40
3	3000	0.34	4.90	0.09 – 1.48	1.55

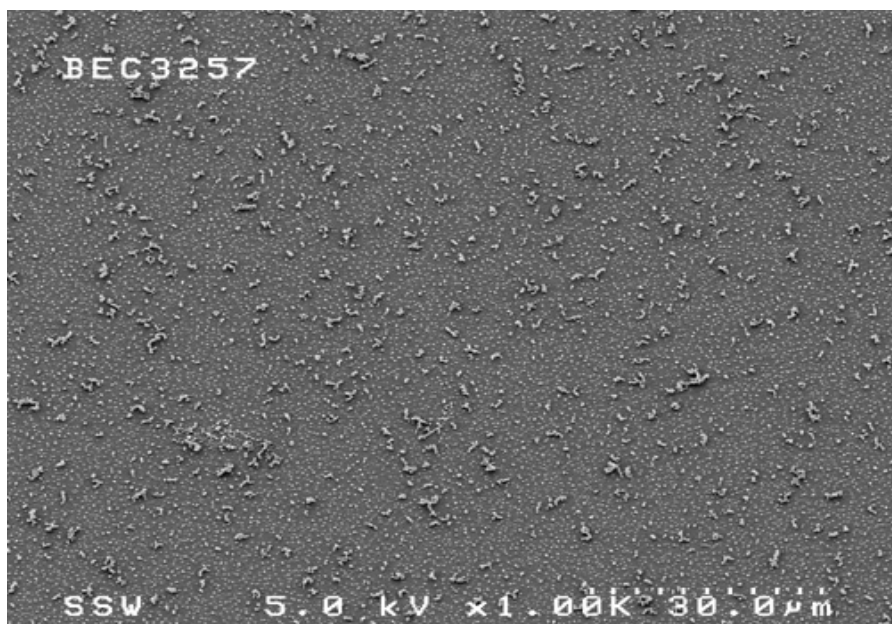


(a)

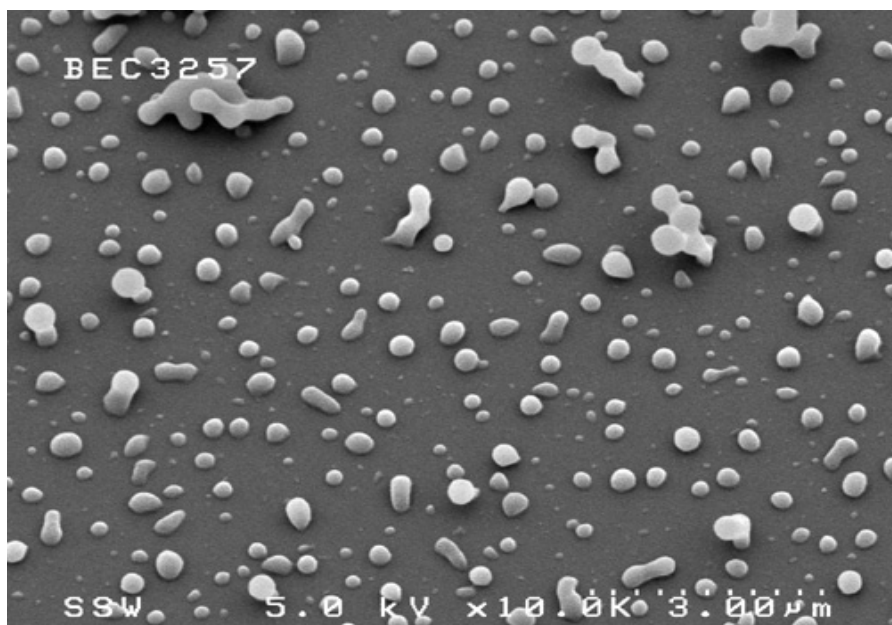


(b)

Figure 4.5.3.2 SEM photographs of BECD produced by RESS at 1900 psi. The experiment conditions were $T_{\text{mix}}=40^{\circ}\text{C}$, Capillary diameter=127microns, Nozzle length=3cm, $y_{\text{BECD}}=8.44 \times 10^{-5}$, Methanol concentration= 5mol%, and Spray distance=1cm

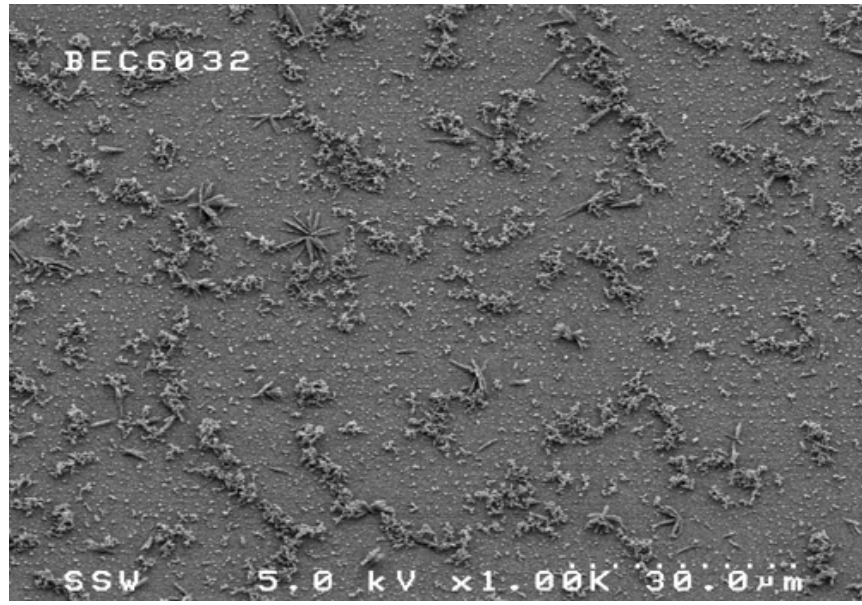


(a)



(b)

Figure 4.5.3.3 SEM photographs of BECD produced by RESS at 2500 psi. The experiment conditions were $T_{\text{mix}}=40^{\circ}\text{C}$, Capillary diameter=127microns, Nozzle length=3cm, $y_{\text{BECD}}=8.43 \times 10^{-5}$, Methanol concentration= 5mol%, and Spray distance=1cm.

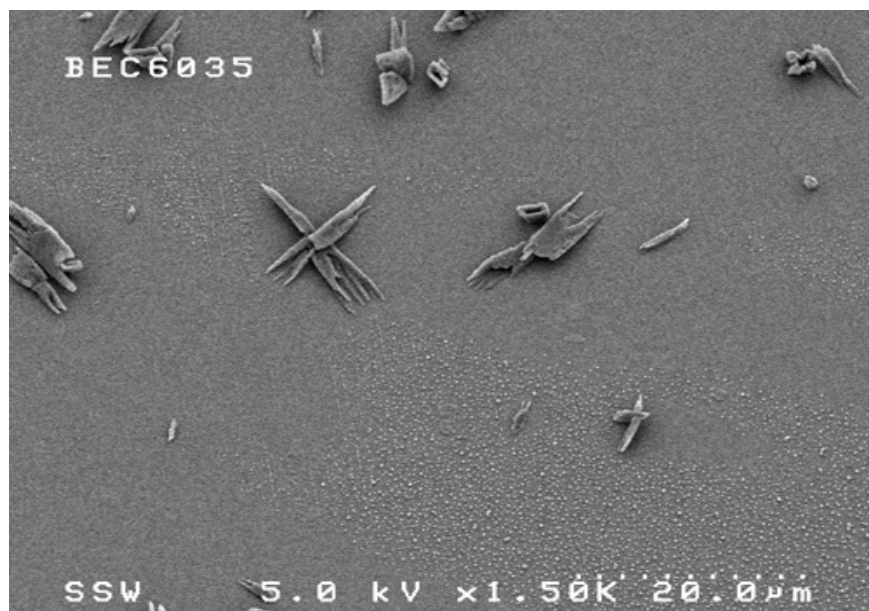


(a)

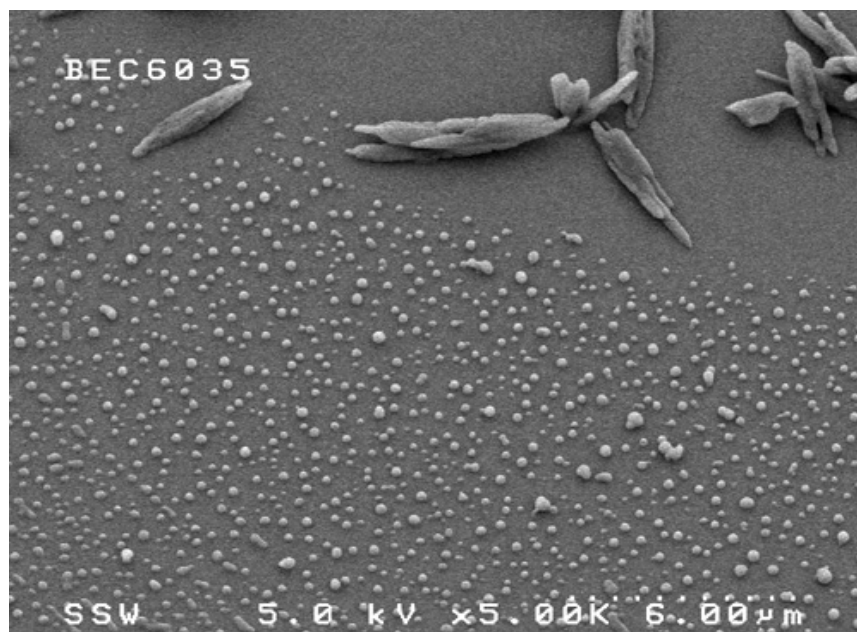


(b)

Figure 4.5.3.4 SEM photographs of BECD produced by RESS at 3000 psi. The experiment conditions were $T_{\text{mix}}=40^{\circ}\text{C}$, Capillary diameter=127microns, Nozzle length=3cm, $y_{\text{BECD}}=8.44 \times 10^{-5}$, Methanol concentration= 5mol%, and Spray distance=1cm



(a)



(b)

Figure 4.5.3.5 SEM photographs of BECD produced by RESS at 4100 psi. The experiment conditions were $T_{\text{mix}}=40^{\circ}\text{C}$, Capillary diameter=127microns, Nozzle length=3cm, $y_{\text{BECD}}=8.44 \times 10^{-5}$, Methanol concentration= 5mol%, and Spray distance=1cm

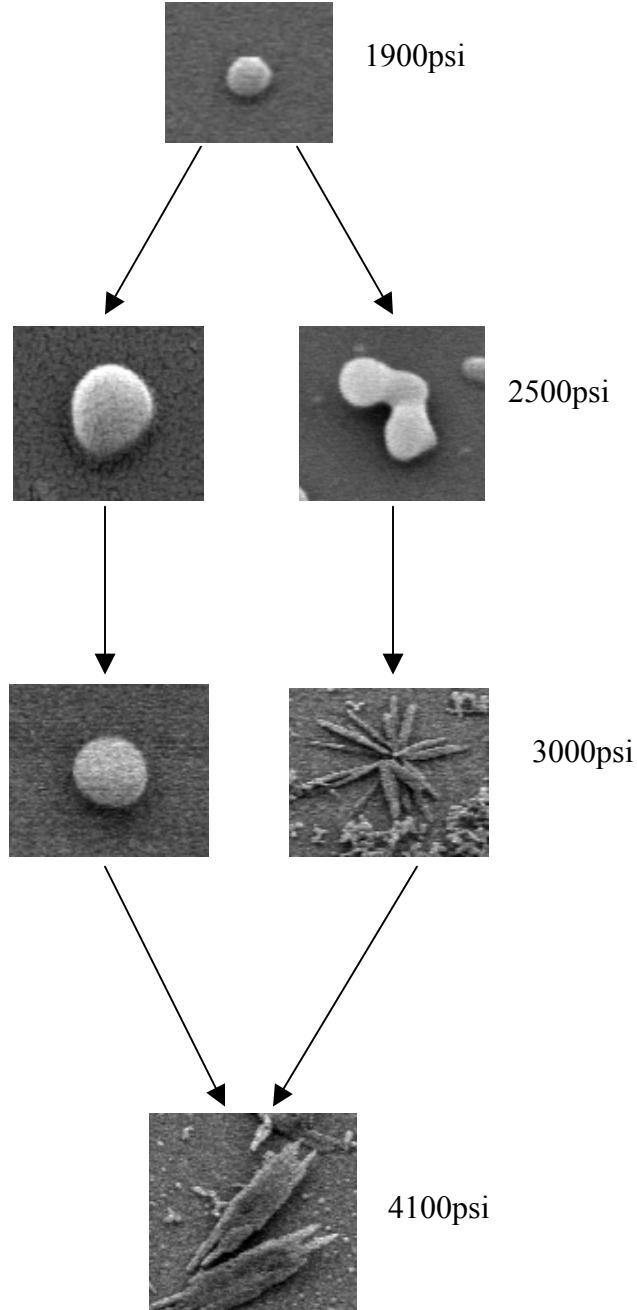


Figure 4.5.3.6 The change of particle size and morphology at different pressures. The experiment conditions were $T_{\text{mix}}=40^{\circ}\text{C}$, Capillary diameter=127microns, Nozzle length=3cm, $y_{BECD}=8.44 \times 10^{-5}$, Methanol concentration= 5mol%, and Spray distance=1cm

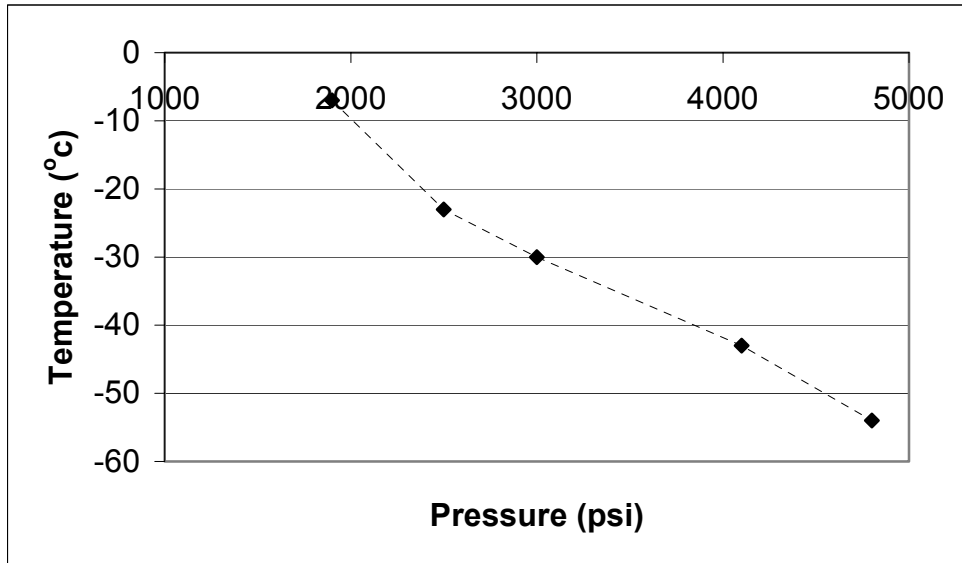


Figure 4.5.3.7 The jet temperatures of CO₂ at different pressures.

4.5.4 Effect of RESS Process Temperature

Table 4.5.4.1 shows the RESS experimental conditions at the various temperatures studied. Figure 4.5.4.1 shows BECD size distribution evaluated at different temperatures. Table 4.5.4.2 shows the mean diameter, standard deviation, size of range and aspect ratio of BECD particles at the different process temperatures. Figures 4.5.4.2 and 4.5.4.3 show SEM photographs of BECD produced by the RESS process at 35°C and 50°C. The morphologies of BECD changed from spherical into short stick crystals by increasing the temperature. Also, the particles grew and coalesced inside the nozzle. Figure 4.5.3.4 shows SEM photographs of BECD produced by the RESS process at 40°C.

Increasing mixture chamber temperature was found to give larger particle sizes. At the same concentration, higher temperature solutions have a higher cloud-point pressure. With respect to all the experiments that were run at the same pressure and concentration, the higher temperature experiments caused the solutions to cross the cloud point first. Although temperatures drop when supercritical solutions are expanded across a nozzle, the pressure-dropping gradient should be similar at the same expansion pressure. Therefore, the temperature-dropping gradient should be the same. A higher temperature solution should still cross the cloud point curve earlier. Hence, particle nucleation will begin earlier. The path length along the nozzle after nucleation is longer than other solutions with lower temperature.

Table 4.5.4.1 RESS Experimental Conditions for Different Process Temperatures.

Run no.	T_{mix} (°C)	P_{mix} (psi)	Capillary diameter (micron)	Capillary length (cm)	BECD concentration y_{BECD}	Methanol concentration (mol%)	Spray distance (cm)
1	35	3000	127	3	8.44×10^{-5}	5	1
2	40	3000	127	3	8.44×10^{-5}	5	1
3	50	3000	127	3	8.44×10^{-5}	5	1

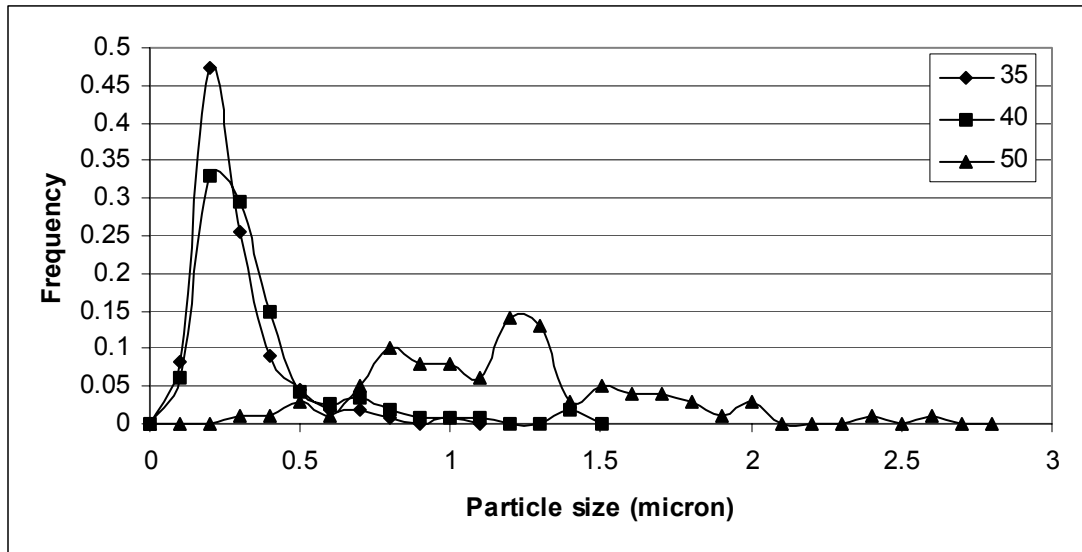
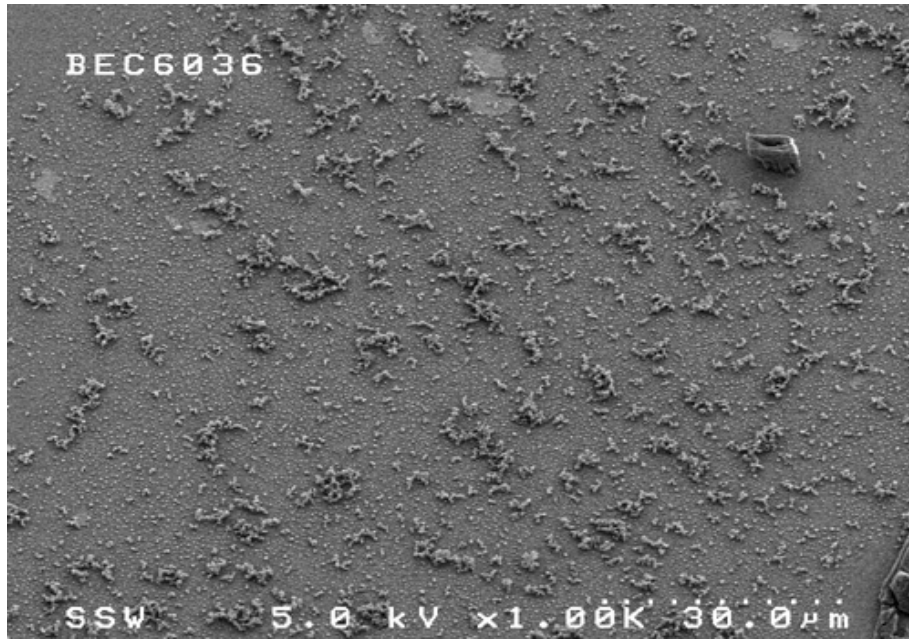


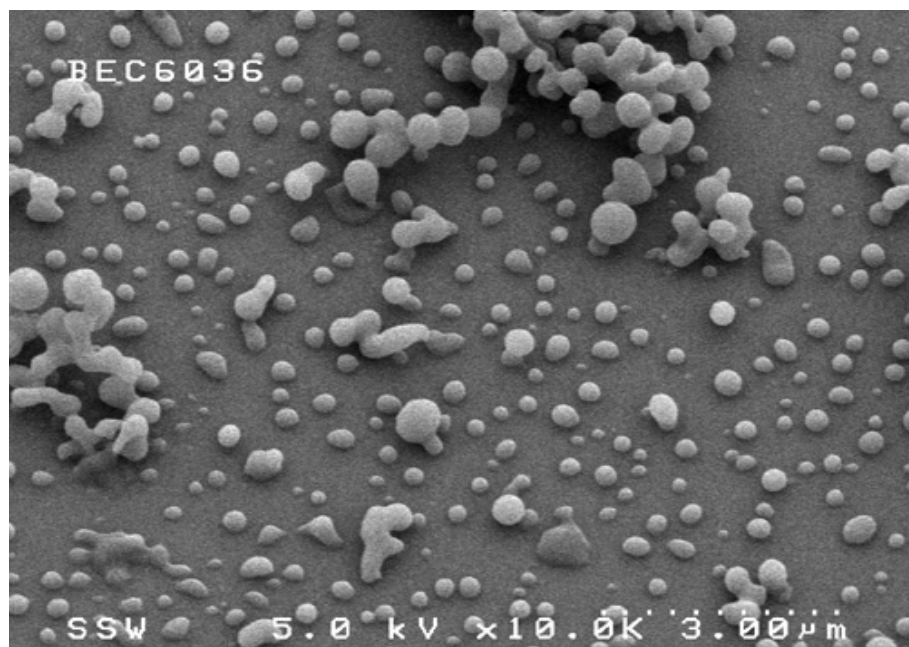
Figure 4.5.4.1 BECD size distribution evaluated at different temperature: 35 °C (◆), 40 °C (■), and 50°C (▲). The experiment conditions were $P_{mix}=3000\text{psi}$, Capillary diameter=127microns, Nozzle length=3cm, $y_{BECD}=8.44 \times 10^{-5}$, Methanol concentration= 5mol%, and Spray distance=1cm.

Table 4.5.4.2 The Mean Diameter, Standard Deviation, Size of Range and Aspect Ratio of BECD Particles at the Different Process Temperatures

Run no.	T_{mix} (°C)	Mean diameter (micron)	Standard deviation (micron)	Size of range (micron)	Aspect ratio
1	35	0.30	4.34	0.07 – 1.01	1.20
2	40	0.34	4.90	0.09 – 1.48	1.55
3	50	1.28	4.03	0.42 – 2.73	2.66

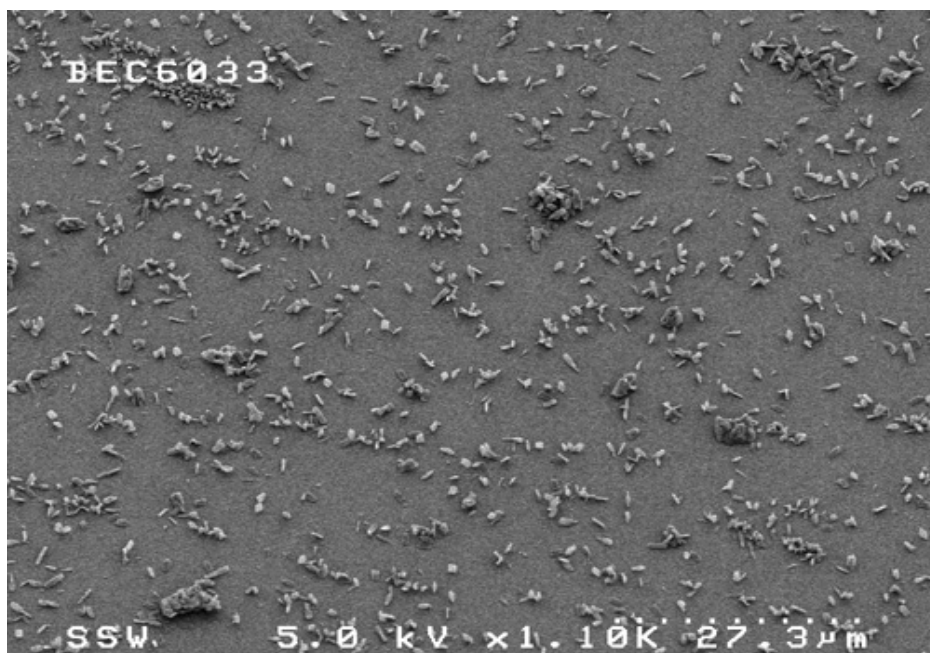


(a)

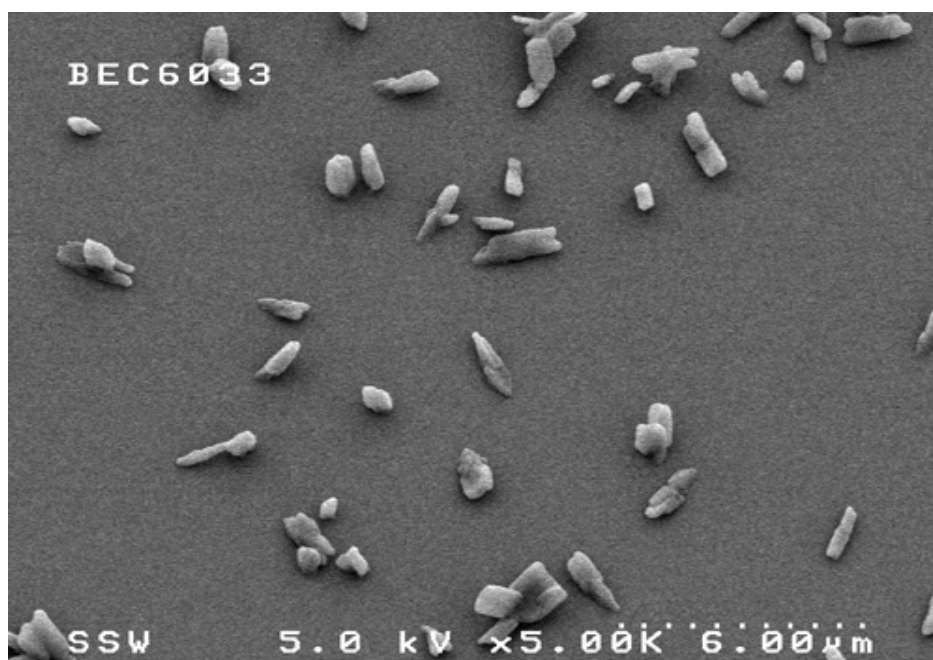


(b)

Figure 4.5.4.2 SEM photographs of BECD produced by RESS at 35°C. The experiment conditions were $P_{\text{mix}}=3000\text{psi}$, Capillary diameter=127microns, Nozzle length=3cm, $y_{\text{BECD}}=8.44 \times 10^{-5}$, Methanol concentration= 5mol%, and Spray distance=1cm.



(a)



(b)

Figure 4.5.4.3 SEM photographs of BECD produced by RESS at 50°C. The experiment conditions were $P_{\text{mix}}=3000\text{psi}$, Capillary diameter=127microns, Nozzle length=3cm, $y_{\text{BECD}}=8.44 \times 10^{-5}$, Methanol concentration= 5mol%, and Spray distance=1cm

4.5.5 Effect of Nozzle Length

Capillary nozzles are of interest in RESS for the reason that the dimensions of the expansion device control the expansion process, and these dimensions can be varied to examine their effect on particle formation. In this report, two lengths of capillary nozzles were studied; 3cm and 4cm.

Table 4.5.5.1 shows the RESS experimental conditions for the different nozzle lengths. Figure 4.5.5.1 shows the BECD particle size distribution evaluated at the different nozzle lengths. Table 4.5.5.2 shows the mean diameter, standard deviation, size of range and aspect ratio of BECD particles at the different nozzle lengths. Increasing the nozzle length leads to larger particle sizes and wider particle size distributions. Figure 4.5.3.4 shows SEM photographs of BECD produced by the RESS process using a nozzle length of 3cm. Figure 4.5.5.2 shows SEM photographs of BECD produced by the RESS process at a nozzle length of 4cm. For BECD, not only the particle size was increased, but also there are two types of morphology being observed, microspheres and microsticks. The residence time that the particles remain inside the nozzle at the same operating condition is longer at the longer nozzle. Therefore, the BECD particles coalesce and grow inside the nozzle.

Table 4.5.5.1 RESS Experimental Conditions for Different Nozzle Lengths

Run no.	T_{mix} (°C)	P_{mix} (psi)	Capillary diameter (micron)	Capillary length (cm)	BECD concentration y_{BECD}	Methanol concentration (mol%)	Spray distance (cm)
1	40	3000	127	3	8.44×10^{-5}	5	1
2	40	3000	127	4	8.44×10^{-5}	5	1

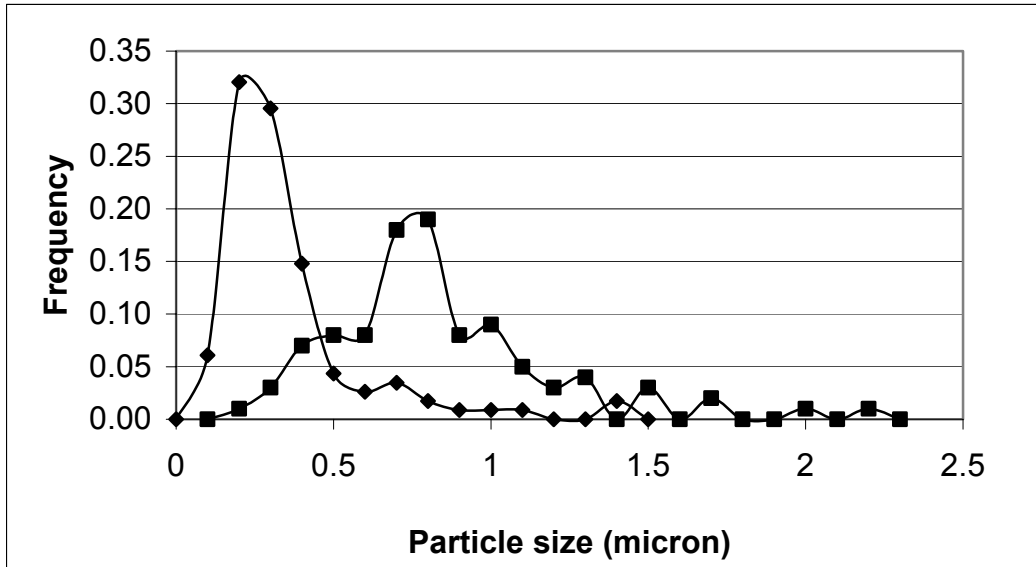


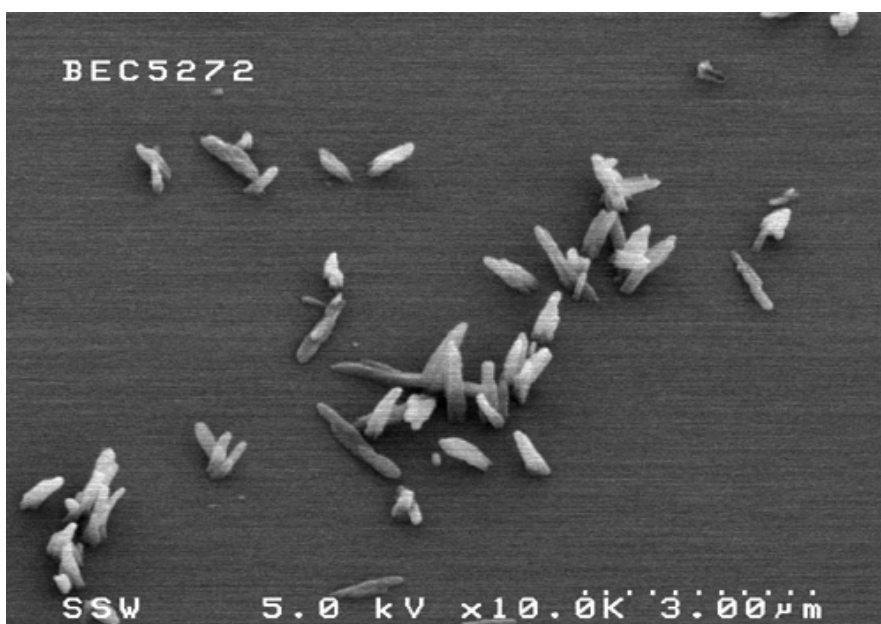
Figure 4.5.5.1 BECD size distribution evaluated at different nozzle length: 3cm (◆) and 4cm (■). The experiment conditions were $T_{mix}=40^{\circ}C$, $P_{mix}=3000psi$, Capillary diameter=127microns, $y_{BECD}=8.44 \times 10^{-5}$, Methanol concentration= 5mol%, and Spray distance=1cm.

Table 4.5.5.2 The Mean Diameter, Standard Deviation, Size of Range and Aspect Ratio of BECD Particles at the Different Nozzle Lengths

Run no.	Capillary length (cm)	Mean diameter (micron)	Standard deviation (micron)	Size of range (micron)	Aspect ratio
1	3	0.34	4.90	0.09 – 1.48	1.55
2	4	0.73	3.53	0.18 – 2.13	2.67



(a)



(b)

Figure 4.5.5.2 SEM photographs of BECD produced by RESS at nozzle length of 4 cm.

The experiment conditions were $T_{\text{mix}}=40^{\circ}\text{C}$, $P_{\text{mix}}=3000\text{psi}$, Capillary diameter=127microns, $y_{\text{BECD}}=8.44 \times 10^{-5}$, Methanol concentration= 5mol%, and Spray distance=1cm.

4.5.6 Effect of Spray Distance

Spray distance, as a parameter, is not studied in most reports. Some researchers think that there is no significant effect on the particle size and morphology (Reverchon et al., 1993; Charoenchaitrakool et al., 2000; Blasig et al., 2002). Another factor affecting the spraying result is the varying spray distance. If the silicon plate is too close to the nozzle, particles may be swept off the surface due to the high-pressure flow exiting the nozzle. On the contrary, if the silicon plate is too far downstream of the nozzle, the flow pattern may extend outside of the silicon plate, and BECD particles may pass by the sample collection without contacting its surface.

The experimental results show that the BECD particle size became larger and morphology changed from spherical into irregular shape by increasing the spray distance from 1cm to 5cm. Table 4.5.6.1 shows the RESS experimental conditions at the different spray distances. Figure 4.5.6.1 shows the BECD size distribution evaluated at different spray distances. Table 4.5.6.2 shows the mean diameter, standard deviation, size of range and aspect ratio of BECD particles at the different spray distances. Figure 4.5.6.2 shows SEM photographs of BECD produced by RESS at a spray distance of 3cm and 5cm. For accuracy, three experiments were repeated at the spray distance of 5cm. The results were duplicated. Figure 4.5.6.3 shows SEM photographs of the BECD particle surface at a spray distance of 3cm and 5cm. The particle surfaces are like honeycomb in appearance. In order to understand more about the relationship between particle size and spray distance, the silicon plate was positioned at the spray distance of 3cm. The results show

that particle size at the spray distance of 3cm is slightly smaller than that at the spray distance of 5cm where the particle morphology does not change. From the SEM photographs at a spray distance of 1cm, 3cm and 5cm, it was found that the particles were aggregated during spraying. The reason behind this phenomenon is unclear.

Phenanthrene particle size and morphology were studied at two-spray distances, 1cm and 5cm. There was no significant effect on particle size and morphology. Charoenchaitrakool and co-workers found that increasing spray distance led to small ibuprofen particles (Charoenchaitrakool et al., 2000). Blasig found that particle size and morphology did not change when a fluoropolymer precipitate was collected 1cm and 10cm downstream of the nozzle (Blasig et al., 2002). The effect of spray distance on particle size and morphology depends on the particular material property. Some materials are sensitive to the spray distance; some are not. BECD is very sensitive to spray distance.

Table 4.5.6.1 RESS Experimental Conditions at the Variant Spray Distance

Run no.	T _{mix} (°C)	P _{mix} (psi)	Capillary diamter (micron)	Capillary length (cm)	BECD concentration y_{BECD}	Methanol concentration (mol%)	Spray distance (cm)
1	40	3000	127	3	8.44×10^{-5}	5	1
2	40	3000	127	3	8.44×10^{-5}	5	3
2	40	3000	127	3	8.44×10^{-5}	5	5

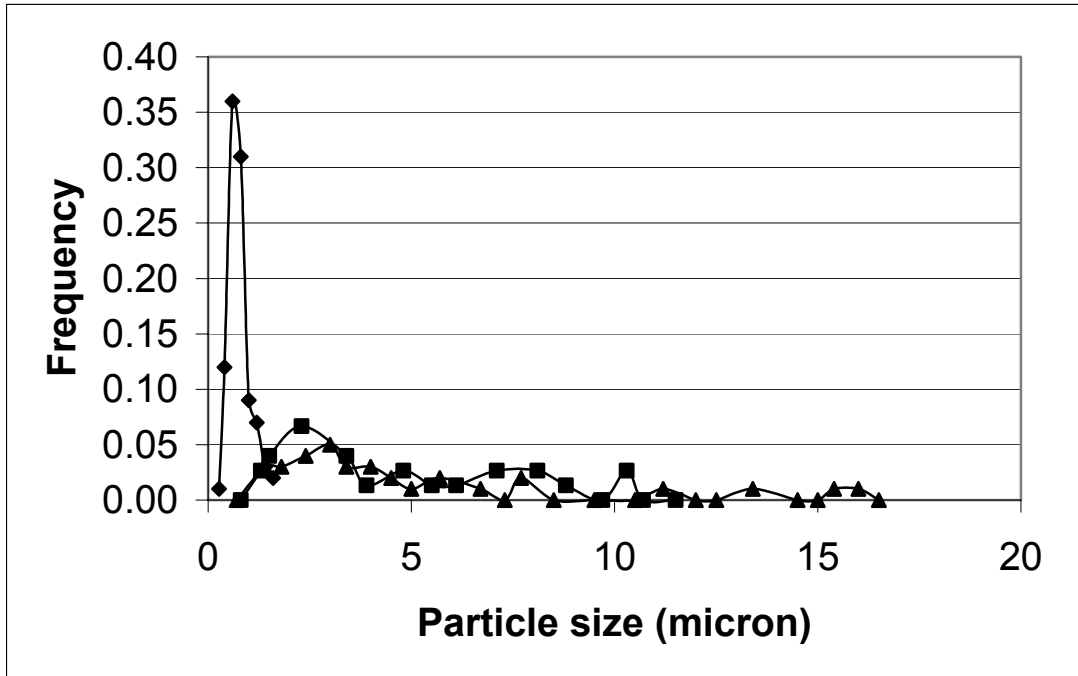
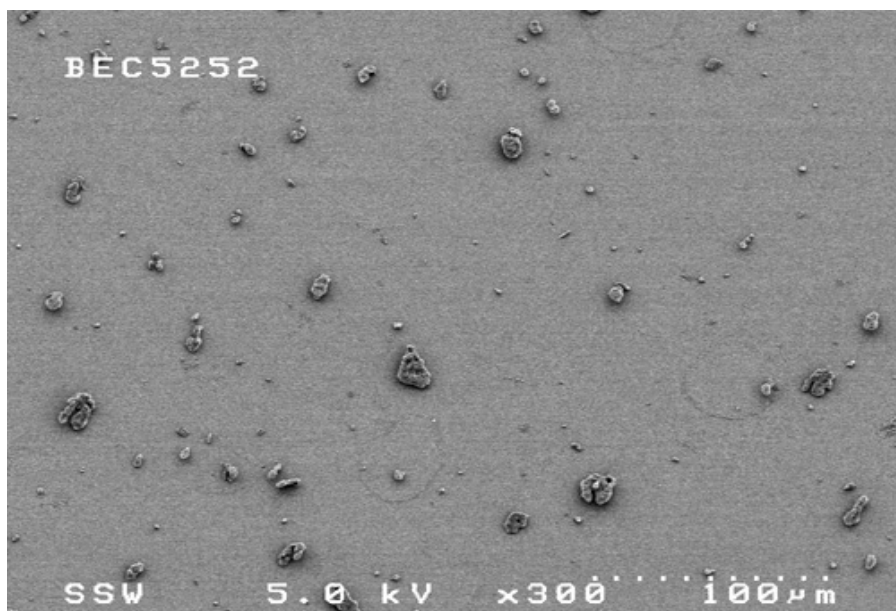


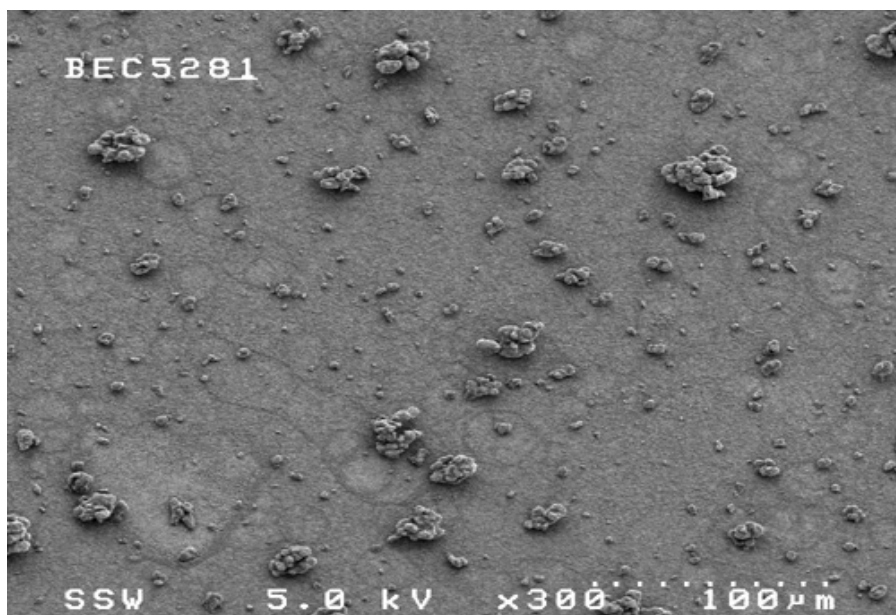
Figure 4.5.6.1 BECD size distribution evaluated at different spray distance: 1cm (◆), 3cm (■), and 5cm (▲). The experiment conditions were $T_{\text{mix}}=40^{\circ}\text{C}$, $P_{\text{mix}}=3000\text{psi}$, Capillary diameter=127microns, Nozzle length=3cm, $y_{\text{BECD}}=8.44 \times 10^{-5}$, and Methanol concentration= 5mol%.

Table 4.5.6.2 The Mean Diameter, Standard Deviation, Size of Range and Aspect Ratio of BECD Particles at the Different Spray Distances

Run no.	Spray distance (cm)	Mean diameter (micron)	Standard deviation (micron)	Size of range (micron)	Aspect ratio
1	1	0.34	4.90	0.09 – 1.48	1.55
2	3	3.73	23.24	1.02 – 10.33	2.05
3	5	4.07	29.12	0.72 - 16.01	1.94

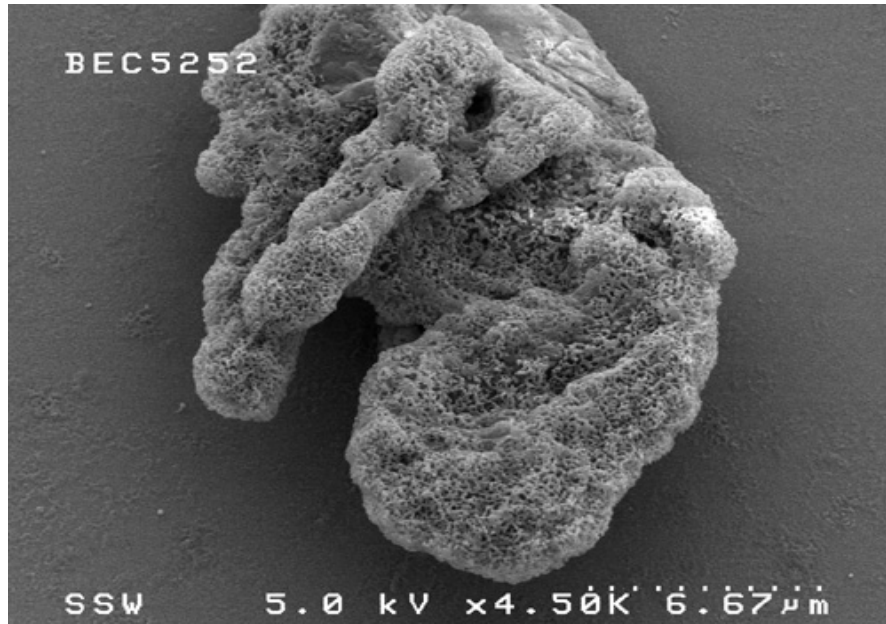


(a)

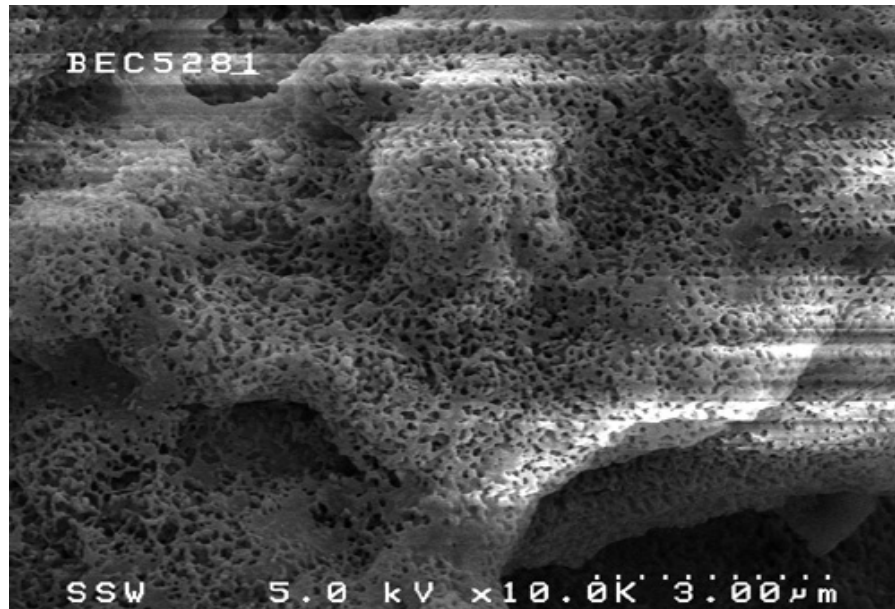


(b)

Figure 4.5.6.2 SEM photographs of BECD produced by RESS at spray distance of (a) 3cm and (b) 5cm. The experiment conditions were $T_{\text{mix}}=40^{\circ}\text{C}$, $P_{\text{mix}}=3000\text{psi}$, Capillary diameter=127microns, Nozzle length=3cm, $y_{\text{BECD}}=8.44 \times 10^{-5}$, and Methanol concentration= 5mol%.



(a)



(b)

Figure 4.5.6.3 SEM photographs of BECD particle surface at spray distance of 3cm(a) and 5cm(b). The experiment conditions were $T_{\text{mix}}=40^{\circ}\text{C}$, $P_{\text{mix}}=3000\text{psi}$, Capillary diameter=127microns, Nozzle length=3cm, $y_{\text{BECD}}=8.44 \times 10^{-5}$, and Methanol concentration= 5mol%.

5 CONCLUSIONS

In this report, the particle formation and solubility of phenanthrene and beclomethasone dipropionate (BECD) were investigated. Experimental results show that the rapid expansion of supercritical solutions (RESS) is a promising method to form small and monodisperse particles.

Although the solvent strength of supercritical CO₂ for BECD was relatively low, adding a small amount of co-solvent enhanced the solubility of BECD in supercritical CO₂ significantly. Methyl alcohol in supercritical CO₂ represents the better solubility enhancement compared with acetone in CO₂, most likely by reason of its hydrogen bond formation between BECD and methyl alcohol. Due to the tunability of supercritical solutions, the solubility of BECD in compressed CO₂ was adjusted by changing the pressure and temperature of CO₂. However, the relation between solvent strength and pressure and temperature is complex. The density of supercritical CO₂ increased with an increase in pressure and a decrease in temperature. Increasing solution density increased the solubility of BECD in compressed CO₂. However, increasing the mixing chamber temperature also increased the solubility of BECD at high-pressure condition, likely by reason that vapor pressure of BECD was increased and the effect of temperature on density became minimal at higher pressures.

Phenanthrene had a relatively high solubility in compressed CO₂ compared with BECD. Therefore, phenanthrene was processed using the experimental RESS system first. The phenanthrene particle size became smaller and the particle size distribution became narrower after the RESS process. Due to the fact that phenanthrene was evaporated under vacuum, optical microscopy was used to observe phenanthrene particle size and morphology after the RESS process instead of Scanning Electron Microscopy (SEM). Increasing concentration resulted in larger mean particle size. The other two studied parameters, pressure and spray distance, had no significant effect on the particle size and morphology in the range of operation conditions studied.

BECD, a synthetic steroid of the glucocorticoid family, was processed on our RESS apparatus. After the RESS process, the BECD mean particle size decreased to sub-micron and nanometer dimensions. An increase in the following parameters, i.e. nozzle diameter, BECD mol fraction, system pressure, system temperature, and L/D ratio of the capillary; led to larger particle sizes. Increasing the following parameters changed the BECD morphology from spherical into long crystals. The spray distance had a strong effect on BECD particle size and morphology. Increasing the spray distance resulted in a larger mean particle size. The particle surface resembled a honeycomb structure.

Particle size and morphology is not only related to processing conditions, but also related to the nature of the material. Spray distance was found to have a significant effect in the BECD study. In contrast, phenanthrene particles were found to be insensitive to changes in this parameter. The effects of the other two parameters, pressure and concentration, on

BECD are more significant than those on phenanthrene within the range of operating conditions studied. For BECD, a small change in process conditions changed particle size and morphology significantly.

Future Work

The experimental results on the formation of phenanthrene and BECD were helpful to understand the relation between particle size and process conditions. Understanding this relation will result in a greater ability to control the particle size, and can also help to build computational models to perform particle nucleation and growth. Future work can try to develop a model to perform parameter studies on particle nucleation and growth.

In this work, the particles were collected on silicon plates. As discussed in the introduction, particles grow during the spraying process. A surfactant could help to impede BECD particle growth and agglomeration. Future experimentation can try to find a biosurfactant and develop a precipitation unit to collect particles. The BECD particles can be sprayed into an aqueous solution directly. The surfactant can be put into this aqueous solution before the RESS process or can be mixed with BECD in the mixture chamber and sprayed into the aqueous solution. Hence, stable suspensions of BECD could be produced by the RESS process.

6. REFERENCES

Alessi, P.; Cortesi, A.; Kikic, I.; Foster, N.R.; Macnaughton, S.J.; Colombo, I. Particle Production of Steroid Drugs Using Supercritical Fluid Processing. *Ind. Eng. Chem. Res.* **1996**, 35, 4718-4726.

Arai, Y.; Sako, T.; Takebayashi, Y. Supercritical Fluid Molecular Interactions, Physical Properties, and New Applications **2002**.

Atkinson, R.M.; Bedford, C.; Child, K.J.; Tomich, E.G. Effect of Particle Size on Blood Grisefulvin-Levels in Man. *Nature* **1962**, 193, 588.

Bausch, A.; Hidber, P. Process for Making Submicron Particles. US patent 6 299 906, **2001**.

Bender, E. Equations of State Exactly Representing the Phase Behavior of Pure Substances. In *Proceedings Fifth Symposium on Thermophysical Properties American Society of Mechanical Engineers New York*, **1970**, 227-235.

Blasig, A.; Shi, C.; Enick, R.M.; Thies, M.C. Effect of Concentration and Degree of Saturation on RESS of a CO₂-Soluble Fluoropolymer. *Ind. Eng. Chem. Res.* **2002**, 41, 4976-4983.

Bradbury, S. *An Introduction to the Optical Microscope* **1984**.

Chang, C.J.; Randolph, A.D. Precipitation of Microsize Organic Particles from Supercritical Fluids. *AIChE Journal* **1989**, 35(11), 1876-1882.

Charoenchaitrakool, M.; Dehghani, F.; Foster, N.R.; Chan, H.K. Micronization by Rapid Expansion of Supercritical Solutions to Enhance the Dissolution Rates of Poorly Water-Soluble Pharmaceuticals. *Ind. Eng. Chem. Res.* **2000**, 39, 4794-4802.

Chernyak, Y.; Henon, F.; Harris, R.B.; Gould, R.D.; Franklin, R.K.; Edward, J.R.; DeSimone, J.M.; Carbonell, R.G. Formation of Perfluoropolyether Coatings by the Rapid Expansion of Supercritical Solutions (RESS) Process. Part 1: Experimental Results. *Ind. Eng. Chem. Res.* **2001**, 40, 6118-6126.

Chrastil, J. Solubility of Solids and Liquids in Supercritical Gases. *J. Phys. Chem.* **1982**, 86, 3016-3021.

Dean, J.R. *Applications of Supercritical Fluids in Industrial Analysis* **1993**.

Dean, J.R.; Kane, M.; Khundker, S.; Dowle, C.; Tranter, R.L.; Jones, P. Estimation and Determination of Steroid Solubility in Supercritical Carbon Dioxide. *Analyst* **1995**, 120(8), 2153-2157.

Debenedetti, P.G. Homogeneous Nucleation in Supercritical Fluids. *AICHE J.* **1990**, 36, 1289-1298.

Dixon, D.J.; Johnston, K.P. Supercritical Fluids. *Encyclopedia of Chemical Technology* 4th **1997**, 23, 452-478.

Domingo, C.; Berends, E.M.; Rosmalen, G.M. Precipitation of Ultrafine Benzoic Acid by Expansion of a Supercritical Carbon Dioxide Solution through a Porous Plate Nozzle. *Journal of Crystal Growth* **1996**, 166, 989-995.

Domingo, C.; Berends, E.M.; Rosmalen, G.M. Precipitation of Ultrafine Organic Crystals from the Rapid Expansion of Supercritical Solutions over a Capillary and a Firt Nozzle. *Journal of Supercritical Fluids* **1997**, 10, 39-55.

Foster, N.R.; Singh, H.; Yun, S.L.J.; Tomasko, D.L.; Macnaughton, S.J. Polar and Nonpolar Cosolvent Effects on the Solubility of Cholesterol in Supercritical Fluids. *Ind. Eng. Chem. Res.* **1993**, 32, 2849-2853.

Gamse, T.; Steinkellner, F.; Marr, R.; Alessi, P.; Kikic, I. Solubility Studies of Organic Flame Retardants in Supercritical CO₂. *Ind. Eng. Chem. Res.* **2000**, 39, 4888-4890.

Godinas, A.; Henriksen, I.B.; Krukonis, V.; Mishra, K.A.; Pace, G.W.; Vachon, G.W. Processes to Generate Submicron Particles of Water-Insoluble Compounds. WO patent 9965469, **1999**.

Goldstein, J.I.; Jr, A.D.R.; Newbury, D.E.; Lyman, C.E.; Echlin, P.; Fiori, C.; Joy, D.C.; Lifshin, E. *Scanning Electron Microscopy and X-Ray Microanalysis: a Text for Biologists, Materials, Scientists, and Geologists* **1992**.

Goodarznia, I.; Esmailzadeh, F. Solubility of an Anthracene, Phenanthrene, and Carbazole Mixture in Supercritical Carbon Dioxide. *J. Chem. Eng. Data* **2002**, 47, 333-338.

Hannay, J.B.; Hogarth, J. On the Solubility of Solids in Gases. *Proc. Roy. Sec.* **1879**, 29, 324.

Helfgen, B.; Turk, M.; Schaber, K. Theoretical and Experimental Investigations of the Micronization of Organic Solids by Rapid Expansion of Supercritical Solutions. *Powder Technology* **2000**, 110, 22-28.

Johnston, K.P.; Penninger, J.M. *Supercritical Fluid Science and Technology* **1988**.

Johnston, K.P.; Lemert, R.M. Supercritical Fluid Technology: Theory and Application. Encyclopedia of Chemical Processing and Design **1996**, 56, 1-45.

Jung, J.; Perrut, M. Particle Design Using Supercritical Fluids: Literature and Patent Survey. *J. Supercrit fluids* **2001**, 20, 179-219.

Karpenko, O.P.; Yalisove, S.M.; Eaglesham, D.J. Surface Roughening During Low Temperature Si (100) Epitaxy. *J. Appl. Phys.* **1997**, 82(3), 1157-1165.

Larson, K.; King, M.L.; Evaluation of Supercritical Fluid Extraction in the Pharmaceutical Industry *Biotechnol. Prog.* **1986**, 2(2), 73-82.

Larson, M.A.; Garside, J. Solute Clustering in Supersaturated Solutions. *Chemical Engineering Science* **1986**, 41(5), 1285-1289.

Lele, A.K.; Shine, A.D. Morphology of Polymers Precipitated from a Supercritical Solvent. *AIChE Journal* **1992**, 38, 742-752.

Lele, A.K.; Shine, A.D. Effect of RESS Dynamics on Polymer Morphology. *Ind. Eng. Chem. Res.* **1994**, 33, 1476-1485.

Liu, G.T.; Nagahama, K. Application of Rapid Expansion of Supercritical Solutions in the Crystallization Separation. *Ind. Eng. Chem. Res.* **1996**, 35, 4626-4634.

Liu, G.T.; Nagahama, K. Solubility and RESS Experiments of Solid Solution in Supercritical Carbon Dioxide. *Journal of Chemical Engineering of Japan* **1997**, 30(2), 293-301.

Liu, S.F.Y.; Ong, C.P.; Lee, M.L.; and Lee, H.K. Supercritical Fluid Extraction and Chromatography of Steroids with Freon-22. *J. Chromatogr.* **1990**, 515, 515-520.

Loth, H.; Hemgesberg, E. Properties and Dissolution of Drugs Micronized by Crystallization from Supercritical Gases. *International Journal of Pharmaceutics* **1986**, 32(2-3), 265-267.

Maguire, K.L.; Denyszyn, R.B. *Modern Supercritical Fluid Chromatography*, New York, **1988**, 45.

Matson, D.W.; Fulton, J.L.; Petersen, R.C.; Smith, R.D. Rapid Expansion of Supercritical Fluid Solutions: Solute Formation of Powders, Thin Films, and Fibers. *Ind. Eng. Chem. Res.* **1987**, 26, 2298-2306.

Matsuyama, K.; Mishima, K.; Umemoto, H.; Yamaguchi, S. Environmentally Benign Formation of Polymeric Microspheres by Rapid Expansion of Supercritical Carbon Dioxide Solution with a Nonsolvent. *Environ. Sci. Technol.* **2001**, 35, 4149-4155.

Mawson, S.; Johnston, K.P.; Combes, J.R.; DeSimone, J.M. Formation of Poly (1, 1, 2, 2, -tetrahydroperfluorodecyl acrylate) Submicron Fibers and Particles from Supercritical Carbon Dioxide Solutions. *Macromolecules* **1995**, 28, 3182-3191.

Mchugh, M.; Krukonis, V. *Supercritical Fluid Extraction* **1986**.

Mchugh, M.; Krukonis, V. *Special Application in Supercritical Fluid Extraction: Principles and Practice* 2nd Edition Butterworths-Heinemann, Boston, **1994**.

Meilchen, M.A.; Hasch, B.M.; Mchugh, M.A. Effect of Copolymer Composition on the Phase Behavior of Mixtures of Poly(ethylene-co-methyl acrylate) with Propane and Chlorodifluoromethane *Macromolecules* **1991**, 24, 4874-4882.

Mohamed, R.S.; Debenedetti, P.G.; Prudhomme, R.K. Effects of Process Conditions on Crystals Obtained from Supercritical Mixtures. *AIChE Journal* **1989**, 35, 325-332.

Pace, G.W.; Vachon, M.G.; Mishra, A.K.; Henrikson, I.B.; Krukonis, V. Processes to Generate Submicron Particles of Water-Insoluble Compounds. US patent 6 177 103, **2001**.

Phillips, E.M.; Stella, V.J. Rapid Expansion from Supercritical Solutions: Application to Pharmaceutical Processes. *International Journal of Pharmaceutics* **1993**, 94(1-3), 1-10.

Reverchon, E.; Donsi, G.; Gorgoglione, D. Salicylic Acid Solubilization in Supercritical CO₂ and Its Micronization by RESS. *Journal of Supercritical Fluids* **1993**, 6, 241-248.

Reverchon, E.; Porta, G.D.; Taddeo, R.; Pallado, P.; Stassi, A. Solubility and Micronization of Griseofulvin in Supercritical CHF₃. *Ind. Eng. Chem. Res.* **1995**, 34, 4087-4091.

Shim, J.; Yates, M.Z.; Johnston, K.P. Latexes Formed by Rapid Expansion of Polymer/CO₂ Suspensions into Water. 1. Hydrophilic Surfactant in Supercritical CO₂. *Ind. Eng. Chem. Res.* **2001**, 40, 536-543.

Sievers, R.E.; Hansen, B.N.; Hybertson, B.M. Chemical Deposition Methods Using Supercritical Fluid Solution. US Patent 4 970 093, **1990**.

Sievers, R.E.; Hybertson, B.M.; Hansen, B.N. Methods and Apparatus for Drug Delivery Using Supercritical Solutions. US patent 5 301 644, **1994**.

Sievers, R.E.; Karst, U. Method and Apparatus for Fine Particle Formation. US patent 6 095 134, **2000**.

Smith, R.D.; Wash, R. Supercritical Fluid Molecular Spray Film Deposition and Powder Formation. US Patent 4 582 731, **1986**.

Smith, R.D. Supercritical Fluid Molecular Spray Thin Film and Fine Powders. US Patent 4 734 451, **1988**.

Span, R.; Wagner, W. A New Equation of State for Carbon Dioxide Covering the Fluid Region from the Triple-Point Temperature to 1100K at Pressures up to 800Mpa. *J. Phys. Chem. Ref. Data* **1996**, 25(6), 1509-1596.

Steckel, H.; Thies, J.; Muller, B.W. Micronizing of Steroids for Pulmonary Delivery by Supercritical Carbon Dioxide. *International Journal of Pharmaceutics* **1997**, 152, 99-110.

Sun Y.P. *Supercritical fluid Technology in Materials Science and Engineering* **2002**.

Tai, C.Y.; Cheng, C.S. Growth of Naphthalene Crystals from Supercritical CO₂ Solution. *AIChE Journal* **1995**, 41(10), 2227-2236.

Tan, H.S.; Borsadia, S. Particle Formation Using Supercritical Fluids: Pharmaceutical Applications. Ashley Publications Ltd. *Exp. Opin. Ther. Patents* **2001**, 11(5), 861-872.

Taylor, L.T. *Supercritical Fluid Extraction* **1996**.

Tom, J.W.; Debenedetti, P.G. Formation of Bioerodible Polymeric Microspheres and Microparticles by Rapid Expansion of Supercritical Solutions. *Biotechnol. Prog.* **1991a**, 7, 403-411.

Tom, J.W.; Debenedetti, P.G. Particle Formation with Supercritical Fluids a Review. *J. Aerosol Sci.* **1991b**, 22(5), 555-584.

Turk, M.; Hils, P.; Helfgen, B.; Schaber, K.; Martin, H.J.; Wahl, M.A. Micronization of Pharmaceutical Substances by the Rapid Expansion of Supercritical Solutions (RESS): a Promising Method to Improve Bioavailability of Poorly Soluble Pharmaceutical Agents. *Journal of Supercritical Fluids* **2002**, 22, 75-84.

York, P.; Hanna, M. Particle Engineering by Supercritical Fluid Technologies for Powder Inhalation Drug Delivery. The Fifth in a Series of International Symposia Organized by the School of Pharmacy of Virginia Commonwealth University April 28-May 2, **1996**.

Young, T.J.; Mawson, S.; Johnston, K.P.; Henriksen, I.B.; Pace, G.W.; Mishra, A.K. Rapid Expansion from Supercritical to Aqueous Solution to Produce Submicron Suspensions of Water-Insoluble Drugs. *Biotechnol. Prog.* **2000**, 16, 402-407.

7. APPENDICES

APPENDIX A. BECD Solubility Measurements

BECD solubility in supercritical CO₂ was measured by SFT phase monitor. The measurement temperature range is from 35 °C to 65 °C. The pressure range is from 1200psi to 3500psi. Figure A.1 provides a schematic of the SFT phase monitor.

Safety Precautions

Safety glasses and a cotton lab coat were worn during all activities in the lab. Gloves were worn all the time when working with tools and operating the SFT phase monitor apparatus. Exhaust gas was vented into a ducted fume hood

Operational Procedure:

1. Loading particles

- Weigh the desired amount of BECD and place into the sample bottle
- Open injection port and load the BECD particles into the vessel

Note: the sample bottle should be weighed before and after loading particles. The weight difference before and after weighing the sample bottle is the mass of BECD particles in the vessel. The mole fraction of BECD was calculated according to equation A.1. According to the SFT vessel volume, the mass of CO₂ can be

determined from the equation A.2. The density of CO₂ was obtained from the equation of Bender for a given temperature and pressure

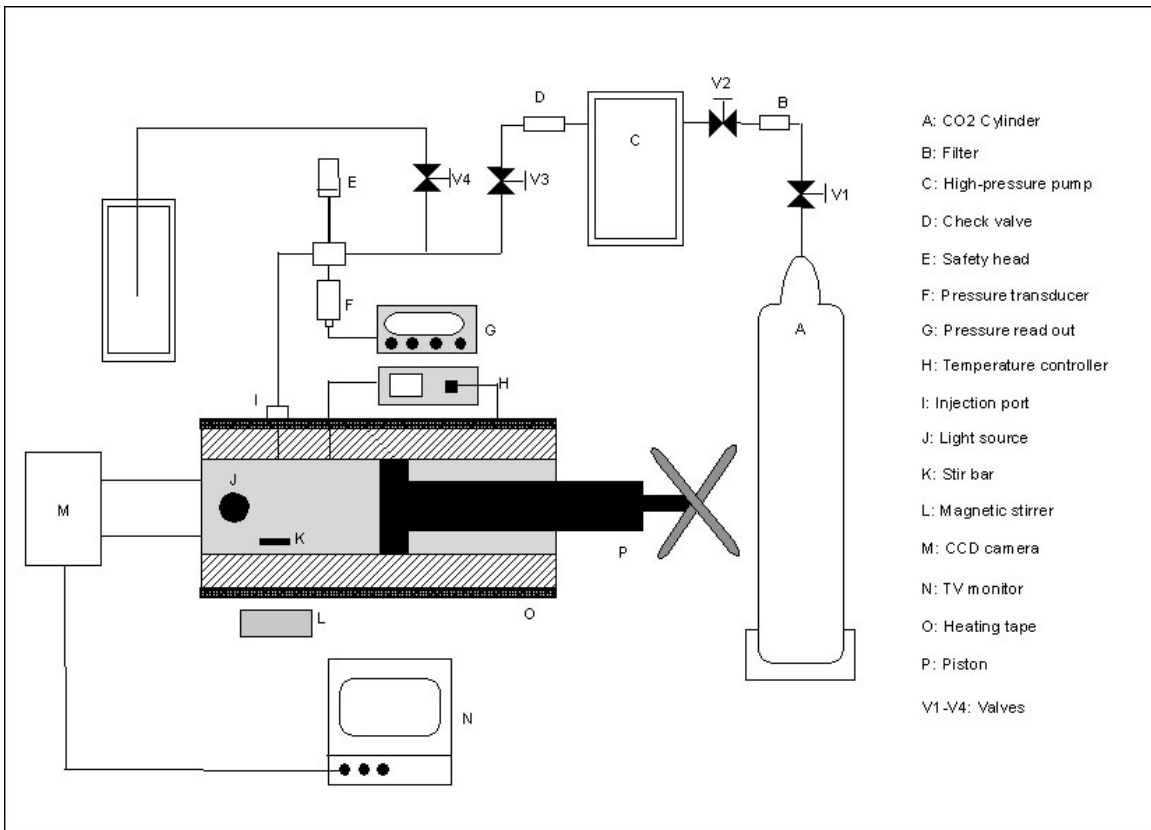


Figure A.1 SFT phase monitor apparatus: A), CO₂ tank; B), filter; C), high-pressure pump; D), check valve; E), safety head; F), pressure transducer; G), pressure read out; H), temperature controller; I), injection port; J), light source; K), stir bar; L), magnetic stirrer; M), CCD camera; N), TV monitor; O), heating tape; P), piston; V1-V4), valves

$$y_{BECD} = \frac{\frac{m_{BECD}}{M_{BECD}}}{\frac{m_{CO_2}}{M_{CO_2}} + \frac{m_{BECD}}{M_{BECD}}} \quad \text{A.1}$$

$$m_{CO_2} = \rho_{CO_2} V_{CO_2} \quad \text{A.2}$$

- Add a desire amount of methyl alcohol into the sample bottle. The volume of methyl alcohol was determined from the equation A.3. The mole fraction of methyl alcohol is pre-determined. The density of methyl alcohol can be obtained from Aldrich website.

$$v_{methanol} = \frac{\frac{m_{CO_2}}{M_{CO_2}}}{1 - y_{methanol}} \times \frac{M_{methanol}}{\rho_{methanol}} \quad \text{A.3}$$

- Close the injection port
 - Remove the air from the vessel by flashing CO₂. Open valve V1, and V2. Close valve V4. Then crack open the top injection port fitting and crack open valve V3 and close immediately. This allows CO₂ from the cylinder to flow into the vessel and blow the air out of vessel.
 - Close valve V3 and tighten injection port fitting.

2 Mixing solution

- Turn on equipment: pressure transducer, temperature controller, variable light source, TV monitor and magnetic stirrer.

- Check that valve V1 and V2 are open and valve V3 and V4 are closed.
- Open valve V3 to introduce the liquid CO₂ into the vessel
- Set the temperature controller to the desired temperature and pressurize the system to the desired pressure. This temperature and pressure is used for the equation of Bender to calculate the density of CO₂.

Note: for this particular system, screwing the piston when valve V4 is closed or using high-pressure pump can increase the vessel pressure. It depends on the experimental requirement.

- Close valve V3 to make the quantity of CO₂ constant in vessel
 - Allow the vessel to remain at desire pressure and temperature about 20 minutes. This is to ensure that all of the materials are dissolved in the supercritical solution.

3 Solubility measurement

- Check that each valve is closed.
- Drop the pressure by backing the piston off. The solute should be precipitated from solution, so the system becomes cloudy.

Note: the pressure needs to be slowly reduced at 5-10 psi/s. The precipitation phenomena can be observed from the TV monitor. If any precipitate forms as a cloud, the image will become bright and cloudy. The cloud-point is a region. In this work, the cloud point pressure is defined as the pressure at which the image started to become bright.

- Measure each cloud point pressure three times at constant temperature and composition to minimize the operator error.
- Set the temperature controller to the higher temperature and measure a new cloud point

4 System shut down

- Open valve V4 to vent the vessel.
- Check that valve V1, V2, and V3 are closed and open valves V4.
- Turn off equipment: pressure transducer, temperature controller, variable light source, TV monitor and magnetic stirrer

5 Cleaning the system

- Close valve V3 and open valve V4 to vent any pressurized solution in the chamber
- Spray acetone inside view cell. Acetone is a very good solvent for BECD used for this experimentation.
 - Use a slim tube to suck the acetone solution out of vessel.
 - Use acetone to rinse the chamber at least two or three times. All the particles must be cleaned by acetone. Otherwise the remained BECD particles will bring in the error to the next measurement.

APPENDIX B. RESS Operational Procedure

The following section covers the procedure for the use of the Rapid Expansion of Supercritical Solutions (RESS) apparatus, and any significant safety precautions. The apparatus was set up for expansion of supercritical organic materials/CO₂ solution to ambient conditions. The process temperature range was from 30°C to 80°C, and pressure range was up to 6000psi. Figure B.1 shows a schematic of the RESS apparatus

Safety Precaution

The basic safety precautions taken were the same as those taken during solubility measurements. Safety glasses, cotton lab coat and gloves should be worn during the RESS operation or other activities in the lab. Phenanthrene and BECD can get into people's lung when the operators breathe it during the rapid expansion of supercritical solutions. Therefore, the hood sash must be closed during the experimental procedure.

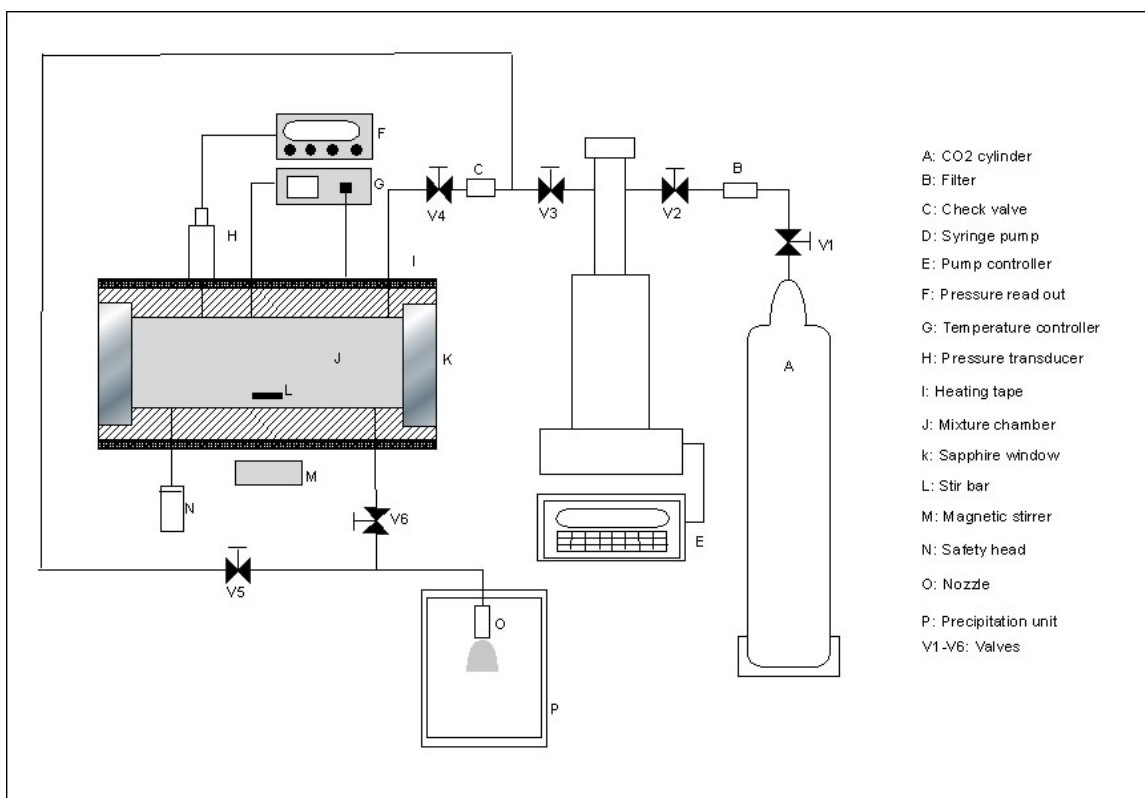


Figure B.1 Rapid expansions of supercritical solutions apparatus: A), CO₂ tank; B), filter; C), check valve; D), syringe pump; E), pump controller; F), pressure readout; G), temperature controller; H), pressure transducer; I), heating tape; J), mixture chamber; K), sapphire window; L), stir bar; M), magnetic stirrer; N), safety head; O), nozzle; P), precipitation unit; V1-V6), valves

Operational Procedure

1. Loading particles

- Determine the amount of material required to produce a pre-determined mole fraction solution from equation B.1:

$$m_{BECD} = \frac{\frac{m_{CO_2}}{M_{CO_2}}}{1 - y_{BECD}} \times M_{BECD} \quad \text{B.1}$$

Note: for this particular system, a constant amount of liquid CO₂ can be collected in the mixture chamber at a given temperature and a pressure. The density of CO₂ can be calculated by the equation of Bender. According to the volume of mixture chamber, the mass of CO₂ can be calculated from equation A.2 in appendix A.

- Weigh the desired amount of material and load into the sample bottle.

Note: for Beclomethasone Dipropionate, methanol should be added in the mixture chamber as co-solvent. The volume of methyl alcohol is provided by equation A.3 in appendix A.

- Remove the mixture chamber lid and sapphire window and place material into the mixture chamber. The BECD particles and methyl alcohol can be placed in the chamber separately, or they can be placed into the chamber together after they are mixed in the sample bottle. For accurate measurements, the sample bottle should be weighted before and after loading the particles into the chamber.

- Put the sapphire window back and tighten the lid. The lid cannot be too tight; or the sapphire window could be crushed.
- Calculate the mole fraction of BECD again from the equation A.1 according to the weight difference of sample bottle before and after loading particles
- Flash CO₂ into the mixture chamber removing the air. Open Valve V1, V2, V3 and V6 and crack open Valve V4 and close immediately. This allows CO₂ from the cylinder to flow into the view cell and blow the air out of the mixture chamber.
 - Close Valve V1, V2, V3, V4, and V6

2. Mixing solution

- Turn on the following equipment: pressure transducer, temperature controller, syringe pump controller and magnetic stirrer.
- Set the temperature controller to the desire temperature
- Check that valves V1 and V2 are open and valve V3, V4, V5 and V6 are closed.
- Fill the syringe pump with liquid CO₂ to the maximum volume (266ml).
- Close valve V2
- Set the pressure of the syringe pump to the desire pressure with the pump controller. Place syringe pump in constant pressure mode.
- Open valve V3, and then open valve V4.

Note: this makes CO₂ flow into the mixture chamber from the syringe pump. As the syringe pump's working condition is constant pressure, the mixture chamber will be pumped to the desired pressure.

- Maintain this condition for at least 20 minutes.

Note: the particle dissolving process takes about 10-20 minutes. The length of dissolving time depends on the solute particular property, the temperature and pressure of the mixture chamber, and the stirring velocity. The solubility progress can be monitored through the sapphire window. The solution will be clear when the material is completely dissolved.

3. Spraying

- Close valve V4 and crack open valve V5 and close immediately.

Note: this allows CO₂ go through bypass tube to clean the way.

- Install the nozzle on the system.
- Open valve V5 first. And then open valve V6, at the mean time, close valve V5.

Note: when supercritical solution sprays through the nozzle, the density of solution will be changed greatly because of depressurization. The solute will be precipitated. The nozzle may be plugged due to this precipitation. Bypass line can help to get rid of initial pressure drop inside the nozzle.

- Collect particles on a silicon wafer or in the precipitation bottle directly. It depends on the experiment requirement.

Note: if the particles need to be collected on the silicon wafer, the silicon plate is put under the nozzle. The collection time is three seconds.

4. Normal shut down

- Take the nozzle off from the system.

- Open valve V6 to vent mixture chamber.
- Check that valve V1, V2, and V3 are closed and open all other valves.
- Turn off equipment: pressure transducer, temperature controller, syringe pump controller and magnetic stirrer.

5. Cleaning the system

- Check valve V4 to be sure that it is closed.
- Open valve V6 to vent any pressurized solution in the chamber.
- Take the mixture chamber lid, sapphire window and Teflon o-ring seal off.
- Remove magnetic stir bar from chamber.
- Spray acetone inside view cell and pass an acetone soaked lint free tissue through the cell.

Note: acetone is easy to vaporize and is a very good solvent for the particles used for this experimentation.

- Clean sapphire window, Teflon o-ring seal, fittings, and magnetic stirrer with acetone and wipe dry with lint off tissues.

6. Emergency shut down

- Turn off all instruments.
- Open valve V5 and close other Valves.

APPENDIX C. Scanning Electron Microscopy (SEM) Operational Procedure

The following section covers the procedure for the use of the SEM. After the “AIR” button was pushed, the specimen chamber door would open automatically after a few seconds. The specimen holder was screwed into a loading rod. Since the SEM only works under the vacuum condition the specimen chamber was evacuated before the sample was loaded into the chamber. “EVAC” button was pressed while the specimen chamber door was shut. It took few seconds to vacuum the chamber. Green lights flashed from high to low on “S.C. VACUUM”. Then, when the vacuum was finished, lights flashed from “S.E.C. VALVE-OPEN” to “S.C. AIR LOCK VALVE-OPEN”. The sample was loaded into the chamber by opening “MV-1” valve. The specimen holder on the loading rod was slid into a slot inside the chamber. The specimen holder was unscrewed and the loading rod was pulled all the way back into the specimen chamber. After the above procedures, the “MV-1” valve was closed.

The next step was to obtain a clear image on Hitachi S-4500 Field Emission SEM screen. “AIR LOCK VALVE” was pulled out and pushed to the left. “READY” light should light up on the control panel to signaling that the SEM is ready to turn on. Several working conditions and parameters need to be set before trying to obtain an image from the SEM. “PF15” button was pressed and the sample data was inputted by keyboard. Voltage and emission were set to 5.0KV and 20 μ A by pressing “ON” button. The working distance was set to between 12-15mm by pressing “PF2” button. In this work,

the working distance was always set to 15mm. Beam alignment was checked by pressing the “PF3” button. In the beam alignment function, a circle was displayed on the screen. The beam was adjusted by using “X” and “Y” knobs on the control panel until the circle filled the screen evenly on all four sides. After aligning the beam, “ENTER” and “PF16” were pressed to exit the beam alignment function. The sample holder tilt was set to 30° by turning “TILT” knob. After these settings, turning the “Z AXIS” knob would bring the sample into focus. Magnification was increased on an area, which was going to be focused. And coarse focus was used to focus the area. Then, the “X” and “Y” knobs on the control panel were used to sharpen the image. Sometimes, moving back and forth between “COARSE FOCUS” and “X” and “Y” to obtain a sharp image was needed. At the same image, the astigmatism should be checked at high magnification. The image started to pulse when the “STIG/AL2” button was pressed. Using “X” and “Y” stigma alignment knobs can correct any astigmatism. Sometimes, the image needed to be switched to low magnification to find the focus location on sample by pushing “LOW MAG” button. Turning “X” and “Y” knobs below the “TILT” knobs can change the focus location. Before acquiring the image from the SEM, the contrast and brightness of the image should be adjusted by using “CONTRAST” and “BRIGHTNESS” buttons.

When the desire image was achieved from SEM, the image should be saved on the computer. After the green button on the top right of computer screen was clicked and “DIRECT” button was pressed on the panel, the computer started to acquire the image from the SEM. The acquire procedure would take a few seconds. The image was saved as TIFF image file.

After the measurements, the SEM was shut down and the “AIR LOCK” was released. Before the sample holder was pulled out from the chamber, the “TILT”, “Z”, “X” and “Y” knobs should be back to 0°, 15, 12.5 and 12.5 respectively. “MV-1” valve was opened. The sample holder was removed from the slot by screwing loading rod into the holder and pulling it all the way back into the specimen chamber. Then, “MV-1” was closed. The air was supplied into the specimen chamber by pressing “AIR” button. Sample holder was removed from loading rod when the loading chamber door opened. In the end, “EVAC” button was pressed while holding the specimen chamber door shut.

APPENDIX D. CO₂ Density Calculation

The density of carbon dioxide was calculated by using the Bender equation. The calculation program shows as follow:

```
% The Density of Carbon Dioxide
% This program is about the calculation of the density of carbon dioxide by the
% equation of Bender.
% The equation of state %
R*T*DEN+B*(DEN^2)+C*(DEN^3)+D*(DEN^4)+E*(DEN^5)+F*(DEN^6)+(G+H*(D
EN^2))*
% (DEN^3)*exp(-n20*(DEN^2))=P
figure;
hold on
% The universal gas constant for carbon dioxide
R=0.188918;
% The coefficients from n1 to n20
n1=0.22488558;n2=-0.13717965e3;
n3=-0.14430214e5;n4=-0.29630491e7;
n5=-0.20606039e9;n6=0.45554393e-1;
n7=0.77042840e2;n8=0.40602371e5;
n9=0.40029509;n10=-0.39436077e3;
n11=0.12115286;n12=0.10783386e3;
```

```
n13=0.43962336e2;n14=-0.36505545e8;  
n15=0.19490511e11;n16=-0.29186718e13;  
n17=0.24358627e8;n18=-0.37546530e11;  
n19=0.11898141e14;n20=0.5000000e1;
```

```
for T=[293:5:393]
```

```
    T=T
```

```
    B=n1*T+n2+n3/T+n4/(T^2)+n5/(T^3)
```

```
    C=n6*T+n7+n8/T
```

```
    D=n9*T+n10
```

```
    E=n11*T+n12
```

```
    F=n13
```

```
    G=n14/(T^2)+n15/(T^3)+n16/(T^4)
```

```
    H=n17/(T^2)+n18/(T^3)+n19/(T^4)
```

```
    % Den: Density
```

```
    % P: Pressure
```

```
    DEN=[0.00:0.001:1.00];
```

```
    P=R.*T.*DEN+B.*(DEN.^2)+C.*(DEN.^3)+D.*(DEN.^4)+E.*(DEN.^5)+F.*(DEN.^6)
```

```
    +(G+H.*(DEN.^2)).*(DEN.^3).*exp(-n20.*(DEN.^2));
```

```
    plot(10*P,DEN);
```

```
end
```

```
xlabel('Pressure (bar)');
```

```
ylabel('Density (g/ml)');
```

```
title('The density of carbon dioxide');
```